Testing Ge- APS's for Ranging Applications in a Cryogenic Environment

Ulrich Schreiber, Christian Schötz
Forschungseinrichtung Satellitengeodäsie
Fundamentalstation Wettzell
D - 93444 Kötzting
Germany

Karl Heinz Haufe
Institut für Angewandte Geodäsie
Fundamentalstation Wettzell
D-93444 Kötzting
Germany

Abstract

The technology for a ranging station that is based on frequency doubled Nd:YAG-lasers is well developed in every aspect. However, when it comes to dualcolor ranging, or to working in the infrared domain, there are still many open questions with respect to suitable detection devices and the propagation properties of the atmosphere. The fact that the infrared tracking channel often seems to have a superior [illegible]

usually used visible channel ($\lambda = 532nm$) and that there is a growing interest in ranging systems that work in the "eyesafe"- region around ($\lambda = 1.54\mu m$) stimulated

2. EXPERIMENTAL SETUP

The germanium avalanche diode under test was placed in a little cryogenic chamber, which allows for a temperature setting between 10 K and room temperature. A window was placed at one side of this chamber, so that short light pulses illuminate the diode, causing a signal induced breakdown of the geiger voltage, which in turn was used as a stop signal on a time interval counter. The start pulse was derived from a frequency generator as a trigger source, running on a frequency of 10 Hz. This ensures that the results obtained are comparable to real ranging. The jitter of the Hamamatsu pulser with respect to the trigger input is of the order of a few picoseconds. However this is not an issue in this type of experiment, since the work presented here focuses mainly on the behaviour of the intrinsic noise of the various tested diodes, relative to the detection of low light level laser pulses. It was made sure that no unwanted background light caused false readings during the experiments. Figure 1 outlines the block diagram of the experimental setup.

Under room temperature conditions it usually takes only about 1 ns for a voltage break down to occur in a germanium avalanche diode. For a well behaved satellite a rangegate of 200 ns is sufficiently large for ranging. Therefore the experiment had set a delay of 170 ns between "gate on" at the detector and the occurence of the laser pulse. The influence of the cooling on the intrinsic noise of a germanium detector could therefore be studied in detail. Figure 2 illustrates the timing arrangement of this experiment. A sample experiment was run to verify the principle of operation and test the setup. The result is shown in Figure 3. The slight deviation from a gaussian distribution is characteristic for a detection based on avalanche diodes. The overall rms was estimated to yield 88 ps and the rate of valid detections is approximately 25 %.

3. INVESTIGATING THE PROPERTIES OF TWO DIFFERENT GERMANIUM DIODES

The sensitivity and scatter of a geiger mode operated avalanche diode is strongly determined by the degree to which the gate voltage, exceeds the breakdown threshold. Increasing the gate voltage leads to higher sensitivity and higher accuracy for the measurement. However, it also increases the probability for an intrinsic noise event. So in the first experiment the gate voltage was varied over the complete working range and the mean time between gate on and the occurence of a noise breakdown was taken from the histogram of the noise. There were two different detectors available for the experiments. One was made by Hamamatsu (type B2834-01) the active chipsize being 100 μm in diameter, while the other was manufactured by Siemens (tpye SRD 00512Z) having a chipsize of only 40 μm across. One has to bear this in mind, when their behaviour is compared. Figure 4 and 5 show the result obtained. All the measurements were taken at a temperature of 10 K. The Hamamatsu diode, operated at a geiger voltage of 3 volts above break down allows a gate width of roughly 200 ns, which is the practical limit for a known good satellite. The far better situation for the Siemens diode of nearly 800 ns at the same level of the geiger voltage has been attributed to smaller size of the active chip area, as mentioned above.

The other important parameter is the detection probability of a laser pulse, again depending on the geiger voltage. Detection probability in this context means the probability of

recording a laser pulse instead of a noise event. The intensity of the pulser signal was high enough so that it can be disregarded in this context. The result of these measurements are shown in figures 6 and 7. In both cases there is a roughly 60 % chance of detecting the signal instead of recording a noise event, when the gate voltage is set to 3 V. This is far from optimum performance for ranging applications but nonetheless it demonstrates the feasibility of the usage of these detectors. Again these measurements were taken at a temperature of 10 K. The timewalk in dependence of the geiger voltage was analysed in the next set of measurements. Since the observed timewalk was small and not significantly dependent on the applied gate, there are no extra plots given in this paper.

In the next set of experiments the behaviour of the thermal noise with respect to the detector temperature was analysed. The gate voltage was set to 3 V above breakdown for this purpose. Once again the probability of recording a valid pulser signal over a noise event was taken as the parameter of interest. Figures 8 and 9 show the result. For both diodes there is a weak temperature dependence in the detection probability of a laser pulse in the temperature range of 10 K to 50 K. However above this upper limit there is a strong increase in the detection of noise events. Above 100 K there is almost no probability of detecting a laser echo which arrives more than 170 ns after the gate was switched on. Both diagrams show roughly the same behaviour. It would be expected that the noise probability would be dependent upon the chip size. However there are obviously other effects masking such behaviour.

In order to characterise germanium diodes with respect to their spectral sensitivity another set of experiments have been carried out. The parameters temperature (10 K) and voltage above breakdown (3 V) were held constant, while measurements were taken at different settings of neutral density filters, which were placed in front of the detector. Figures 10 and 11 show the result. In this case one can see that the Hamamatsu detector is obviously superior to the Siemens diode. This again is attributed to the larger chip of the B2834-01. Unfortunately it is not possible to obtain the sensitivity of the germanium diode for the application in the infrared wavelength domain, since the pulser is operating on $\lambda = 0.776\mu m$. On the other hand both detectors were treated in the same way, so that their relative difference in sensitivity can be compared. From figure 10 one can see, that at a level of four optical densities the single photon domain is obviously reached. Towards higher optical densities one can find a strict proportional relationship between the number of valid signal recordings and the applied attenuation of the pulse source. The Siemens diode appears to be far less sensitive. It is assumed that this is due to the smaller sensitive area, since the light pulse was not focused onto the detector, but applied as a collimated beam.

The variation of timewalk of a detector with respect to the receive signal intensity is one of the important parameters, which has also been investigated. In figure 12 and 13 one can see the respective behaviour of the two diodes, as the signal amplitude is decreased. The measurements yield a timewalk of nearly 1 ns for the diode B2834-01 over 5 magnitudes in intensity, while the detector SRD00512Z shows 200 ps over 3 magnitudes. The rms of the histogram taken over the pulser events is below 90 ps in all cases. When exposed to a high signal level, values of less than 40 ps were obtained. This is caused by a change of the multiplication factor for the avalanche growth process. This parameter is intensity

dependent and this behaviour is well known from the application of silicon avalanche diodes.

4. CONCLUSIONS

At the WLRS in Wettzell a laboratory system has been set up which allows the analysis of sensitive detectors capable of single photon detection. This experiment can be operated completely independent of the routine tracking system. A cryogenic chamber has been added, in order to allow the investigation of the properties of germanium diodes as sensitive detectors in the infrared wavelength domain. The construction of the chamber is such that it can also be operated as part of the WLRS. All relevant parameters for a tracking application were investigated for two different types of germanium diodes, as they became available. Their general properties are close to those of silicon diodes, however the intrinsic noise of the germanium avalanche diodes places additional demands on the tracking experiment. The cryo chamber was found to be completely adequate to meet these requirements. The major differences between the two specimens under test were found with respect to sensitivity and the amount of intrinsic noise. This was attributed to the different size of the semiconductor chip between the two diodes.

5. ACKNOWLEDGEMENTS

The authors would like to thank the WLRS team for assisting in the work presented here.

References

[1] A. W. Lightstone, R. J. McIntyre; "Avalanche Photodiodes for Single Photon Detection", *IEEE Trans. Electron Devices*, **ED-28**, 1210 (1981)

[2] U. Schreiber, K. H. Haufe, J. F. Manging, J. M. Torre and Chr. Veillet; "Operating the APD SP 114 at the LLR Station in Grasse", *Lidar Techniques for Remote Sensing, Chr. Werner, Editor*, Proc. SPIE 2310, **2**, (1994)

[3] I. Prochazka, K. Hamal; "Recent Achievements in Solid State Detector Technology for Laser Ranging", *Proceedings Of 9th International Workshop on Laser Ranging Instrumentation*, Canberra, 1994

[4] U. Schreiber, St. Riepl; "Measuring atmospheric dispersion employing avalanche photo diodes", *Lidar Techniques for Remote Sensing, Chr. Werner, Editor*, Proc. SPIE 2310, **25**, (1994)

[5] Ch. Veillet, E. Bois, J. E. Chabaudie, C. Dumoulin, D. Feraudy, M. Glentzlin, J. F. Mangin, J. PhamVan, J. M. Torre; "The Cerga Lunar Laser Ranging Station", *Proceedings Of 7th International Workshop on Laser Ranging Instrumentation*, Matera, 1989

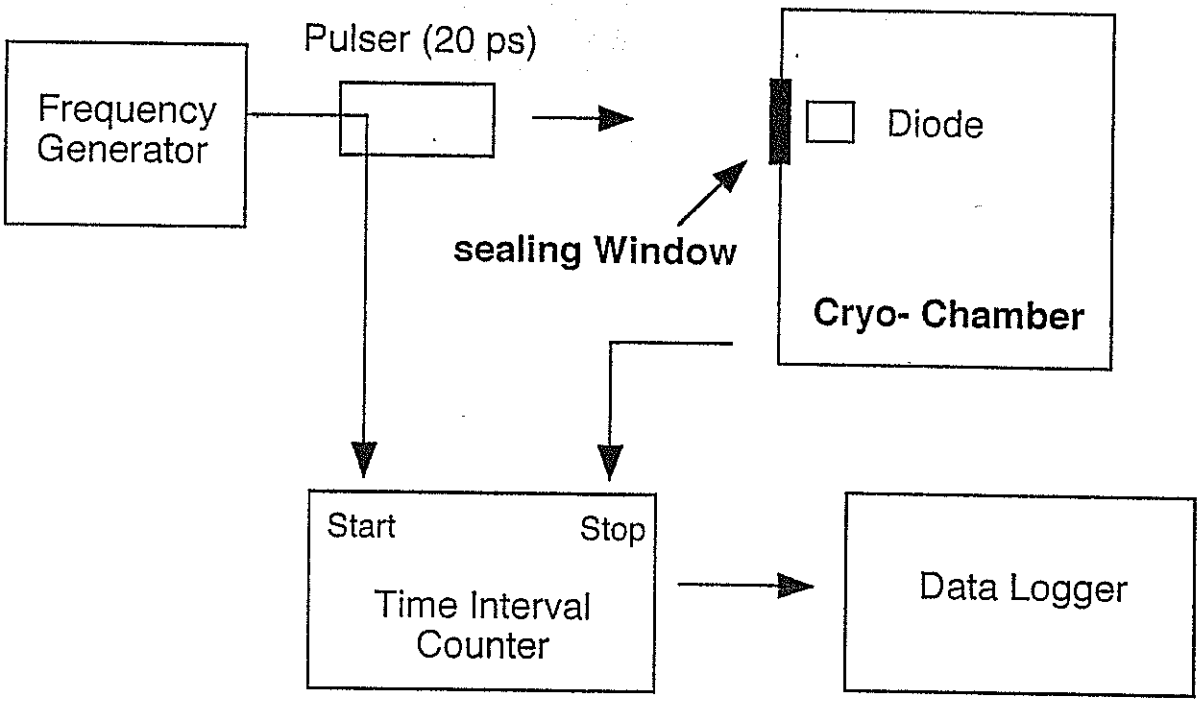

Figure 1: The block diagram of the experimental setup. The diode was placed inside the cryogenic chamber, while the signal source and the time interval counter were set up for an indoor ranging experiment

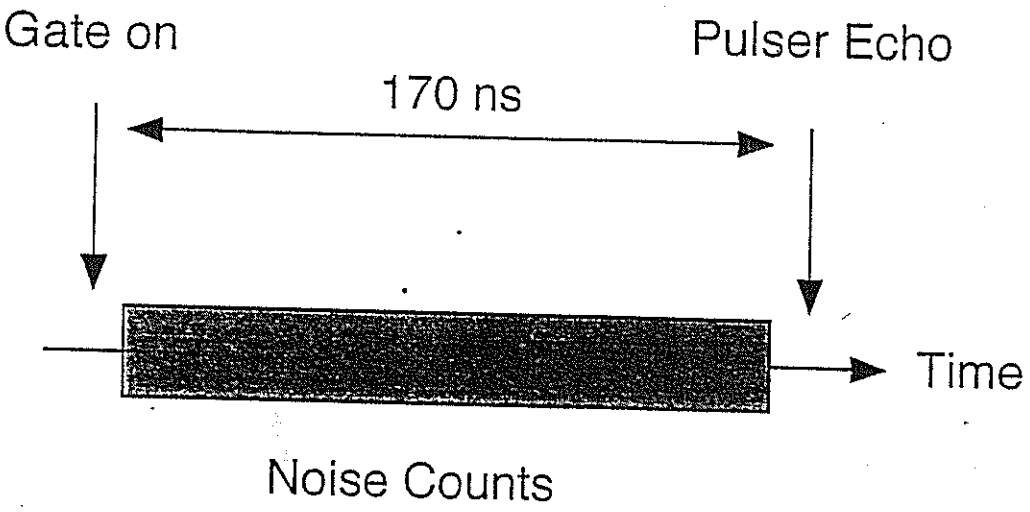

Figure 2: The simplified timing diagram of the discribed experiment. A period of 170 ps was set before the laser pulse hits the diode. This allows the effect of cooling on the diode to be studied

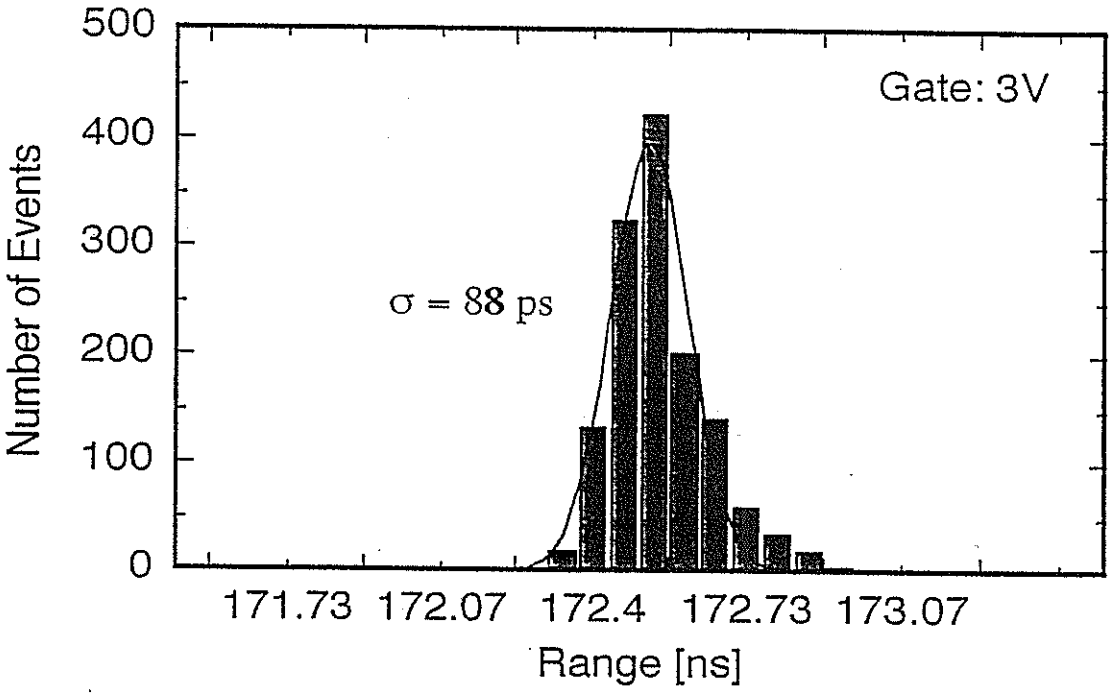

Figure 3: Histogram of a test ranging run for a typical germanium avalanche diode. The obtained overall rms was 88 ps. The detection rate is close to 25%

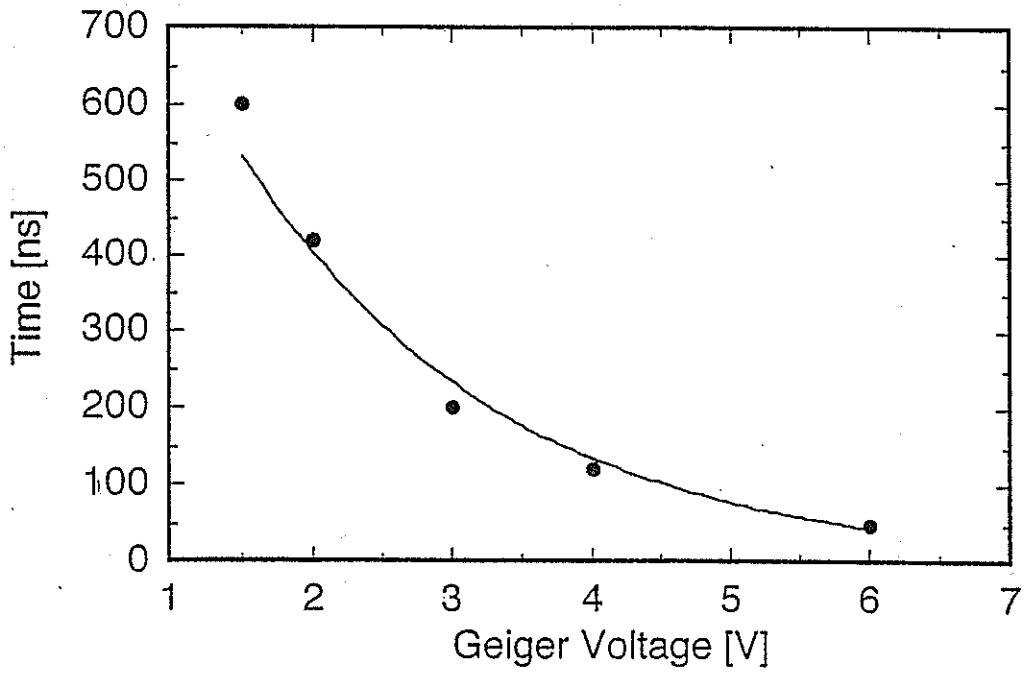

Figure 4: The average time between "Gate On" and a noise "Breakdown" over the Geiger pulse voltage for the diode B2834-01. A geiger voltage of 3 V seems to be the highest reasonable value. The temperature is 10 K

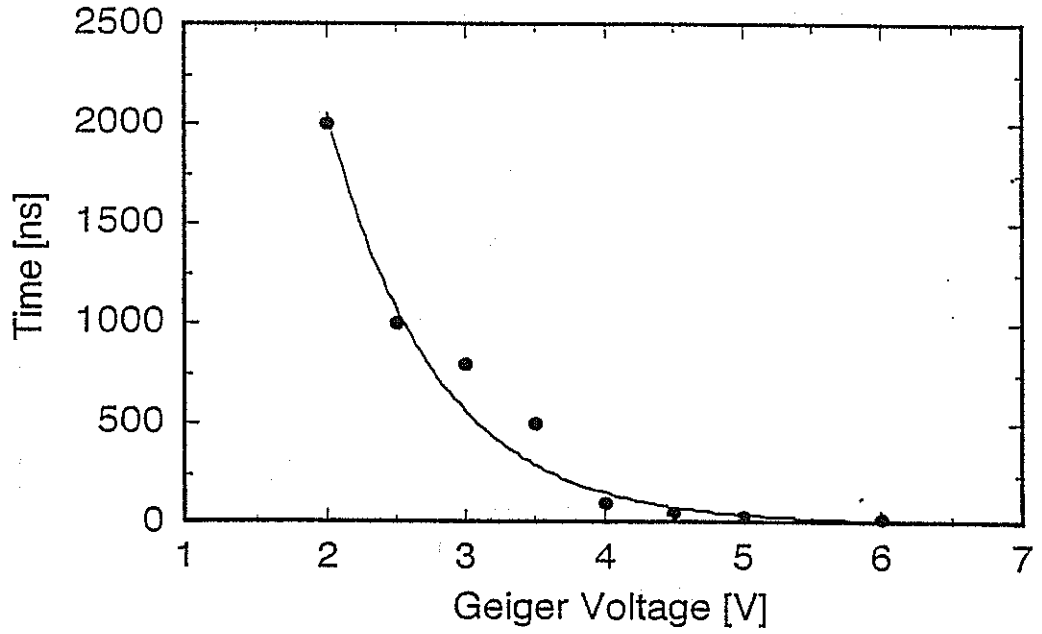

Figure 5: The average time between "Gate On" and a noise "Breakdown" over the Geiger pulse voltage for the diode SRD 00512Z. A geiger voltage of 3 V seems to be a good operating value. The temperature is 10 K

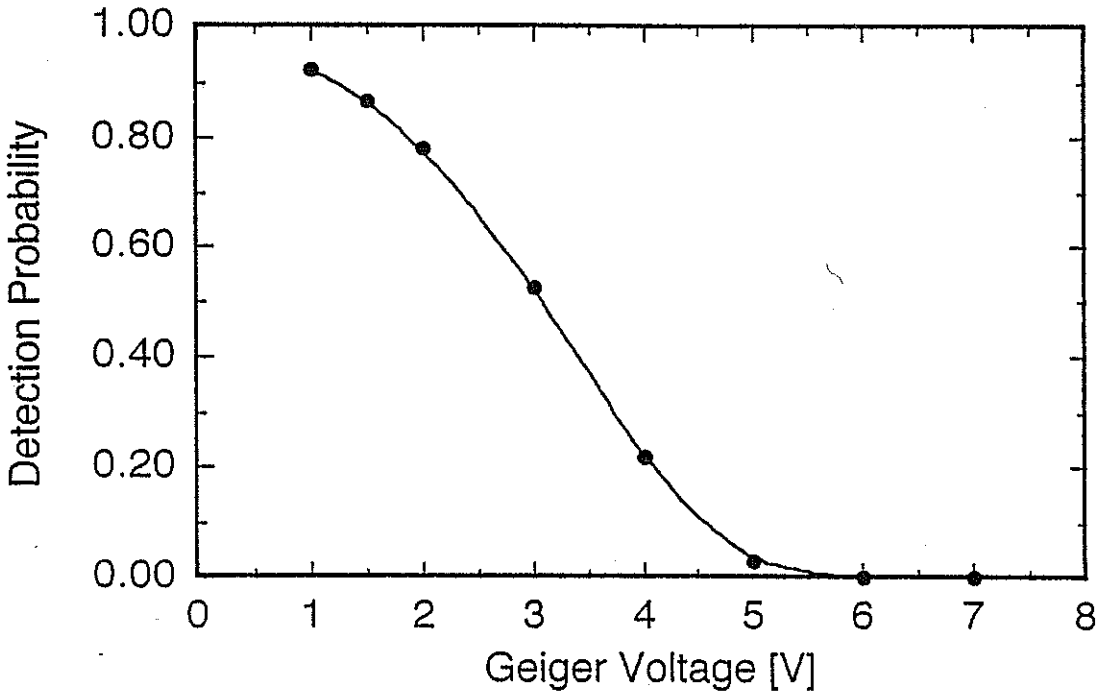

Figure 6: The probability of recording a signal instead of a noise event over the Geiger pulse voltage for the diode B2834-01. A geiger voltage of 3 V seems to be a good operating value. The temperature is 10 K

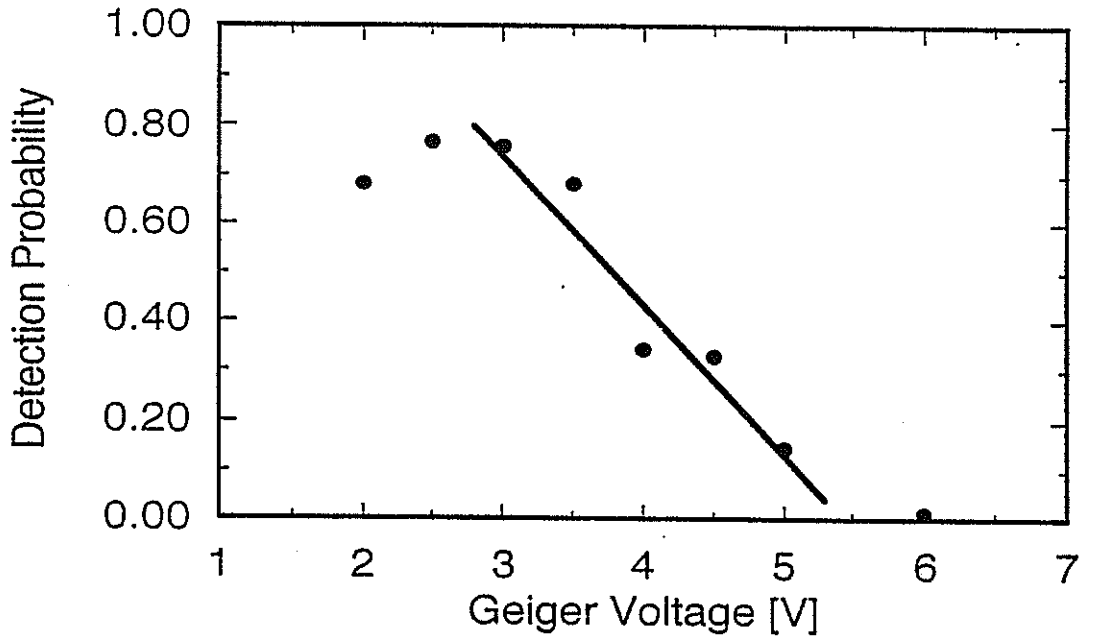

Figure 7: The probability of recording a signal instead of a noise event over the Geiger pulse voltage for the diode SRD 00512Z. A geiger voltage of 3 V seems to be a good operating value. The temperature is 10 K

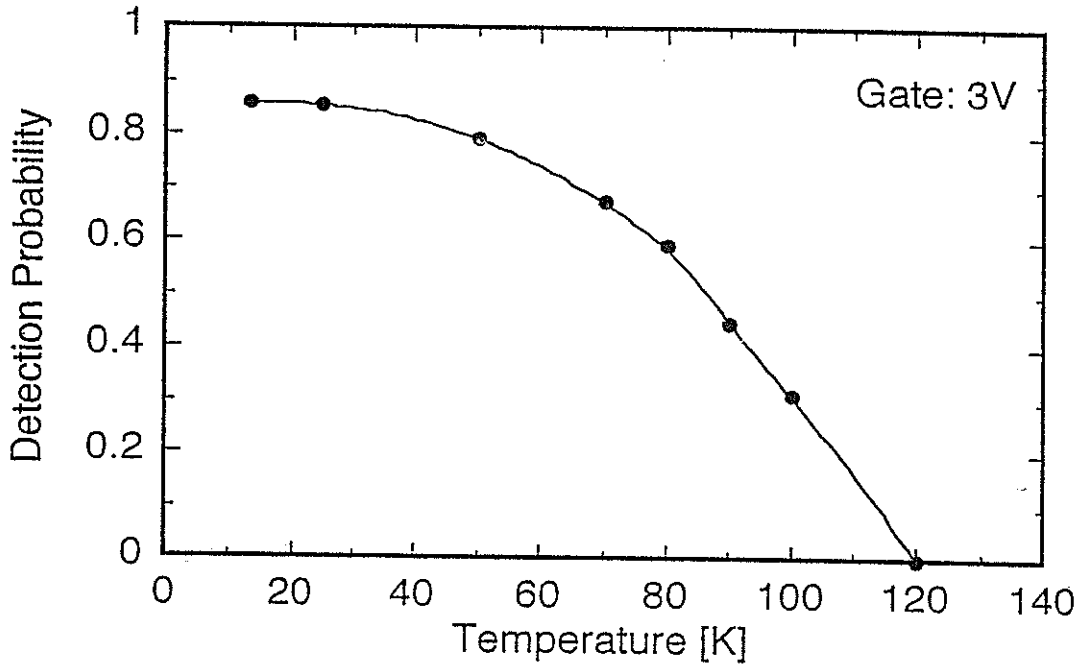

Figure 8: The probability of recording a signal instead of a noise event over the detector temperature for the diode B2834-01. A geiger voltage of 3 V was applied. Above 50 K there is a strong increase of the noise

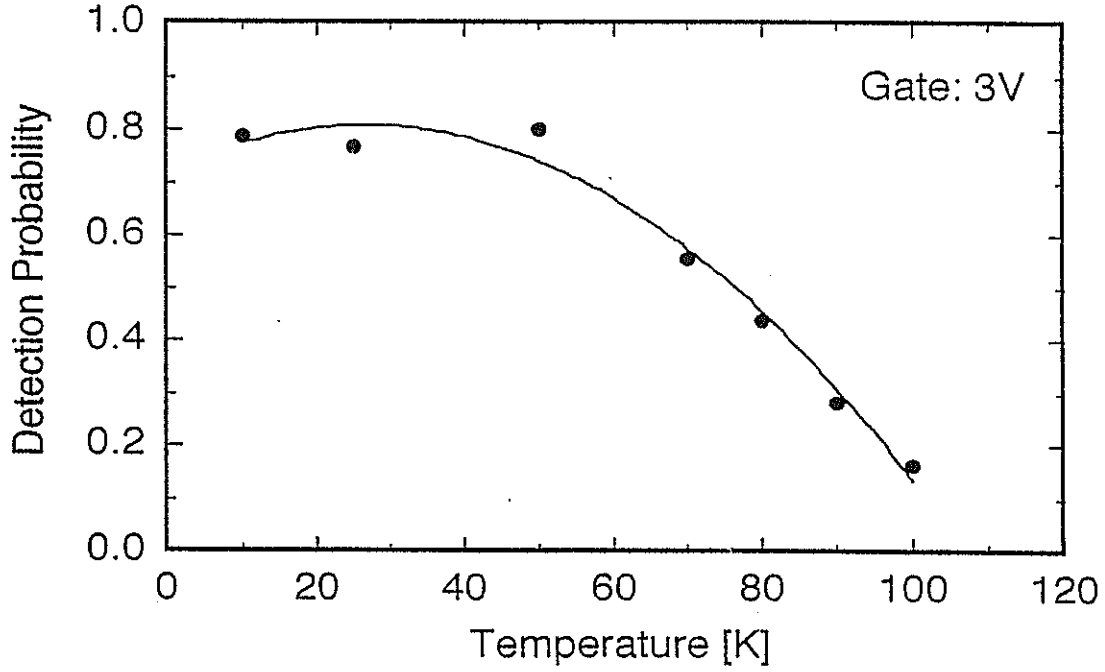

Figure 9: The probability of recording a signal insted of a noise event over the detector temperature for the diode SRD 00512Z. A geiger voltage of 3 V was applied. Above 50 K there is a strong increase of the noise

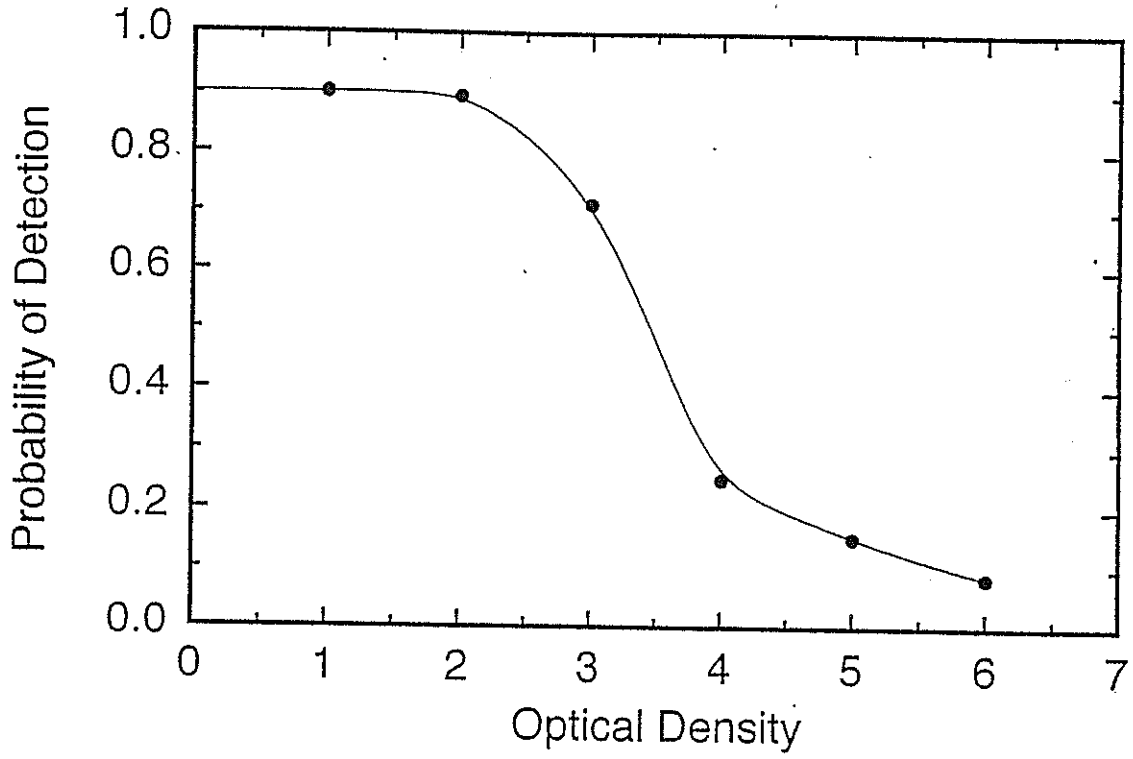

Figure 10: The spectral sensitivity of the diode B2834-01 at $\lambda = 0.776\mu m$. A geiger voltage of 3 V and a temperature of 10 K was applied to the detector

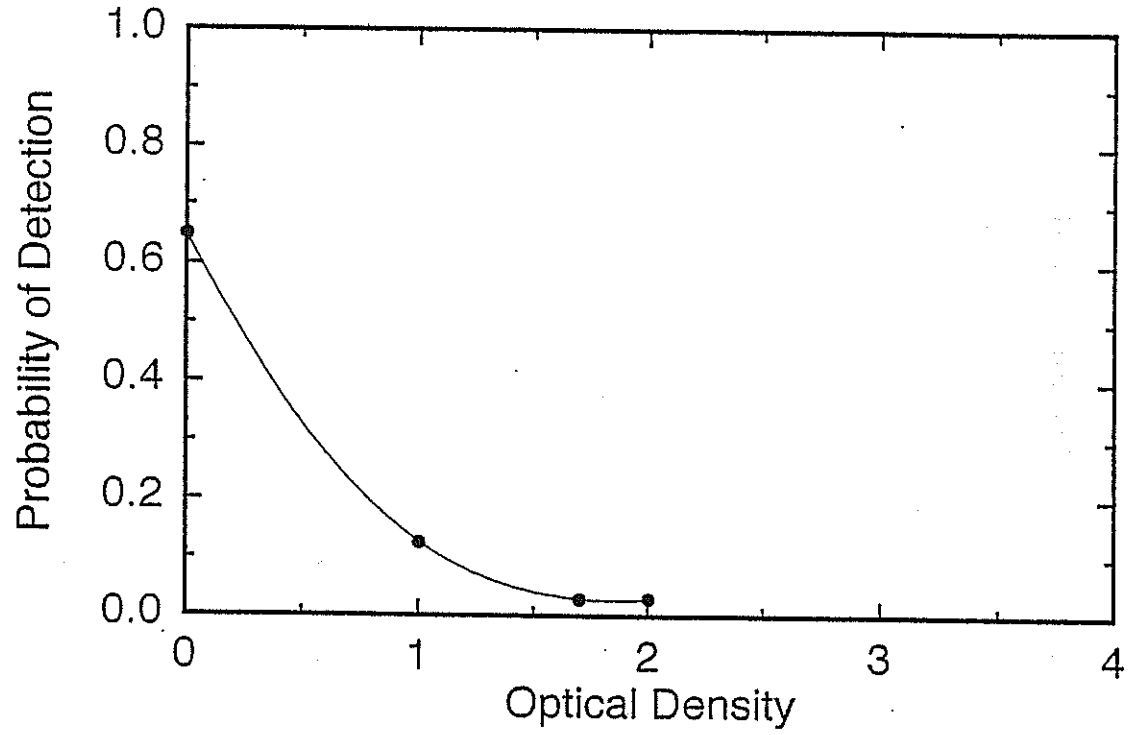

Figure 11: The spectral sensitivity of the diode SRD 00512Z at $\lambda = 0.776\mu m$. A geiger voltage of 3 V and a temperature of 10 K was applied to the detector

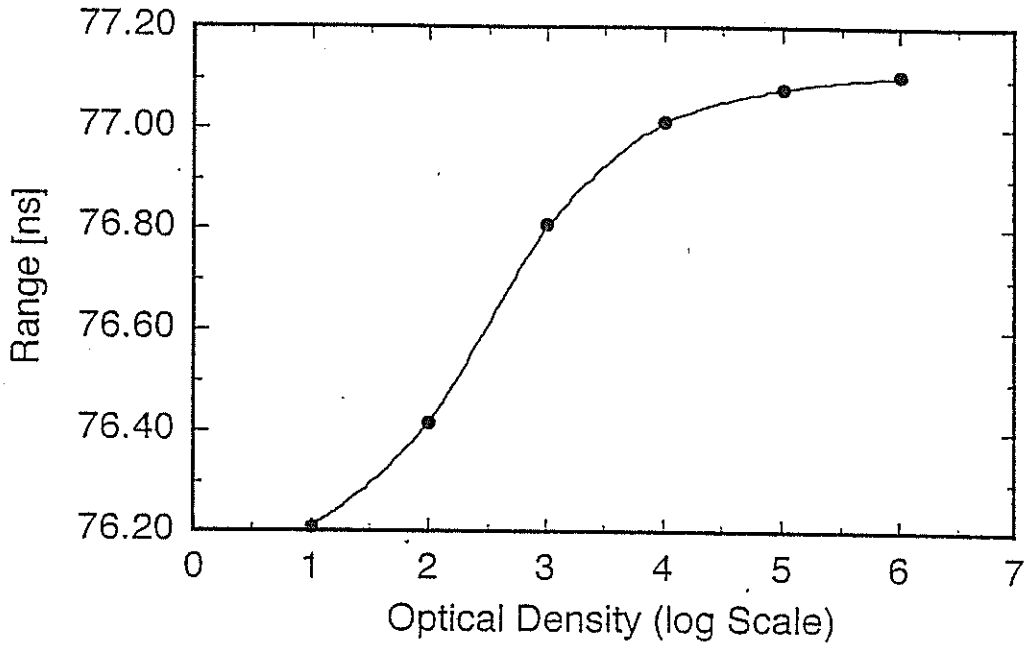

Figure 12: The experienced timewalk of the diode B2834-01 under various signal intensities. A geiger voltage of 3 V and a temperature of 10 K was applied to the detector

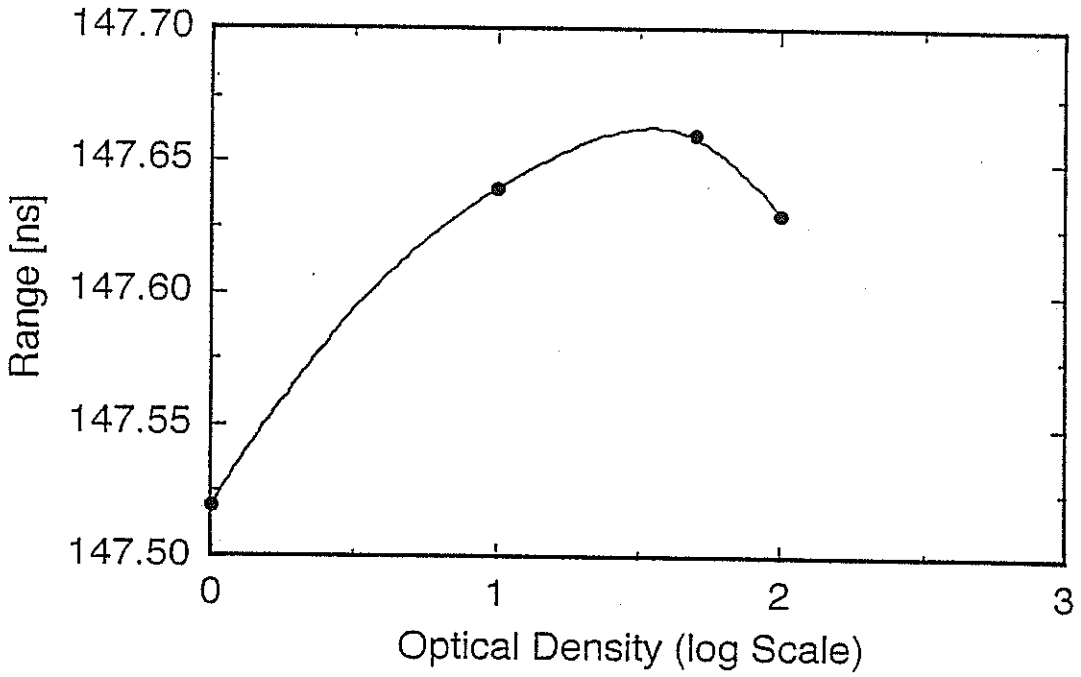

Figure 13: The experienced timewalk of the diode SRD 00512Z under various signal intensities. A geiger voltage of 3 V and a temperature of 10 K was applied to the detector

Effects of Common Gating Schemes on SPAD/APD Bias.

Suzanne Jackson
Orroral Observatory
Australian Surveying & Land Information Group.
Phone: +61 6 235 7111. Fax: +61 6 235 7103. Email: suzyj@auslig.gov.au

Abstract:

Through our use of APD detectors at single-photon level over the last two years, we have noticed that different gating schemes in use in the SLR community can contribute significant biases to the data received. Our use of extremely short range calibrations, necessitating narrow gate pulses for calibration data has highlighted many of the traps in APD/SPAD use. This paper discusses some of the contributors to these biases, and how best to avoid them.

1. Introduction:

Considerable effort has been put into gaining a thorough understanding of the signal strength dependent time walk inherent to all APDs [1, 2]. It is now common practice to ensure that APDs are run in a single photon per return regime, or else more recently to gather data on the number of received photons using either a separate MCP or avalanche rise time so that this walk may be compensated out[3].

Less well known, it seems, is the effect that asymmetric calibration/satellite gates have on time bias.

Sharing a common aperture for transmit and receive has many advantages, such as improved transmit beam collimation and most effective use of available aperture. This technique also allows real-time calibration data to be gathered simply by placing a retro-reflector within the telescope tube. Unfortunately on the Orroral telescope[4], the calibration retro-reflector is not the only source of receive energy. The use of refractive optics in the common transmit/receive path, with their associated on-axis reflections, provides a number of other signal sources, any of which will trigger a gated APD.

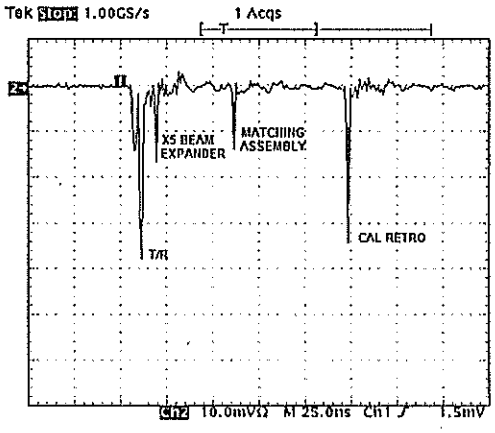

Figure 1: OTDR Plot of Orroral Common T/R Path.

The waveform in Figure 1 illustrates the time and amplitude relationship of return sources from telescope refractive optics. The waveform was captured by monitoring the MCP output with a 1GS/s digital oscilloscope. Of particular concern is the reflection from the Coudé matching

optics. This signal source is only three times weaker than the calibration retros, yet occurs just 65nsec before.

In order to ensure that only calibration returns trigger the APD, it is necessary to position the gate leading edge such that the APD is biased on in the interval between the matching assembly returns and the real calibration returns.

The necessary gate asymmetry has been found to introduce range biases, due to instabilities in the HV bias voltage at the start of the gate. Several gating schemes have thus been trialed at Orroral, in order to improve the gate switching speed, whilst ensuring stable bias for a reasonable gate period without increasing APD dissipation.

2. Relationship between APD voltage and response time:

Examination of the physics of geiger mode operation makes it clear that the response time of an APD is dependent on the excess bias voltage above the diodes breakdown voltage. As the electric field in the depletion layer becomes stronger with increased bias, avalanche events have more energy, and thus liberate more charge carriers in a given time. The avalanche spreads through the active area faster, leading to a faster time response at higher bias voltage, with correspondingly reduced jitter.

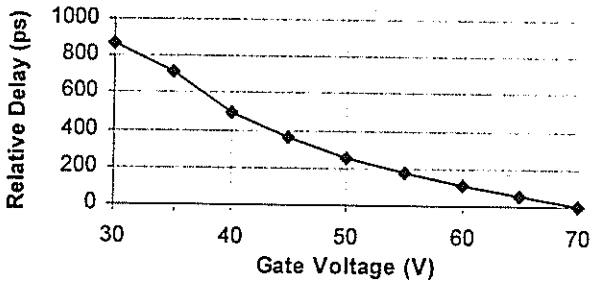

Figure 2: Relationship Between SSO-230 Gate Voltage and Delay.

The plot of delay versus gate voltage shown in Figure 2 was taken with the current Orroral APD, a Silicon Sensor SSO-230, cooled to -40°C with the HV bias set to -135V, 10V below breakdown. A gated passive quenching circuit was employed, with the gate leading edge positioned 200ns before the returns. At a typical operating gate voltage of 50V, there is a 22ps/V dependence between gate voltage and delay.

This figure illustrates that it is crucial to ensure that the bias voltage is the same for both calibration returns and satellite returns. On a system utilising real-time calibration data, where calibration and satellite gates are necessarily asymmetric, the bias driver plays an important role in ensuring that bias levels are consistent for the duration of the gate.

It should also be noted that varying the temperature of the diode has a corresponding effect on response time, as the breakdown voltage changes with temperature. Given a coefficient for breakdown of 600mV/°C [5], we get a variation of 13ps/°C at 50V gate. It is thus also important to ensure that the temperature of the APD is the same for calibration returns and satellite returns, just as with bias voltage. Indeed, in a system where calibration returns are gathered every shot, the possibility of range dependent time bias, due to the diode being cooled for a longer period on long ranges, exists where the diode cooling has a small time constant. This effect is minimised by ensuring that an avalanche event causes minimal dissipation within the APD.

3. Common gating schemes:

Numerous circuits have been devised to allow operation of APDs in the geiger mode. They are presented in order of complexity.

3.1 Ungated passively quenched.

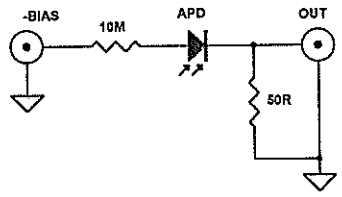

Figure 3: Ungated Passively Quenched Circuit.

The biasing technique depicted in Figure 3 is common when APDs are used for simple photon counting applications.

When an avalanche event occurs, current is drawn from the bias supply, through the 10M series resistor. The bias voltage on the APD collapses, quenching the avalanche. The quenching time here is dependant on the time constant of the diode capacitance (typically a few pF) and the series resistance. Unfortunately, there is a corresponding reset time, after the avalanche has been quenched.

The likelihood of receiving a photon within the quench/reset time is quite high for all but the most noise-free APDs. The bias is not constant during this time, so the sensitivity and response speed is very unpredictable, making this type of bias circuit impractical for satellite ranging.

3.2 Gated passively quenched.

In order to make the passively quenched design work with noisy APDs, it is necessary to gate the device. This is usually done by reducing the bias voltage to less than the APD breakdown voltage, and capacitively coupling a low impedance, fast gate pulse to bring the voltage across the APD (the algebraic sum of the bias supply and the gate supply) to above the breakdown voltage. Avalanche quenching still occurs due to the collapse of the high impedance bias input, as for the ungated passively quenched circuit, but now the gate coupling capacitor adds to the diode capacitance to increase the quenching time constant (see Figure 4).

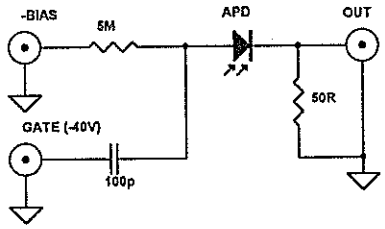

Figure 4: Gated Passively Quenched Circuit.

The advantage with this circuit over the ungated one is that we can be reasonably sure that the APD voltage will remain constant for a time after the gate pulse is applied. The important considerations here are the gate leading edge time, as this dictates the time between the start of the gate and the time when the APD voltage is stable, and also the fact that the voltage will 'bleed off' over the gate time through the resistor to the bias supply. For the circuit in Figure 4, with the bias supply set to 10V below the APD breakdown, and a 20us 50V gate, the reduction in APD voltage is given by:

$$\Delta V = V(1-e^{-1/RC}) = 50\left(1-e^{-20E^{-6}/500E^{-6}}\right) = 2.0V$$

Referring again to figure 2, this bias change represents a 43ps shift in time delay. Increasing the value of the gate coupling capacitor reduces this effect, but at the expense of increased dissipation in the APD due to a corresponding increase in the quench time constant, and increased gate ramp up time. At Orroral, we are currently using a compromise of 220pF gate coupling capacitor, and 10M HV series resistance, for a delay change of 5ps over a 10us 50V gate.

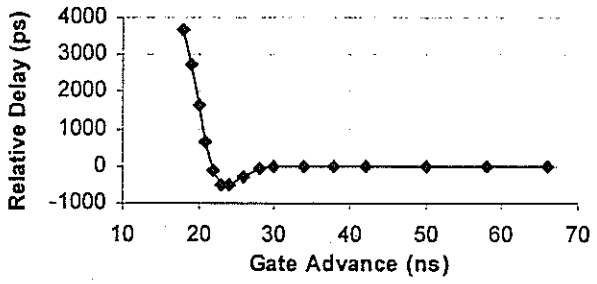

Figure 5: Delay vs Gate Advance for Gated Passively Quenched SSO-230

Figure 5 shows the actual measured bias with the gate edge placed close to the return. The gate on time is extremely short, being only 30ns or so. No returns were evident for the first 18ns. The bias has settled down (within 10ps) after 40ns, and remains stable all the way to 5us (the limit for ground ranging). This graph was created by firing at the ground target (1.1Km distant), using a HP5359A time synthesiser to generate a gate from the start detector output.

An important point to note with this circuit (and the actively quenched circuits) is that a portion of the change in bias at the APD will be capacitively coupled to the output. It is important to disable the output comparator or discriminator during the gate switch-on period, in order to stop the circuit from triggering on the leading edge of the gate.

To summarise, long gates must be avoided, even if the detector has a low enough noise count. There is a temptation to reduce the value of the HV series resistor, but this decreases the time constant of the bias discharge. Increasing the value of the gate coupling capacitor has a detrimental effect on APD dissipation, due to increased quenching time constant. The gate must be active a reasonable time before the return (say 50ns), to allow the bias to settle.

3.3 Actively quenched with 'Class A' bias driver.

To guarantee a constant bias voltage with long gates, whilst minimising APD dissipation, it is advantageous to actively control the bias voltage with a low impedance driver, as depicted in Figure 6.

Here the APD is driven by a relatively low impedance (10K) directly to the final bias voltage. In order to quench the avalanche, a transistor is employed to sink current from the bias source, thus reducing the APD voltage below breakdown. The quenching transistor is driven by the output of a flip flop, which is set by the avalanche event (detected by a fast comparator) and reset by the gate edge. By utilising a fast comparator, flip-flop, and quenching transistor, we are able to quench the avalanche in well under 100ns, limiting APD dissipation to acceptable levels.

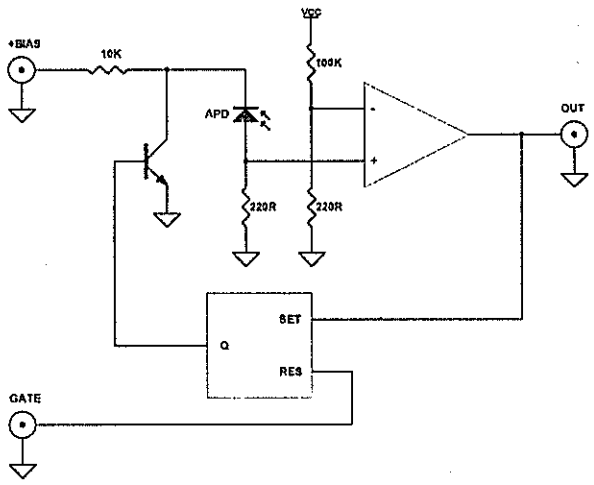

Figure 6: Actively Quenched 'Class A' Circuit.

Although this circuit appears significantly more complex than the passively quenched versions, the presence of the avalanche comparator on-board negates the need for an external discriminator.

This circuit exacerbates the problem with slow ramp up of APD bias at the start of the gate because of the 10K resistor sourcing current into the APD and quenching transistor capacitance. Reducing the value of the source resistor increases power dissipation in the quenching circuitry, and also increases the power requirements placed on the bias supply.

In summary, charging time constant is dependent on diode/transistor capacitance and bias series resistance. Decreasing charging resistance improves gate on time at the expense of extra dissipation in the quenching transistor and bias supply. Bias voltage is constant until the detector is triggered, however, so noise count is the only limiting factor on gate duration with this circuit. APD dissipation is dependent on the propagation delay of the comparator, flip-flop, and driving transistor.

3.4 Actively quenched with 'Class A-B' bias driver.

The slow ramp up times experienced by the simple class-A bias driver may be improved by adding a buffer stage to the driver, so that it can source current as well.

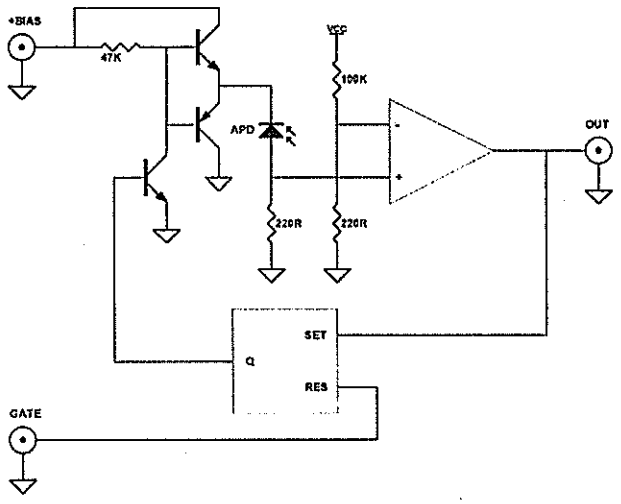

Figure 7: Actively Quenched 'Class A-B' Circuit.

Gate on time is reduced to a few tens of nanoseconds (dependant on the quenching circuit transistor speed and the quenching voltage difference), as with the passively quenched circuit. Bias current requirements are reduced over that of the class-A circuit. Note however that gate on times will not be as fast as for the passively quenched circuit, as bipolar transistor switch-off times are longer than switch-on times.

The APD bias voltage is now driven rapidly and accurately to the full supplied bias, and maintained until an avalanche event triggers the quenching circuit.

To summarise, Charging time constant is dependent on speed of bias driving transistors, diode capacitance, and decoupling. The power supply for the bias need only supply a few milliamps of current. As with the gated passive design, it is still important to activate the gate (say) 100ns or so before the return is expected, to ensure that the bias voltage has stabilised. After this point, bias voltage is constant until the detector is triggered. As with the class A circuit, APD dissipation is dependent on the propagation delay of the comparator, flip-flop, and bias driver transistors.

4. Conclusion:

There are numerous issues affecting the performance of APD/SPAD photon detectors when used for satellite laser ranging, beyond the simple multi-photon timewalk.

Gating circuitry, in particular the type of gating circuit used and the time relationship between the gate edge and the received photon, plays a considerable role in determining the overall accuracy of SLR measurements made with APD/SPAD detectors. Improper gating can contribute centimetre level errors to otherwise good data. It is of critical importance to ensure that calibration and satellite data are captured under identical conditions, in terms of receive energy, bias voltage, and temperature.

When faced with other constraints, such as the need to tightly gate calibration return sources on the Orroral telescope, the gating circuit must be carefully optimised to avoid biases.

5. Acknowledgment:

The author would like to thank Dr Ulrich Schreiber, of Satellitenbachtungstation Wettzell for supplying the SSO-230 APD, as well as device data and considerable assistance in setup.

6. References:

1. Appleby, G. Gibbs, P. "Monitoring Potential Range Biases in Single Photon SLR Systems", Proc. Ninth International Workshop on Laser Ranging Instrumentation, Canberra, Australia, November 1994.

2. Schreiber, U. Maier, W. Haufe, K. H. and Kriegel, B. "Properties of Avalanche Photo Diodes", Proc. Ninth International Workshop on Laser Ranging Instrumentation, Canberra, Australia, November 1994.

3. Greene, B. Private communications, 1996.

4. Luck, J. McK. "Performance of the Upgraded Orroral Laser Ranging System", Proc. Eighth International Workshop on Laser Ranging Instrumentation, Annapolis, USA, May 1994.

5. Product Datasheet, SSO-AD230H-TO8PELT, Silicon Sensor GmbH Berlin.

Lsaer Technology Development

Cr:LiSAF / Ti:Sapphire based solid state Laser System

for Two Color Satellite Laser Ranging

Peter Sperber, Armin Böer
Institut für Angewandte Geodäsie
Fundamentalstation Wettzell
D-93444 Kötzting
Germany

Eugen Pop
Astronomical Institute
University Berne
Sidlerstr. 5
CH-3012 Berne
Switzerland

Frederic Estable, Luc Vigroux
B.M. Industries
CE 2901
F-91029 Evry
France

Franck Falcoz
Institut d'Optique
Univ. Paris Sud
Cedex BP 147
F-91403 Orsay Cedex
France

Abstract: This paper is reporting on a diode pumped ps-Cr:LiSAF laser seeding a Ti:Sapphire regenerative and multipass amplifier.

This system produces pulses with 20 - 100 ps with an energy of about 100 mJ at 846/847 nm, combining the optimum wavelength for two color satellite ranging with the transmission of the atmosphere and the detection probability of high accuracy single photon detectors.

1. Introduction

During the last years Satellite Laser Ranging (SLR) using picosecond Nd:YAG Lasers achieved an accuracy of better than one cm. At this level of accuracy more emphasis has to be placed on the influence of satellite geometry and the atmospheric dispersion, causing errors up to a few cm /1,2,3/. The control and refinement of these models can be done with multiple wavelength ranging, measuring the Differential Time Interval between two wavelengths /4,5/. Taking into account the difference in the refractive index, the atmospheric transmission and the sensitivity of single photon detectors, best results are expected with wavelengths around 425 nm and in the near Infrared.

To fulfill all the requirements for a two color satellite laser ranging system in terms of peak power, pulse width, wavelength and repetition rate an all solid state Laser System based on a diode pumped ps Cr:LiSAF Oscillator and Nd:YAG pumped Ti:Sapphire amplifiers was designed and realized under contracts of B.M. Industries with the University Berne and the Institut für Angewandte Geodäsie.

2. System overview

2.1. Chromium LiSAF

Discovered in 1989, the Chromium:LiSAF crystal consists of a $LiSrAlF_6$ matrix doped with Cr^{3+} ions /6/. Like other solid state crystal, as Titanium Sapphire, this new material exhibits a large band off fluorescence in the near infrared between 800 and 1000 nm (see figure 1). The main advantage of this crystal is its absorption band between 600 and 700 nm (see figure 2) which is overlapping the emission wavelength of GaAlInP red diodes (at 670 nm). The Cr^{3+}:LiSAF is therefore an ideal candidate for tunable all solid state diodepumped lasers.

2.2. Titanium:Sapphire

It consists of a Sapphire matrix (Al_2O_3) doped with Titanium ions Ti^{3+} /6/. Titanium:Sapphire offers a very large band of fluorescence in the near infrared between 650 and 1100 nm (see figure 3). The absorption band is lying from 400 to 600 nm (see figure 4). This allows to pump this crystal with a source like Argon ion laser or Nd:YAG laser.

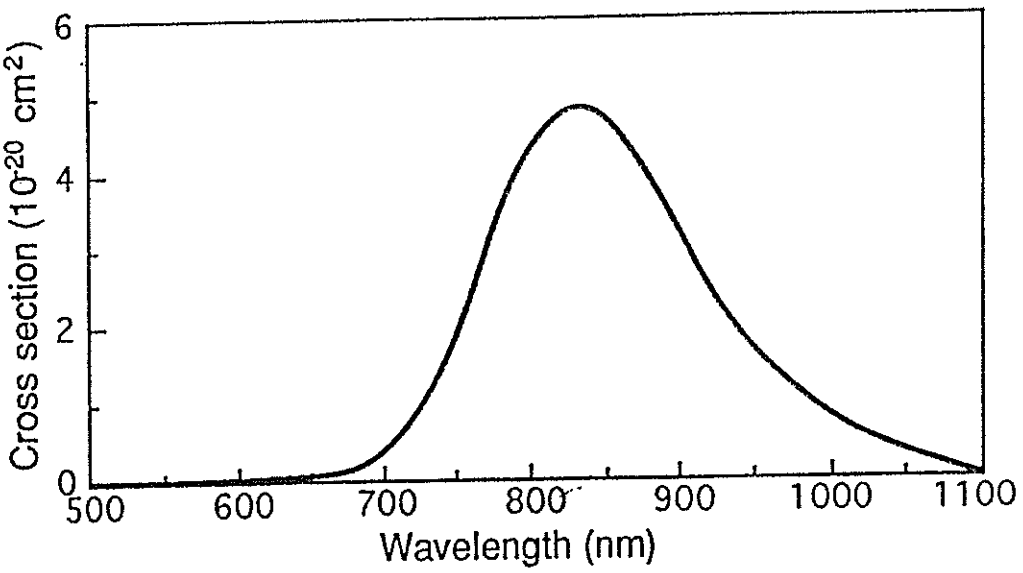

Figure 1: Shape of the emission spectrum of Cr^{3+}:LiSAF on the polarisation parallel to the c-axis

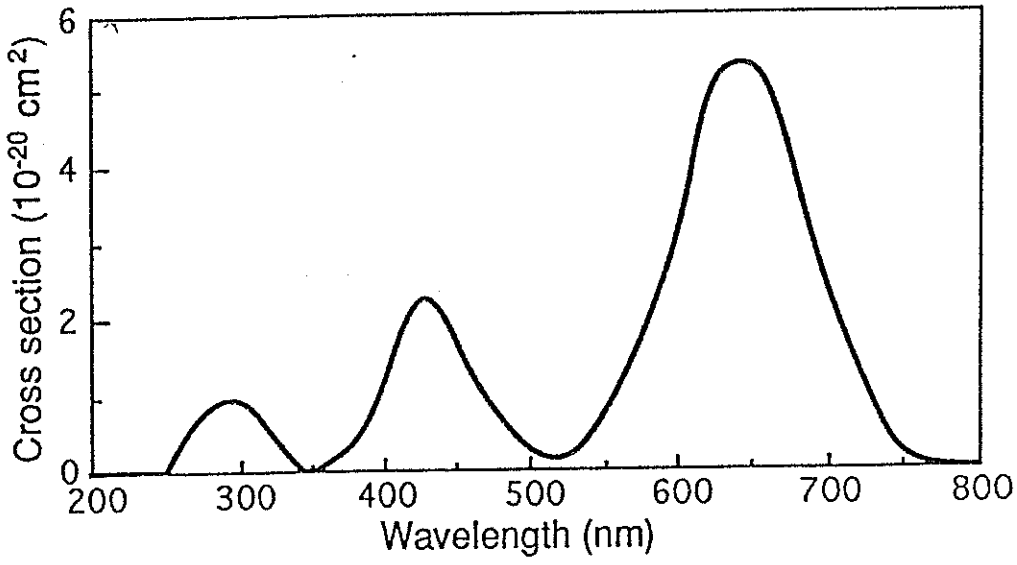

Figure 2: Shape of the absorption spectrum of Cr^{3+}:LiSAF on the polarisation parallel to the c-axis

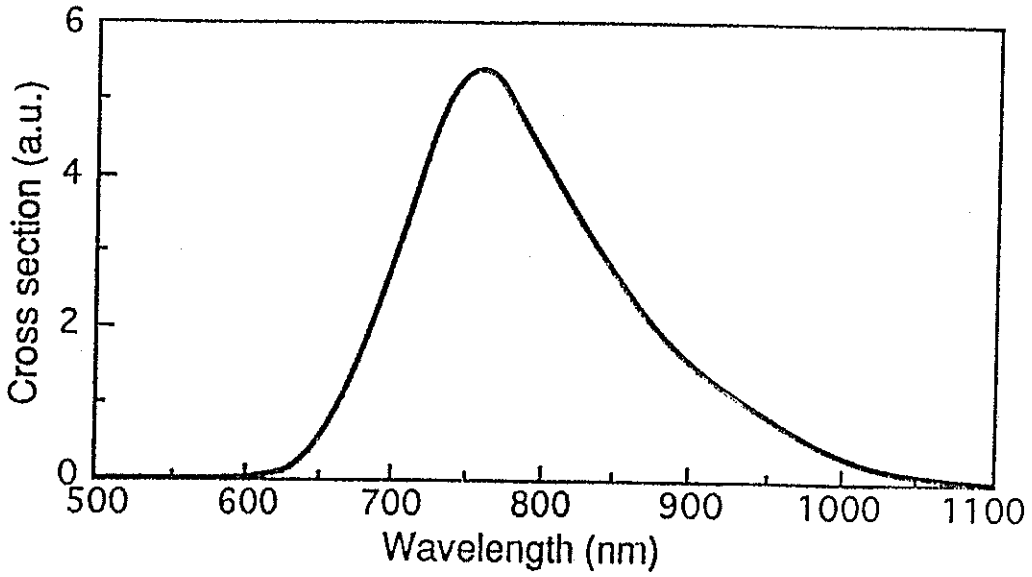

Figure 3: Shape of the emission spectrum of $Ti^{3+}:Al_2O_3$ on the polarisation parallel to the c-axis

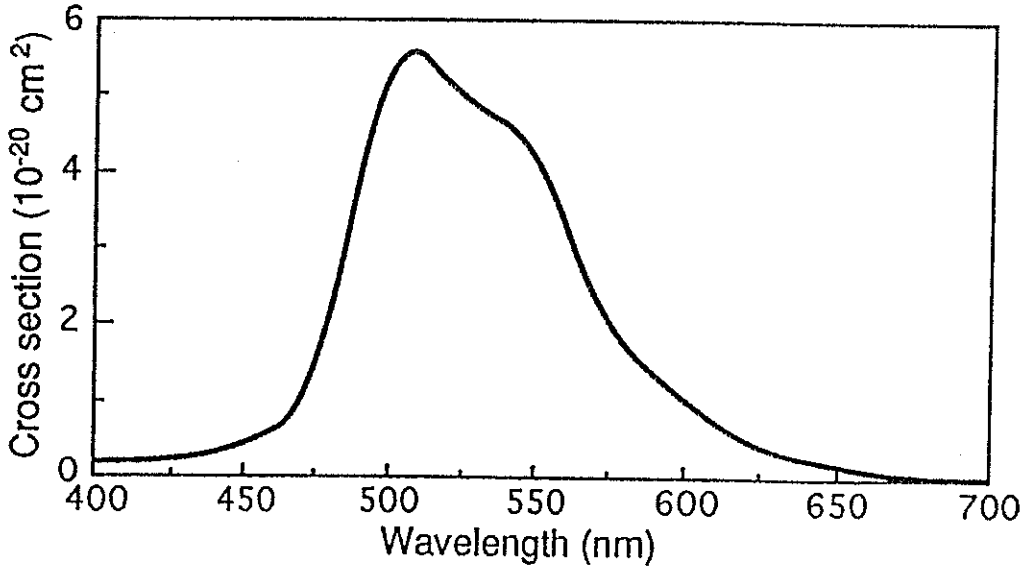

Figure 4: Shape of the absorption spectrum of $Ti^{3+}:Al_2O_3$ on the polarisation parallel to the c-axis

2.3. General Description

The Chromium:LiSAF-Titanium:Sapphire system consists of a Cr:LiSAF oscillator, an optical path selector, a regenerative amplifier, two multipass amplifiers and a second harmonic generator (see the general setup in figure 5). The "pump distributor" is used to split the pump beam in order to supply the different amplifiers.

The oscillator use Chromium:LiSAF as gain medium to generate a picosecond pulse train. The cw mode locking effect is achieved by using an acousto-optic modulator. The output wavelength can be tuned with the intra-cavity birefringent filter.
The optical path selector consists of a Faraday rotator with a half wave plate between two polarisers. This device rotates the polarisation of 90° in one direction, but does not change the polarisation in the other direction. It is used to send the beam from the oscillator to the regenerative amplifier at the first pass, and from the regenerative amplifier to the multipass amplifiers at the second pass.
The regenerative amplifier is used to increase the energy of the pulse to the milliJoule level. It consists of a resonator with Titanium:Sapphire as gain medium. The pulse is seeded and dumped out of the cavity by using a double step Pockels cell device. The repetition rate of the output train is fixed by the repetition rate of the Nd:YAG laser.
Two multipass amplifiers allow to increase the energy of the pulse. Different high reflection mirrors are used to make several passes into the Titanium:Sapphire crystals. The multipass preamplifier is pumped by the same Nd:YAG laser than the regenerative amplifier. The other Nd:YAG output is exclusively used by the main multipass amplifier.
The second harmonic generation is achieved by a non linear crystal with high conversion efficiency. The two wavelengths are separated and recombined by dichroic mirrors.
All the mechanical components are directly set on an optical table provided with covers.

Two similar systems are actually operational at the Astronomical Institute of University Berne and at the Institut für Angewandte Geodäsie in Wettzell. The general specifications of the systems are listed in Table 1. (If the specifications of the two systems are slightly different, the number for the Bernese system is marked by *.

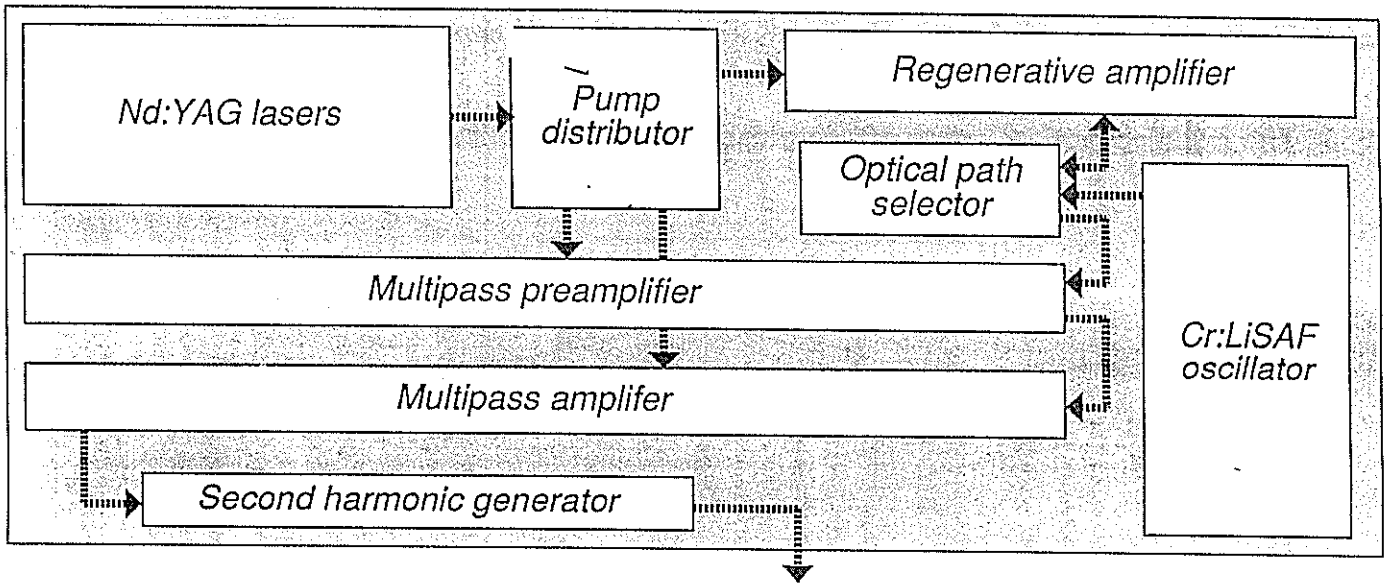

Figure 5: General Setup of the Cr:LiSAF/Ti:Sapphire Laser System

Oscillator	cw-modelocked diode pumped CR:LiSAF
Amplifier	Nd:YAG pumped Ti:Sapphire regenerative amplifier Two Nd:YAG pumped Ti:Sapphire multipass amplifiers
Wavelength	847/846* and 423.5/423* nm
Spectral width	< 0.5 Angström
Pulse duration	50/100* ps
Pulse energy	30/50* mJ
Repetition rate	10 Hz
Spatial mode	TEM 00
Divergence	< 1.5 mrad

Table 1: General system specifications

3. Optical Setup

To get the best flexibility for future improvements, the laser system is setup from several standard parts that can be exchanged independently. This philosophy also makes the adjustment of the whole system quite easy as each part can be adjusted separately, the optical interfaces between the different parts are clearly defined.
The detailed optical setup of the pulse generation is shown in Figure 6.

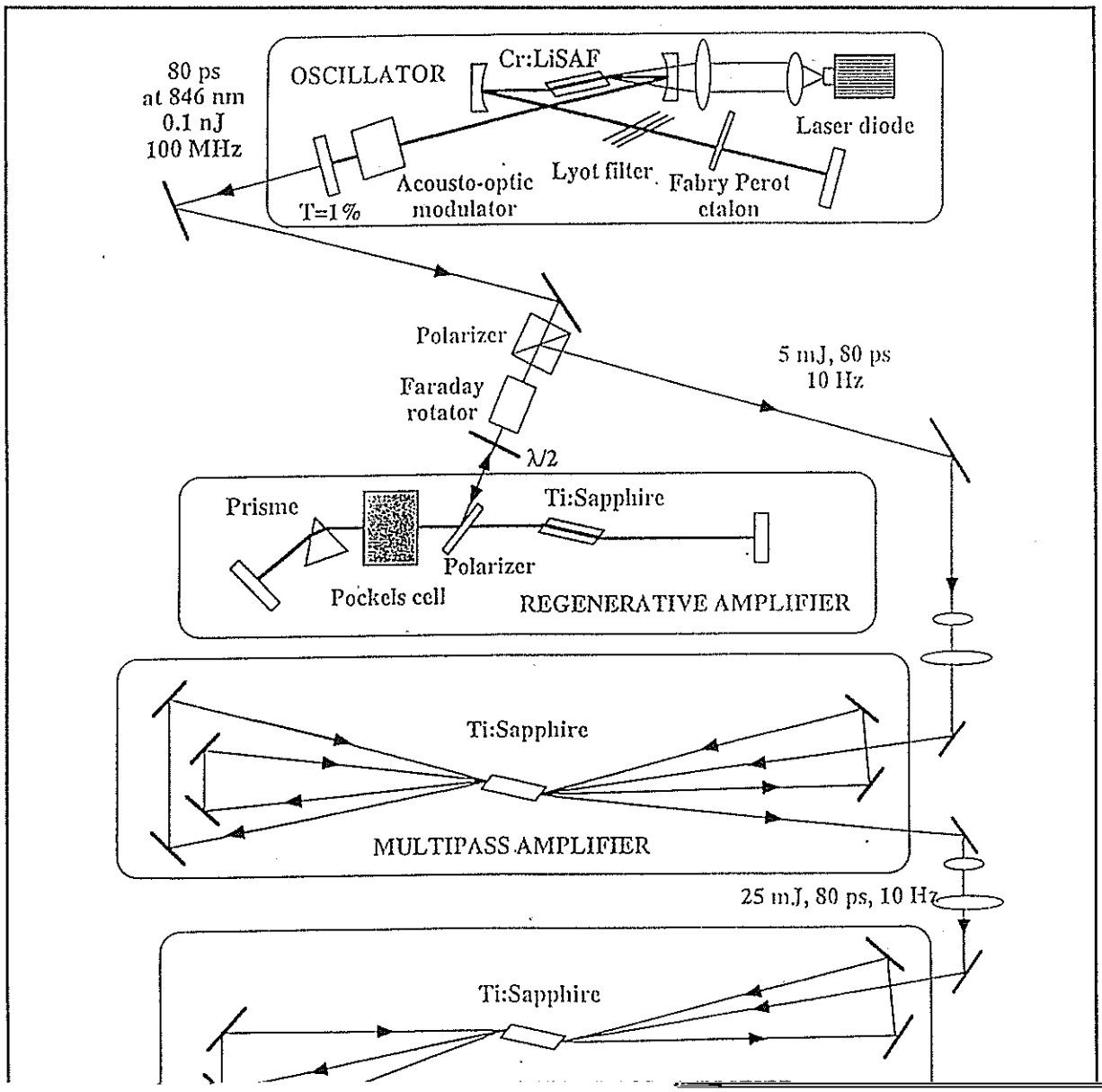

3.1. Cr:LiSAF Oscillator

The oscillator is an actively mode-locked, diodepumped Cr:LiSAF-laser. A single stripe GAALJnP laser diode (400 mw cw at 670 nm) pumps a 5 mm long Brewster cut LiSAF crystal. The cavity consists of four mirrors, two concave mirrors (150 mm radius of curvature) around the crystal, a plane high reflector end mirror and a plane output coupler with 1% transmission between 800 and 900 nm. For the adjustment of the wavelength and the reduction of the spectrum width, a three-plate birefringent filter is used. In this case, pulses as short as 15 ps with a bandwidth of 0.06 nm around 850 nm have been obtained, indicating, that the pulses are transform limited. With different etalons, the pulse width can be adjusted between 50 ps and 200 ps. The average output power is around 15 mW at 100 MHz repetition rate corresponding to an energy per pulse of 0.1 nJ.
The output specifications of the oscillator are summarized in Table 2.

Cr:LiSAF oscillator	
Active medium	Cr^{3+}:LiSAF
Typical output power of oscillator	> 5 mW
Tuning range	820 - 900 nm
Operating wavelength	847/846* nm
Spectral width	< 0.5 Å
Repetition rate	100 MHz
Spatial mode	TEM_{00}
Polarisation	Linear horizontal
Pulse duration	variable 60/100* ps

Table 2: Specifications of the oscillator

3.2. Regenerative amplifier

Through an optical path selector, the pulses from the oscillator are switched into an regenerative Ti:Sapphire amplifier pumped at 10 Hz by a Q-switched frequency-doubled Nd:YAG laser. At moderate pulse durations of 50 ps or higher the peak power in the amplifier is still low enough to avoid the classical Chirped Pulse Amplification (CPA) Technic. Therefor the setup is quite simple. The only additional element needed is a prism in the cavity to reduce the width of the free running spectrum and to match the central wavelength to that of the oscillator. The pump energy is about 50 mJ and the output energy at 846/847 nm is 5 mJ. The detailed specifications are summarized in Table 3.

Regenerative amplifier	
Active medium	Titanium: Sapphire (Ti^{3+}:Al_2O_3)
Tuning range	750 to 850 nm
Operating wavelength	847/846*nm
Repetition rate	10 Hz
Pump energy	40 mJ
Output energy (1)	> 2 mJ at 10 Hz
Spatial mode	TEM_{00}
Beam divergence	< 1.5 mrad
Pulse duration (FWHM) (2)	50 - 100 ps
Output polarisation	Linear vertical

(1) Measured just at the output of the regenerative oscillator. The cavity is then unseeded.
(2) For the seeded cavity only. This specification depends on the oscillator specifications.

Table 3: Specifications of the regenerative amplifier

3.3. Multipass Amplifiers

To increase the pulse energy to the required 60 mJ - 100 mJ two multipass amplifiers are used. The beam is expanded to avoid nonlinear effects in the amplifier crystals. The crystals of the two amplifiers are pumped from both sides to keep the pump fluence under 1.5 J/cm². After the first four pass amplifier an output energy of about 25 mJ is obtained for a pump energy of 150 mJ.

In the second (three pass) amplifier an output energy of 100 mJ is obtained. An independent Nd:YAG laser producing 350 mJ in the green is used to pump this amplifier. The use of two pump lasers gives the possibility to adjust the time delay between the two pump pulses and to optimize the pump arrival time in the second multipass amplifier. So we could take into account the build up time of the gain in the regenerative amplifier. Table 4 show the detailed specifications of the multipass amplifier chain.

Multipass preamplifier	
Active medium	Titanium:Sapphire
tuning range	750 to 850 nm
Operating wavelength	847/846* nm
Repetition rate	10 Hz
Pass number	4
Pump energy	200 mJ
Input energy	> 2 mJ
Output energy	> 25 mJ
Typical average power	> 250 mW at 10 Hz
Spatial mode	Single transverse
Beam divergence	< 1 mrad
Pulse duration (2)	50 - 100 ps
Output polarisation	Linear horizontal
Multipass amplifier	
Active medium	Titanium:Sapphire
Tuning range	750 to 850 nm
Operating wavelength	847/846* nm
Repetition rate	10 Hz
Pass number	3
Pump energy	400 mJ
Input energy	> 25 mJ
Output energy	> 65 mJ
Typical average power	> 650 mW at 10 Hz
Spatial mode	Single transverse
Beam divergence	< 1 mrad
Pulse duration (2)	50 - 100 ps
Output polarisation	Linear horizontal

(2) Specification depends on the oscillator specifications

Table 4: Specifications of the multipass amplifier chain

3.4. Second harmonic generation

The optical setup of the second harmonic generation is shown in Figure 7. A BBO type 1 crystal with a conversion rate of app. 50% generates pulses of 30 mJ at 846/847 nm and 423/423.5 nm. The wavelengths are split and each pulse can be independently attenuated to optimize the relative return level of both wavelengths during ranging. A lens telescope is used to adjust the different divergence of the two beams before recombining the two wavelengths into one beam.

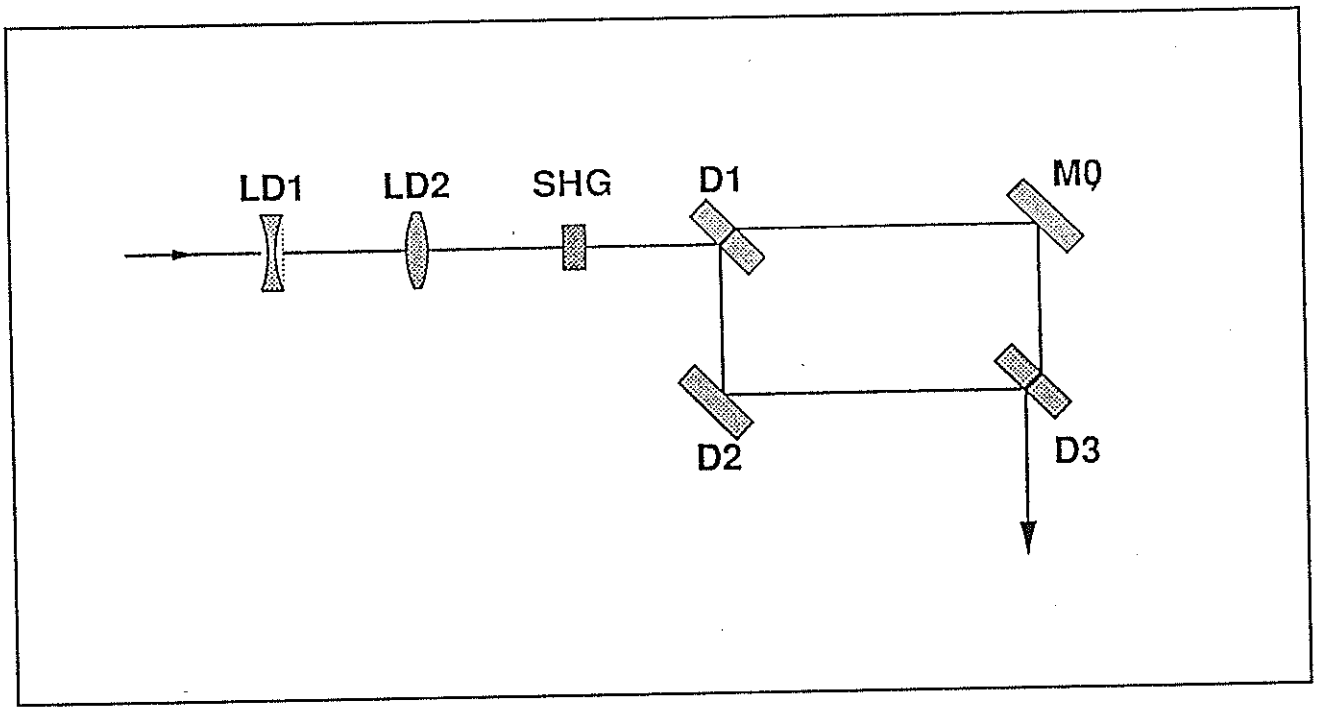

Figure 7: Optical setup of the Second Harmonic Generation

3.5. Pump laser

The Ti:Sapphire amplifier chain is pumped by a q-switched Nd:YAG laser with two independent channels (Figure 8). Channel one is used to pump the regenerative amplifier (50 mJ) and the first multipass amplifier (150 - 200 mJ).

The whole energy of channel two (400 mJ) can be used to pump the second multipass amplifier. With this pump energy an output energy of 100 mJ at 846/847 nm is available. At pulse durations below 100 ps the pump energy and therefor the output energy of the amplifier has to be reduced by slight misalignment of the Quarterwaveplate to prevent damage of the optical components in the multipass amplifier.

The specifications of the pump laser are listed in Table 5.

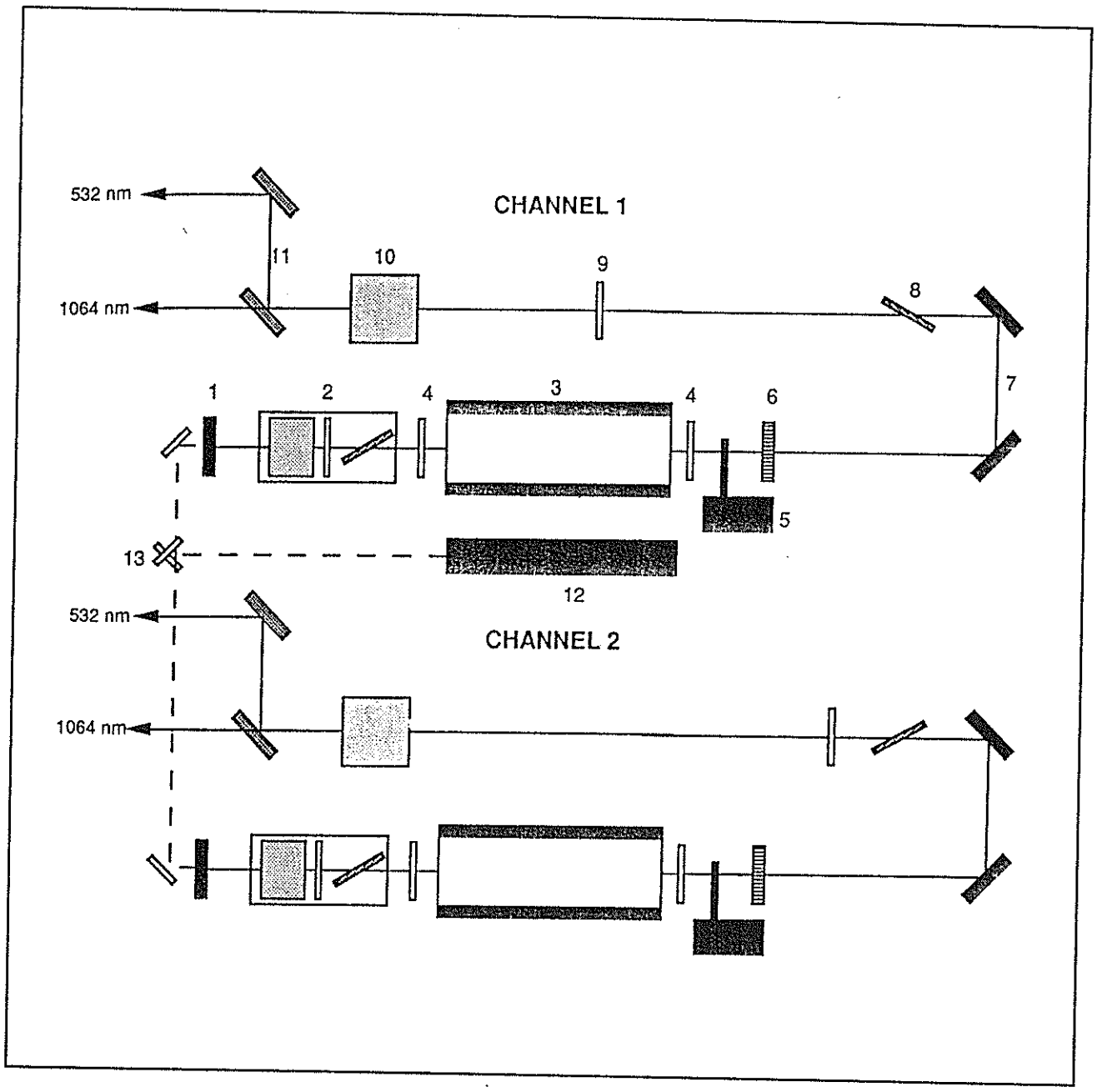

Oscillator 1&2:
1. High reflective mirror; 2. Electro-Optic Q-switch; 3. Pumping structure
4. Compensating quarter-wave plate; 5. Intracavity beam shutter;
6. Graded reflective output coupler; 7. Deflecting mirror

Second Harmonic Generation 1&2:
8. Polariser at 1064 nm; 9. Quarter-wave plate at 1064 nm;
10. Temperature regulated frequency doubler; 11. Dichroic mirror 532 nm

Micellaneous:
12. He-Ne Laser; 13. Silvered mirrors; 14. Control photodiode

Figure 8: Layout of the Nd:YAG Pump Laser

Nd:YAG pump laser	Model: 5000 D.NS 10
Typical output power on channel 1	> 450 mJ @ 1064 nm > 240 mJ @ 532 nm
Typical output power on channel 2	> 850 mJ @ 1064 nm > 400 mJ @ 532 nm
Repetition rate	10 Hz
Pulse duration (FWHM)	~ 7 ns
Beam diameter on channel 1	7 mm
Beam diameter on channel 2	9 mm
Spatial mode	Single transverse
Beam divergence	< 0.5 mrad
Polarisation	Linear vertical
Spectral width	~ 1 cm^{-1}

Table 5: Specification of the pump laser

4. Summary

In this paper we described a very flexible and modular laser system generating ps-pulses at wavelengths which are optimal for two colour satellite laser ranging. The laser is an all solid state system working already very reliable at the two new state-of-the-art SLR Systems in Zimmerwald and Wettzell (TIGO).

References:

/1/ Degnan I. I., Millimetre Accuracy Satellite Laser Ranging: A Review, Geodynamics Series Vol. 25, Contributions of Space Geodesy to Geodynamics, American Geophysical Union, Washington (1993), 125

/2/ Neubert R., An Analytical Model of Satellite Signature Effects, Australian Government Publishing Service, Proceedings of the 9th International Workshop on Laser Ranging Instrumentation, Canberra (1994) 82

/3/ Appleby G. M., Satellite Signatures in SLR Observations, NASA Conference Proceeding 3214, 8th International Workshop on Laser Ranging Instrumentation, Annapolis (1992) 2-1

/4/ Kirchner G., Koidl F., Hamal K., Prochazka I., Multiple Wavelength Ranging in Graz, Australian Government Publishing Service, Proceedings of the 9th International Workshop on Laser Ranging Instrumentation, Canberra (1994) 609

/5/ Schreiber U., Maier W., Riepl S., Measuring atmospheric dispersion employing avalanche photodiodes, in Lidar Techniques for Remote Sensing, Christian Werner, Editor, SPIE 2310, 2 - 10, (1994)

/6/ W. Koechner, Solid State Laser Engineering, Springer series in Optical Science, Vol. 1, Fourth Edition, p. 66ff, (1996)

OPTIMAL DESIGN OF PASSIVELY Q-SWITCHED MICROLASER TRANSMITTERS FOR SATELLITE LASER RANGING

John J. Degnan
NASA Goddard Space Flight Center
Greenbelt, MD 20771 USA

ABSTRACT

The workhorse for third generation satellite laser ranging systems has been the modelocked Nd:YAG laser which produces pulsewidths measured in tens to hundreds of picoseconds. These systems are typically large (> 1 m long), complex, and require relatively sophisticated modulation and switching electronics, passive or active thermal control of the resonator length, and, in some cases, the use of limited lifetime dyes and carcinogenic solvents. Their complexity and reliance on inexpensive but short-lived flashlamps for pumping, with their attendant high voltage power supplies and ionozation circuits, further ensures a high level of maintenance by onsite personnel.

Recently, tiny Q-switched Nd-based microlasers, having lengths on the order of a millimeter and pumped by a single laser diode, have been demonstrated. These devices have operated at multikilohertz rates with pulsewidths as short as 115 picoseconds and single pulse output energies up to several tens of microjoules. Microlasers have been Q-switched via both active (e.g electro-optic) and passive (e. g. saturable absorber) means and generate more stable and temporally smooth profiles than many modelocked systems. Various passive diode-pumped multipass amplifier schemes have been devised for amplifying the microlaser output to millijoule levels without resorting to the use of fast switching or pulse selection devices. Thus, microlasers make ideal transmitters for the eyesafe SLR 2000 system and are a natural and inexpensive alternative to modelocked oscillators and/or regenerative amplifiers in higher power systems.

At GSFC, we have studied the manner in which both active and passive Q-switched lasers can be optimized for maximum efficiency (and coincidentally for minimum pulsewidth) and have examined the effects of thermalization among Stark sublevels and lower multiplet relaxation on pulse temporal profiles. More recently, we have begun to experimentally characterize the saturation properties of passive absorbers, such as chromium-doped YAG and Lithium Fluoride commonly used to Q-switch Nd-based lasers, as a function of pulsewidth. These theoretical and experimental efforts are combined in the present paper to derive optimum designs for an all diode-pumped SLR 2000 transmitter with the following characteristics: pulse energy $\geq$100 μJ at 532 nm, repetition rate $\geq$ 2 KHz, and pulsewidth $\leq$ 140 picoseconds.

1. INTRODUCTION

The workhorse for third generation satellite laser ranging systems has been the modelocked Nd:YAG laser which can produce pulsewidths measured in tens to hundreds of picoseconds. These systems are typically large (> 1 m long), complex, and require relatively sophisticated modulation and high voltage switching electronics, passive or active thermal control of the resonator length, and, in some cases, the use of limited lifetime modelocking dyes and carcinogenic solvents. Their complexity and reliance on inexpensive but short-lived flashlamps for pumping, with their attendant high voltage power supplies and ionization circuits, further ensures a high level of maintenance by onsite personnel. Field lasers typically generate 100 mJ of energy per pulse at repetition rates of 5 to 10 Hz for the frequency doubled wavelength at 532 nm. This corresponds to an average green power output of only 0.5 to 1.0 Watts although single pulse peak powers are typically in the Gigawatt range.

Recently, tiny Q-switched Nd-based microlasers, having lengths on the order of a millimeter and pumped by a single laser diode, have been demonstrated. These tiny oscillators have operated at multikilohertz rates with pulsewidths as short as 115 picoseconds in active Q-switching mode using a resonant end reflector and have produced single pulse output energies up to several tens of microjoules [1]. Microlasers have also been switched via passive saturable absorbers and generate more stable and temporally smooth profiles than many modelocked systems [2,3] although they have not yet achieved the very short pulsewidths on the order of 10 picoseconds available from modelocked systems. In some cases, the gain and saturable absorber media can be doped into the same host crystsal, such as Neodymium and Chromium ions, and optical coatings deposited on both ends to form a single element, monolithic laser [3]. Furthermore, various passive diode-pumped multipass amplifier schemes have been devised for amplifying the microlaser output to millijoule levels without resorting to the use of active regenerative amplifiers which require nanosecond rate switching or pulse selection devices [4]. One can therefore design a laser ranging transmitter which operates off a single DC voltage by using a combination of CW diode pumping for both the oscillator and amplifier, passive Q-switching by saturable absorbers, and passive multipass amplifier configurations. Since the resulting transmitter would produce average powers comparable to that of current field SLR systems ($\leq$ 1 Watt) , but at much lower pulse energies and multikilohertz rates, the photon detection rate would also be similar. By allowing the low energy pulse train from the microlaser transmitter to fill the transmit/receive telescope aperture (<50 cm diameter), one can also meet current eye safety standards while maintaining average power levels comparable to current systems. Thus, microlasers make ideal transmitters for the eyesafe SLR 2000 system [5] and are a natural and very inexpensive alternative to modelocked oscillators and/or regenerative amplifiers in seeding higher power systems.

The author has previously studied the manner in which both actively [6] and passively [7] Q-switched lasers can be designed for maximum energy efficiency (and coincidentally for minimum pulsewidth in most cases of interest) and has further examined the effects of thermalization among Stark sublevels and lower multiplet relaxation on Q-switched laser energy and pulse temporal profiles [8]. More recently, Xiao and Bass [9] have demonstrated the manner in which excited state absorption, which occurs in some saturable absorbers, can be accomodated in Degnan's passive Q-switch optimization process. More recently, we have begun to experimentally characterize the saturation properties of passive absorbers, such as chromium-doped YAG and Lithium Fluoride commonly used to Q-switch Nd-based lasers, as a function of pulsewidth [10]. These theoretical and preliminary experimental efforts are combined in the present paper to derive optimum designs for an all diode-pumped SLR 2000 transmitter with the following characteristics: pulse energy $\geq$100 μJ at 532 nm, repetition rate $\geq$ 2 KHz, and pulsewidth $\leq$ 140 picoseconds.

2. OPTIMIZATION EQUATIONS FOR A CW-PUMPED, PASSIVELY Q-SWITCHED SYSTEM

Using Eqs. (21), (35), (36) and (38) in [7], one can show that, in order to optimize the output energy of a CW-pumped, passively Q-switched laser, the following three equations

$$z = \frac{\left(1-e^{-\alpha\rho}-\alpha\rho\right)^2}{\left(1-e^{-\alpha\rho}-\alpha\rho\right)\left(1-e^{-\alpha\rho}-\alpha\rho e^{-\rho}\right)-\alpha\left(1-e^{-\rho}-\rho\right)\left(1-e^{-\alpha\rho}-\alpha\rho e^{-\alpha\rho}\right)} \tag{1a}$$

$$z = z_{cw}\frac{1-\exp\left(-\tau_c/\tau_a\right)}{1-\delta\exp\left(-\tau_c/\tau_a\right)} \equiv z_{cw}F \tag{1b}$$

$$\delta = 1-\frac{f_a}{\gamma}\left(1-e^{-\rho}\right) \tag{1c}$$

must be solved simultaneously for the parameters z, δ, and ρ where

$$z = \frac{2\sigma n_i l}{L} = \frac{2\ln(G_o)}{L} \tag{2a}$$

$$\rho = \ln\left(\frac{n_i}{n_f}\right) \tag{2b}$$

and δ is the fraction of the original inversion remaining from the previous Q-switch cycle as determined from a steady state analysis.

Alternatively, equations (1a) through (1c) can be combined to yield a single transcendental equation for the value of ρ in the optimized case, i.e.

$$z_{CW} = \frac{\left(1-e^{-\alpha\rho}-\alpha\rho\right)^2\left[1+\frac{f_a}{\gamma}\frac{\left(1-e^{-\rho}\right)}{\exp\left(\tau_c/\tau_a\right)-1}\right]}{\left(1-e^{-\alpha\rho}-\alpha\rho\right)\left(1-e^{-\alpha\rho}-\alpha\rho e^{-\rho}\right)-\alpha\left(1-e^{-\rho}-\rho\right)\left(1-e^{-\alpha\rho}-\alpha\rho e^{-\alpha\rho}\right)} \tag{3}$$

Parameters appearing in (3) , which are assumed to be known or estimated apriori, are:

$z_{cw} = 2\,\sigma n_{cw} l/L = 2\ln(G_o)/L$ where G_o is the roundtrip CW small signal power gain in the absence of Q-switching, L is the dissipative roundtrip optical loss (which excludes the mirror transmission and saturable absorption loss), σ is the spectroscopic stimulated emission cross-section; n_{cw} is the population inversion density produced by the CW pump, and l is the gain length.

$\alpha = \frac{F_{sat}^{amp}}{F_{sat}^{abs}}$ = the ratio of the saturation fluences for the amplifying and absorbing media

τ_n = upper laser multiplet relaxation time = 230 μsec for Nd:YAG

τ_c = desired Q-switch cycle time (inverse of repetition rate) = 500 μsec for SLR 2000 at 2 KHz

f_a = fractional Boltzmann population of laser Stark sublevel within the upper multiplet = .41 for Nd:YAG

γ = inversion reduction factor[6] where $f_a \leq \gamma \leq 2$and takes on the upper value (2) when all thermalization and terminal level relaxation processes are slow relative to the resonator photon decay time and the lower value (f_a) when the processes are all relatively fast [8] . We have assumed a value of $f_a + f_b = 0.6$ for these Nd:YAG calculations which implies thermalization among Stark sublevels is fast but lower multiplet relaxation is slow compared to the resonator photon decay time.

By substituting (1c) in (1b), the quantity F, which represents the amount the initial Q-switch gain is reduced from its CW value due to the pulse repetition rate, can be written in the form

$$F = \left[1 + \frac{f_a}{\gamma} \frac{\left(1 - e^{-\rho}\right)}{\exp\left(\tau_c / \tau_a\right) - 1}\right]^{-1} \tag{4}$$

and computed once ρ is computed from (3). One can then use equations (22), (23), and (30) in [7] to compute the optimum unsaturated absorber transmission (T_{opt}) , the optimum mirror reflectivity (R_{opt}), and the optimized laser output energy (E_{opt}). For our CW-pumped case, these equations can be written in a somewhat more transparent form, i.e.

$$T_{opt} = \exp\left[-\sigma n_{cw} l F \frac{\alpha\left(1 - e^{-\rho} - \rho\right)}{\left(1 - e^{-\alpha\rho} - \alpha\rho\right)}\right] \tag{5a}$$

$$R_{opt} = \exp\left[-\left(2\sigma n_{cw} l F + 2\ln(T_{opt}) - L\right)\right] \tag{5b}$$

$$E_{opt} = \frac{h\nu A\rho}{2\sigma\gamma} \ln\left(\frac{1}{R_{opt}}\right) \tag{5c}$$

and computed sequentially in the order the equations are given. In (5c), A is the effective beam area in the gain medium and hν is the laser photon energy. The time averaged output power of the energy-optimized, CW-pumped microlaser is in turn given by

$$P_{ave} = \frac{E_{opt}}{\tau_c} = \frac{h\nu A\rho}{2\sigma\gamma\tau_c} \ln\left(\frac{1}{R_{opt}}\right) \tag{6}$$

One can also derive an expression for the laser pulsewidth using (32) in [7] which is given by

$$\tau = \frac{t_r}{\left[L - \ln\left(R_{opt}\right)\right]} \frac{1 - e^{-\rho} + \frac{\ln\left(T_{opt}\right)}{\alpha\sigma n_{cw} lF}\left(1 - e^{-\alpha\rho}\right)}{1 - \frac{g_t(\alpha,\rho)}{2\sigma n_{cw} lF} + \frac{\ln\left(T_{opt}\right)}{\alpha\sigma n_{cw} lF}\left(1 - \left[\frac{g_t(\alpha,\rho)}{2\sigma n_{cw} lF}\right]^{\alpha}\right) + \frac{L - \ln\left(R_{opt}\right)}{2\sigma n_{cw} lF} \ln\left[\frac{g_t(\alpha,\rho)}{2\sigma n_{cw} lF}\right]} \tag{7a}$$

where the roundtrip threshold gain, $g_t(\alpha,\rho)$,is obtained from an iterative solution of the equation [7]

$$g_t(\alpha,\rho) = \left[L - \ln\left(R_{opt}\right)\right] - 2\ln\left(T_{opt}\right)\left[\frac{g_t(\alpha,\rho)}{2\sigma n_{cw} lF}\right]^{\alpha} \tag{7b}$$

3. CW DIODE END-PUMPING OF A MICROLASER

Since our design goal is a short pulse comparable to that used in current centimeter accuracy SLR systems (<140 psec at 532 nm), the length of the microlaser must be kept fairly short, and therefore end-pumping by a single diode or fiber-coupled diode array is the only viable approach. Longer rods favor increased pump efficiencies which results in higher small signal gains, higher output energies, and higher average powers. However, the beneficial effects of higher gain on reducing laser pulsewidth are more than offset by an increase in the resonator roundtrip transit time. Thus, pulsewidth must be traded off against other important parameters such as pulse energy, peak power, or average power.

In order to begin our computation of the parameters for the optimized laser, we must compute the quantity z_{cw} appearing in Eqs. (1b) and (3) as a function of the diode pump intensity. For a CW-pumped laser, this is given by

$$z_{cw} = \frac{2\sigma n_{cw} l}{L} = \frac{2\sigma T_p \eta_p f_a \tau_a \eta_a I_p}{h\nu_p L} \tag{8}$$

where I_p is the CW pump intensity, $h\nu_p$ is the pump photon energy (= 2.46 x 10^{-19} J at 808 nm), η_p is the efficiency with which the energy deposited in the pump bands gets deposited into the upper laser multiplet (believed to be ≅1 for the $^4F_{3/2}$ level in Nd:YAG), T_p is the transmission of the entrance face at the pump wavelength, and η_a is the fraction of the optical pump power entering the laser medium which is absorbed. The latter is given by the expression

$$\eta_a = \left[1 - \left(1 - R_p\right)e^{-\alpha_p l} - R_p e^{-2\alpha_p l}\right] \tag{9}$$

where, α_p is the pump absorption coefficient (~4.5/cm for Nd:YAG at a pump wavelength of 808 nm) and R_p is the reflectivity of the rod exit face at the pump wavelength. For one way pumping, the back face of the rod is AR-coated for the pump and laser wavelengths so that $R_p \cong 0$ whereas , for ideal two-way pumping, $R_p \cong 1$. In reality, the reflectivity of the pump wavelength must be traded off against the transmission at the laser wavelength which contributes to the dissipative loss, L, so that $R_p < 1$.

4. NUMERICAL RESULTS FOR A MONOLITHIC Nd^{3+};Cr^{4+}:YAG CRYSTAL

We now use our theoretical expressions (3) through (7) to study the laser properties of a "monolithic" YAG crytal which is simultaneously doped with the ions producing gain (Nd^{3+}) and ions producing saturable absorption (Cr^{4+}) [3]. Since short pulses are our goal, use of a monolithic structure results in the simplest and shortest passively Q-switched laser resonator possible. In performing our numerical computations, we will assuime the following values for previously undefined parameters: T_p=1, L=.02, R_p =1, F_{sat}^{amp} = 480 mJ/cm^2 [7], F_{sat}^{abs} = 179 mJ/cm^2 [10]. We allow the length of the laser rod, l, to vary between 1 and 5 mm and assume that the optimum absorber doping for maximum laser efficiency can be accomodated within this crystal length. Figures 1 and 2 show plots of the optimum mirror reflectivity, optimum absorber transmission, and laser pulsewidth as a function of the CW diode pump intensity for different crystal lengths. The CW pump intensity was allowed to vary between 0 and 20 Watts/mm^2. The pulse energy curves are plotted against the same parameters for a total diode pump power of 1.2 Watts corresponding to the output of a Spectra Diode Labs Model SDL-2372-P3 diode laser which provides a high brightness beam in a 100 μm diameter spot via fiber optic coupling.

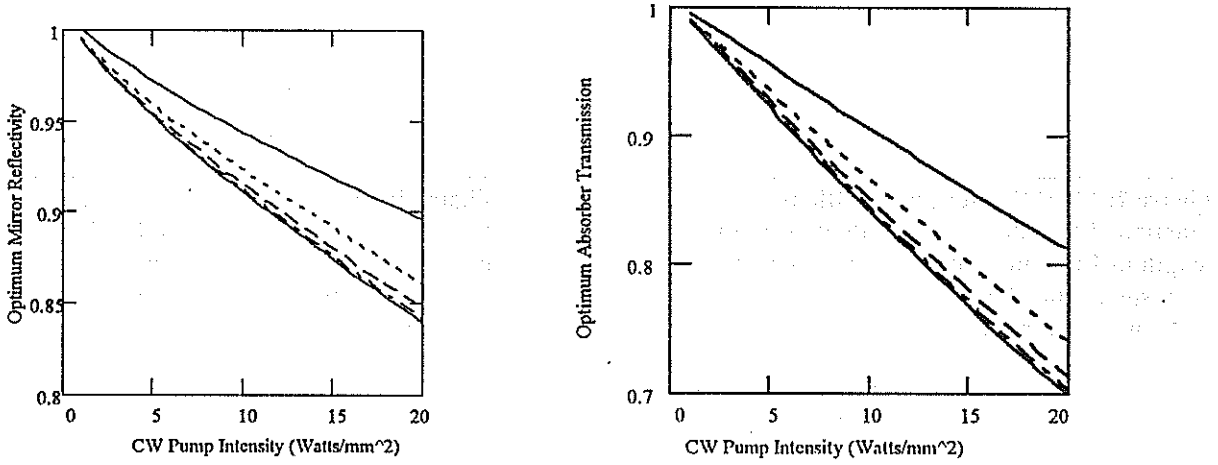

Figure 1: Optimum mirror reflectivity and absorber transmission as a function of CW pump intensity and rod length in 1mm increments. The top curve corresponds to a rod length of 1 mm and the bottom curve to a length of 5mm.

5. PASSIVE MULTIPASS AMPLIFIER

Coyle [4] has described a clever passive multipass amplifier design based on a rectangular slab shown in Figure 4. The slab is pumped on up to four sides by linear diode arrays. Typical cm long commercial arrays each produce up to 20 Watts of CW power.

One can define an amplifier "cell size", a, such that the length and width of the amplifier are equal to L = na and W = ma respectively where n and m are integers. One corner of the amplifier slab can be polished off to serve as an entrance face ,i.e. the entrance cell is cut in half along its diagonal and perpendicular to the beam.Thus, the beam size must be less than $\sqrt{2}a$ to fit within the entrance face. In addition, the beam size should be less than the width of the pumped volume in the slab. Once inside the slab, the beam will reflect internally off the sides of the amplifier at a 45° angle until it encounters another corner. This corner can be polished off (exit cell halved) to serve as an exit face.

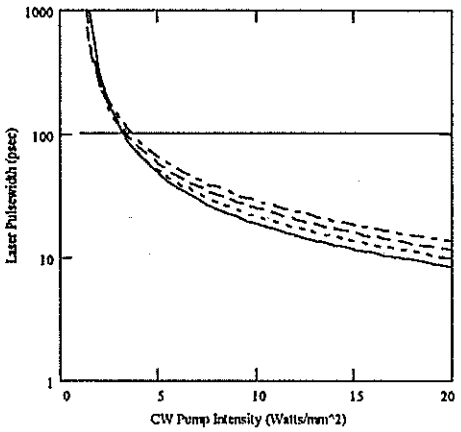

Figure 2: FWHM laser pulsewidth as a function of CW diode pump intensity and rod length in 1 mm increments. Bottom curve corresponds to a length of 1 mm and top curve to a length of 5 mm.

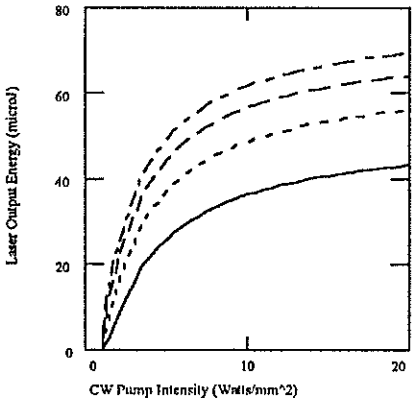

Figure 3: Laser pulse energy as a function of CW diode pump intensity and rod length in 1 mm increments for a total input power of 1.2 Watts. Bottom curve corresponds to a length of 1 mm and top curve to a length of 5 mm.

If m and n are chosen to have no common factors, one can show from a simple graph paper analysis that the effective multipass gain length before encountering a corner is given by

$$l_{eff} = \sqrt{2}a(mn-1) = \sqrt{2}\left(\frac{LW}{a}-1\right) \tag{10}$$

where $\sqrt{2}a$ is the diagonal length of a single "cell" and (mn-1) is the number of cell diagonals traversed before encountering a corner (one cell is lost by halving the entrance and exit cells to create the entrance and exit faces). Furthermore, the beam undergoes a number of 45° reflections inside the amplifier given by

$$n_r = m+n+2 \tag{11}$$

so that the net multipass power gain in the amplifier is

$$G_{net} = \exp\left(\sigma n_{cw} l_{eff}\right) R_{45°}^{n_r} \tag{12}$$

where $R_{45°}$ is the reflectivity of the amplifier face at 45° incidence.

If the integers m and n are odd, the beam exits the amplifier from the corner opposite to the entrance face. If one integer is odd and the other even, the entrance and exit corners are adjacent to each other and lie on the same even numbered side.

If m and n have a common factor f, graphical analysis shows that the beam encounters a corner more quickly, and the effective gain length is reduced to

SLR 2000 LASER TRANSMITTER

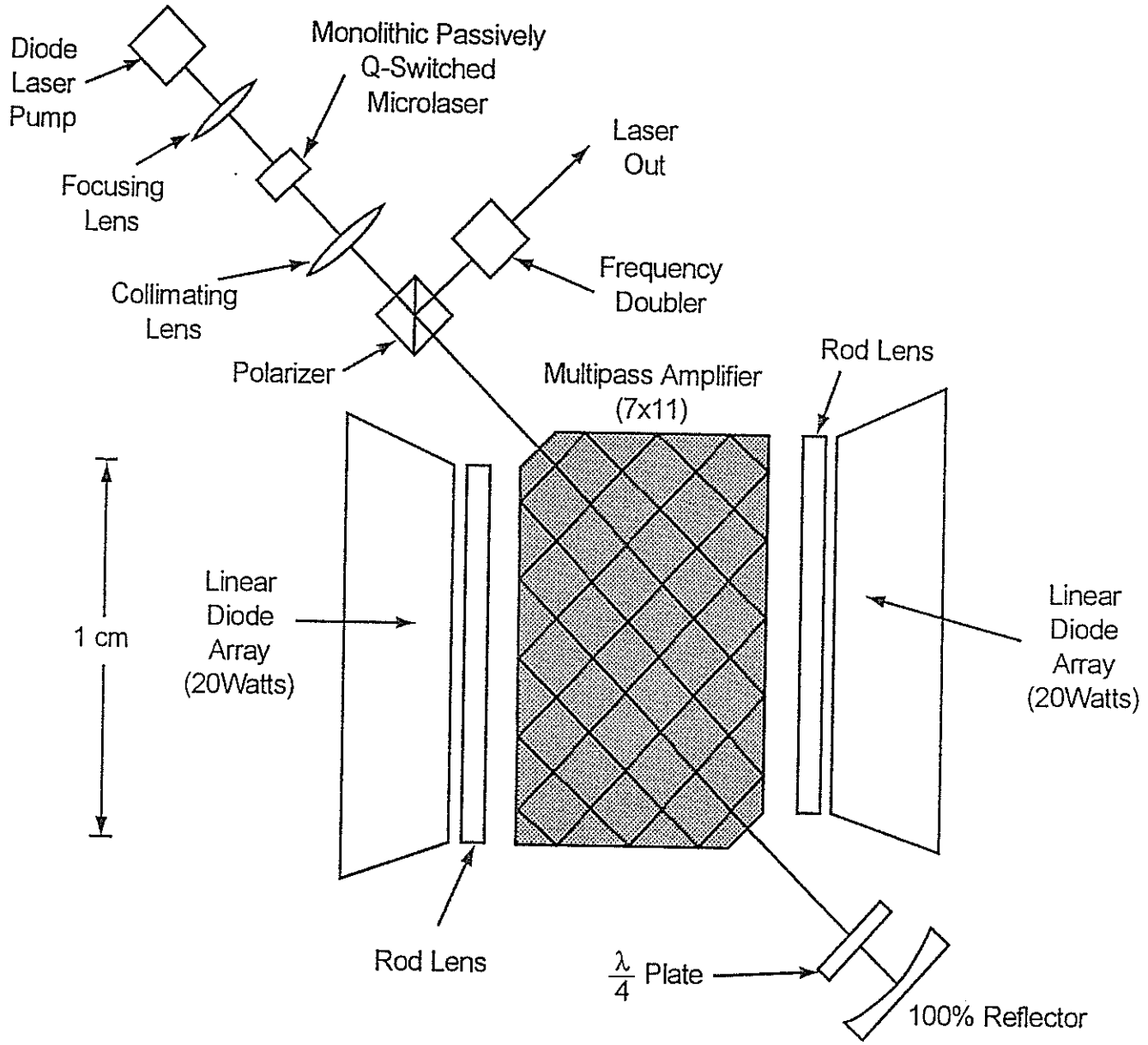

$$l_{eff} = \sqrt{2}a\left(\frac{mn}{f} - 1\right) = \sqrt{2}\left(\frac{LW}{fa} - 1\right) \tag{13}$$

and this represents a "bad" design.

If L and W are both on the order of a cm (corresponding to a standard laser diode array length) and a is on the order of a mm (a typical slab pump width [4]) , then, from (12), the effective multipass gain length, on a single pass through the amplifier, can be as large as 14 cm. Placing a mirror at the exit face, as in the SLR2000 transmitter block diagram in Figure 4, allows the multipass amplifier to be used in a double-pass configuration, resulting in an effective gain length of 28 cm. Our computations show that such a configuration, pumped by two linear diode arrays, each producing 20 watts of CW power, can produce a double-pass small signal power gain of 16 if the diode pump light is focused into a typical 1.2 mm width. Thus, a 25 μJ pulse from the oscillator can be amplified to 400 μJ, which is more than adequate for SLR2000. Significant additional gain can be achieved, if necessary, by adding arrays to the two remaining unpumped sides of the amplifier as in [4], roughly squaring the small signal gain.

6. CONCLUSIONS

A comprehensive theoretical model has been developed for the passively Q-switched microlaser which (1) can be fit well to existing experimental data, (2) is useful in estimating unknown parameters, and (3) can guide prototype hardware design. Furthermore, a simple model for a totally passive CW laser diode-pumped multipass amplifier has been developed. This compact amplifier, with a ~1cm by 1 cm by 1mm pumped volume, produces gains much higher than can be achieved in a conventional single or double pass configuration pumped by the same diode power. Our calculations predict a maximum single pass gain of 4 and a maximum double pass gain of 16 for a slab multipass amplifier pumped by two 20 watt laser diode arrays, and this can be increased substantially by adding additional arrays. The resulting oscillator/amplifier design has no high speed pulsing or switching circuits and should easily achieve the laser energy, pulsewidth, and repetition rate goals of SLR2000.

REFERENCES

1. Zayhowski, J. and C. Dill III, "Coupled-Cavity Electro-optically Q-switched ND:YVO_4 Microchip Lasers", Optics Letters, 20, pp. 716-718, April, 1995.

2. Zayhowski, J. and C. Dill III, "Diode Pumped Passively Q-switched Picosecond Microchip Lasers", Optics Letters, 19, p. 1427-1430, 1994.

3. S. Li, S. Zhou, P. Wang, Y. C. Chen, and K. K. Lee, , "Self Q-switched Diode End-Pumped Cr, Nd: YAG with Polarized Output", Optics Letters, 18, pp. 203-204, February 1993.

4. Coyle, D. B., "Design of a High Gain Laser Diode Array Pumped Nd:YAG Alternating Precessive Slab (APS) Amplifier", IEEE J. Quantum Electronics, 27; pp. 2327-2331, October, 1991.

5. Degnan, J. , J. McGarry, T. Zagwodzki, P. Titterton, H. Sweeney, H. Donovan, M. Perry, B. Conklin, W. Decker, J. Cheek, A. Mallama, P. Dunn, and R. Ricklefs; "SLR2000: An Inexpensive, Fully Automated, Eyesafe Satellite Laser Ranging System", these proceedings.

6. Degnan, J. J. , "Theory of the Optimally Coupled Q-switched Laser", IEEE J. Quantum Electronics, 25, pp. 214-220, February, 1989.

7. Degnan, J. J., "Optimization of Passively Q-switched Lasers", IEEE J. Quantum Electronics, 31, pp. 1890-1901, November, 1995.

8. Degnan, J. J., D. B. Coyle, and R. B. Kay, "Effects of Thermalization on Q-switched Laser Parameters", IEEE J. Quantum Electronics, accepted with revisions.

9. Xiao G., and M. Bass, "A Generalized Model for Passively Q-switched Lasers Including Excited State Absorption in the Saturable Absorber", IEEE J. Quantum Electronics, 33, pp. 41-44, January 1997.

10. Gompers S. and J. Degnan, unpublished

EYE SAFE RAMAN LASER

K.Hamal, J.Blazej, I.Prochazka

Czech Technical University, Brehova 7
115 19 Prague 1, Czech Republic
fax +42 2 85762252, prochazk@mbox.cesnet.cz

To build the eye safe transmitter we were using the Raman cell filled by methane shifting the 1.064 micrometer Nd:YAG laser pulses to 1.54 micrometer wavelength. We examined the Raman process at 30, 60, 100 and 200 picoseconds long laser pulses using the active passive mode locked laser at methane pressure ranging from 5 to 11 Bars (the indoor experiment in Prague) and the active active mode locked laser at 180 picoseconds and 40 Bars (CRL Tokyo). The conversion efficiency varies from 5 to 10 percent. Using the CCD we tested the Raman beam structure. The beam divergence is generally 1.2 times smaller than the incoming 1.06 μm beam, the fluctuations from shot to shot are within the same value. Using the streak camera we measured the temporal structure, the Raman pulse duration was approximately 1.5 times shorter then the pumping pulse, however for longer pulse and higher pumping above the Raman threshold the pulse shape deterioration is pronounced and consequently influencing the overall single shot jitter of the laser ranging system. Testing the energy we found out that the Raman energy fluctuations increase by a factor 5 in comparison to 1.06 μm pump. In Tokyo SLR, using 10 milliJoules of 1.54 μm energy, all satellites up to 20 000 kilometers have been ranged.

10th International Workshop on Laser Instrumentation, Shanghai, China, November '96

Optical block scheme

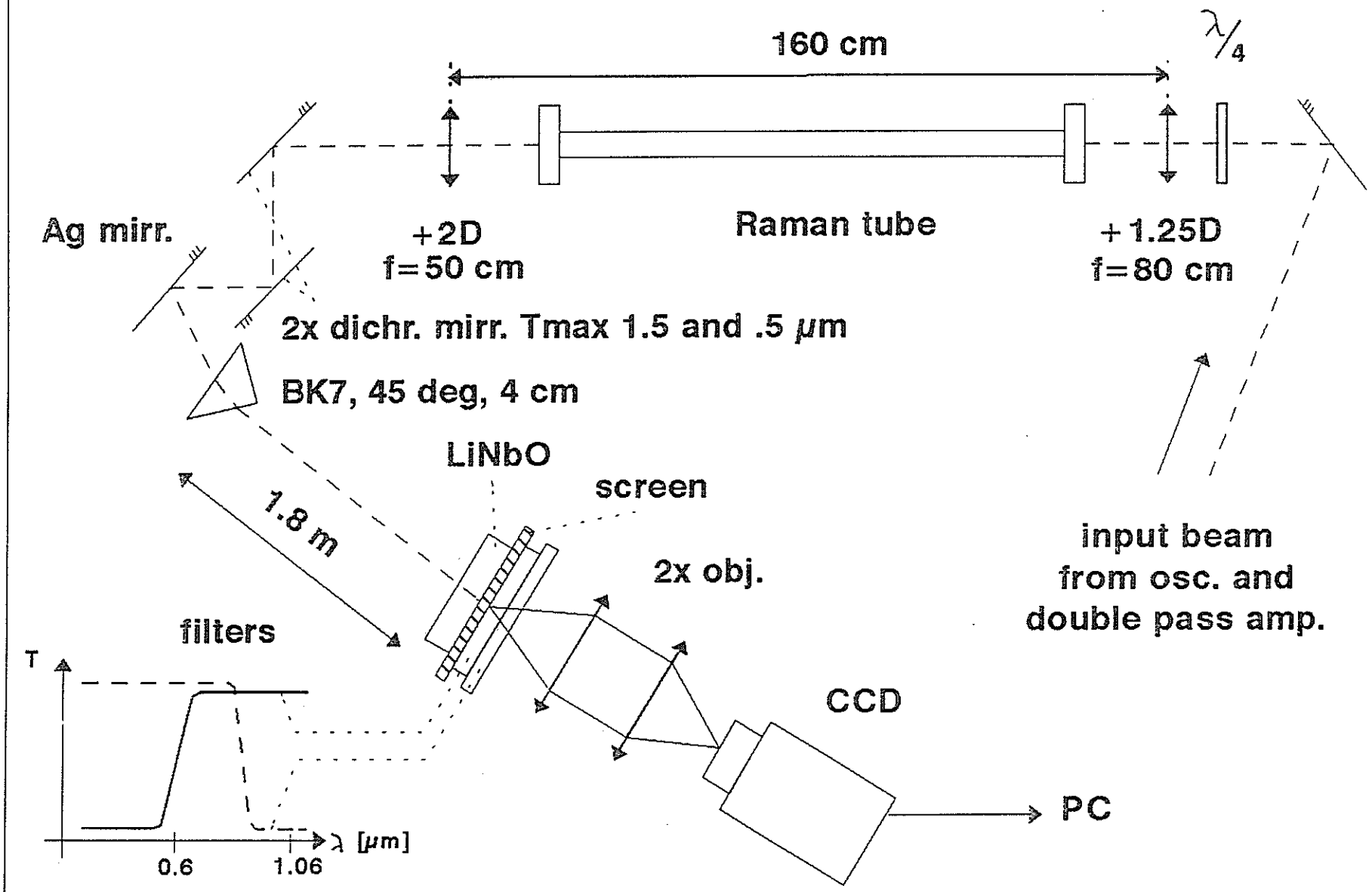

K.Hamal,J.Blazej,I.Prochazka, Shanghai '96

Eye Safe Raman Laser

Raman scattering in methane
Energy conversion

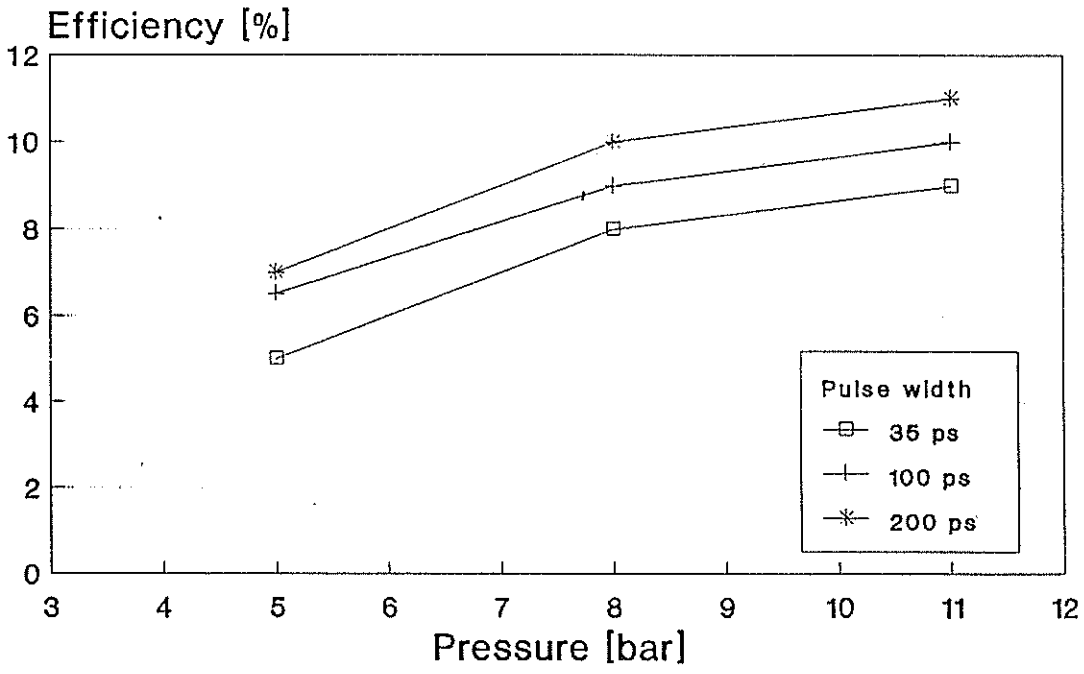

K.Hamal,J.Blazej,I.Prochazka, Shanghai '96

Eye Safe Raman Laser

Energy output stability

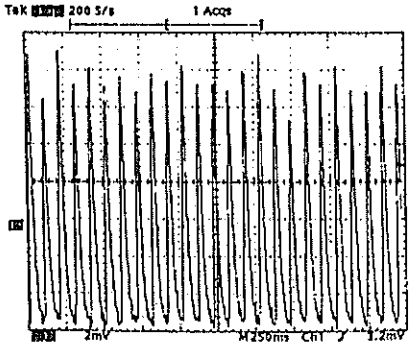

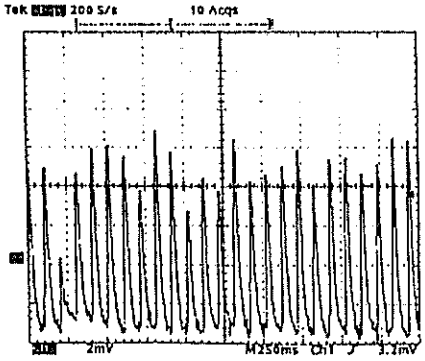

1.06 pumpe output

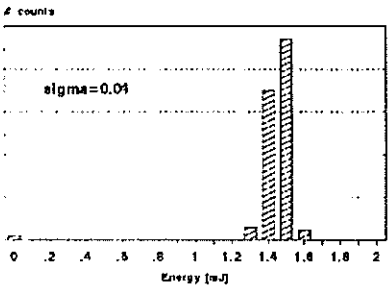

1.54 Raman tube output

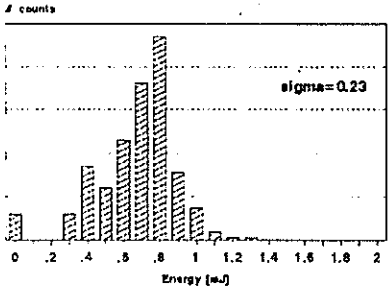

K.Hamal,J.Blažej,I.Procházka, Shanghai '96

Eye Safe Raman Laser

Spatial structure
methane 8 bar, 12 mJ, 35 psec

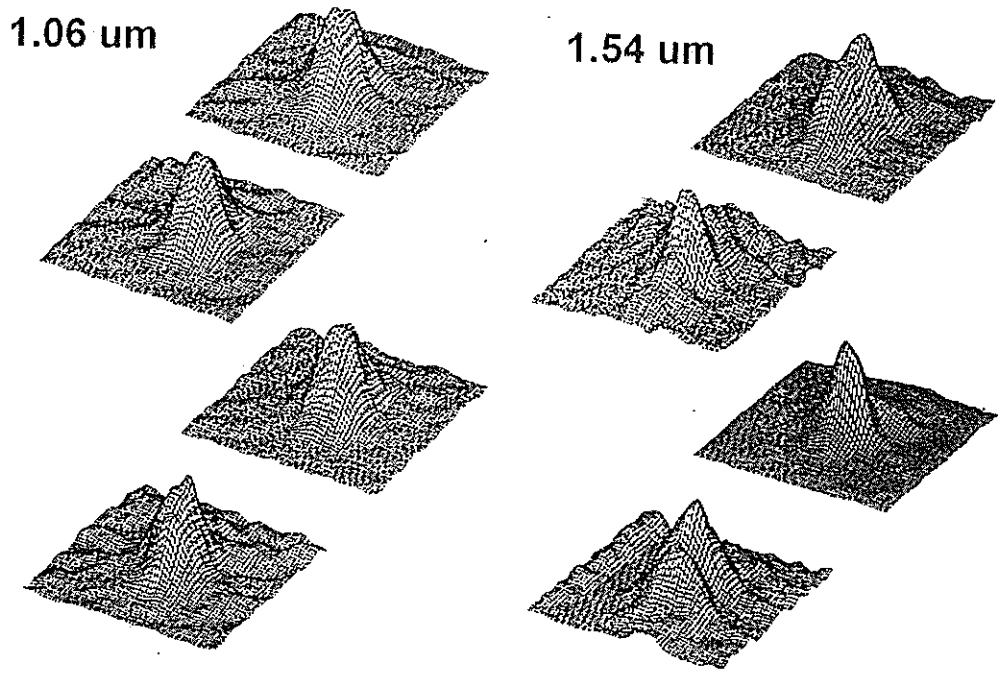

K.Hamal,J.Blažej,I.Procházka, Shanghai '96

Eye Safe Raman Laser

Spatial fluctuation - superposition of 30 shots
methane 8 bar, 12 mJ, 35 psec

K.Hamal,J.Blažej,I.Procházka, Shanghai '96

RAMAN LASER TEMPORAL PROFILE

Raman Stokes 1540 nm, 1.7 kV

Streak record

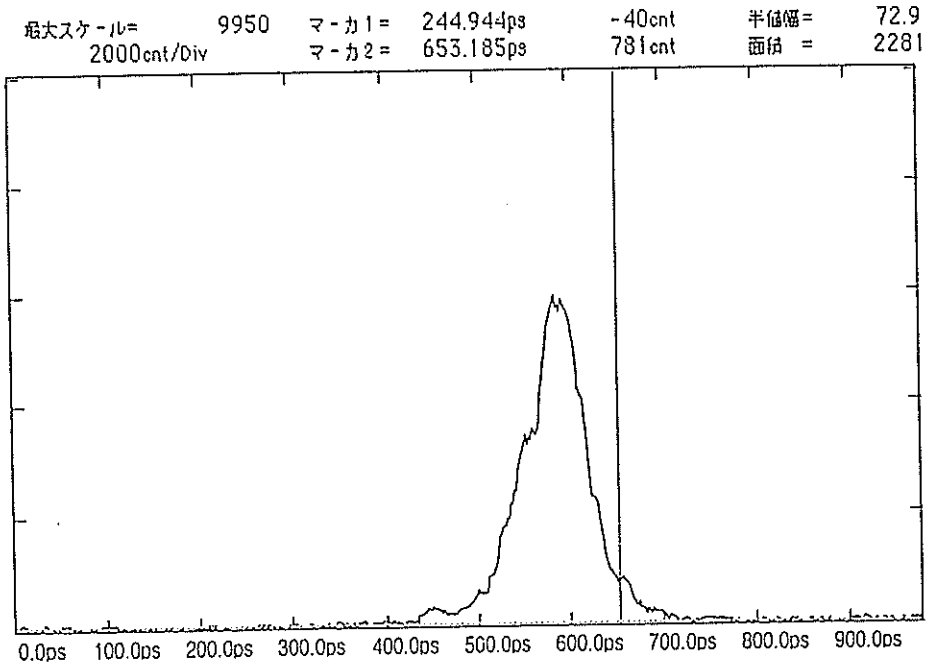

CRL Tokyo, January 20- February 11,'95

RAMAN LASER TEMPORAL PROFILE

Fundamantal 1064 nm, depleted, 1.4kVpump

Streak record

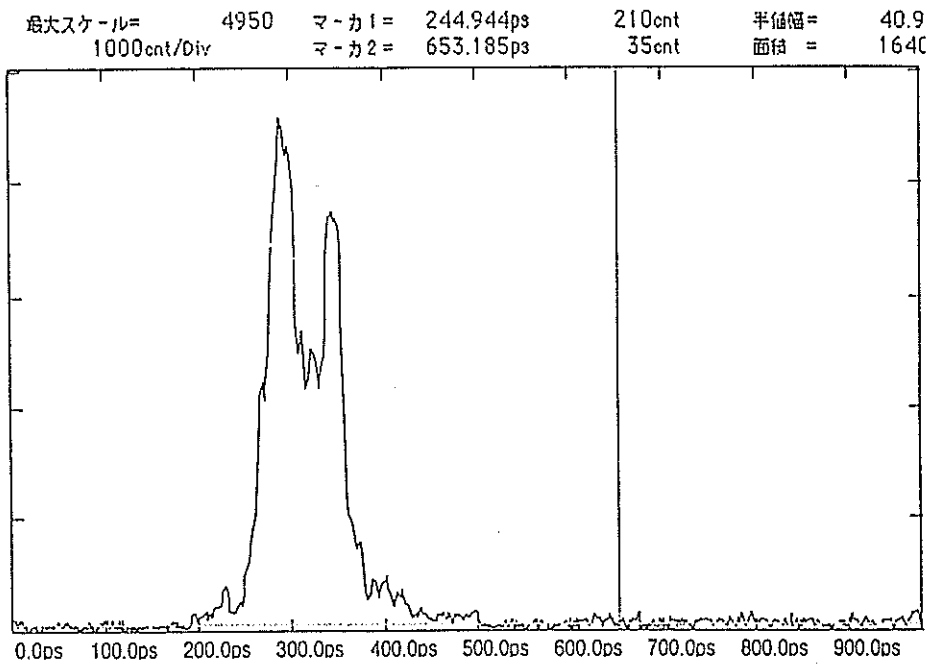

CRL Tokyo, January 20- February 11,'95

A Compact Modified SFUR Passively Mode-Locked Nd: YAG Laser for Satellite Ranging

Sun Zhan'ao, Yang Xiangchun, Zhu Xiaolei, Wu Zhaoqing

(Shanghai Institute of Optics and Fine Mechanics, Academia Sinica, China)

Yang Fumin, Chen Wanzhen, Xiao Chikun

(Shanghai Observatory, Academia Sinica, China)

Abstract

A compact frequency doubled Nd:YAG laser for satellite ranging is presented. In this system, a self-filtering unstable resonator (SFUR) in new modified configuration and linear colliding pulse mode-locked (CPM) scheme have been adopted. The typical parameters are:

Wavelength	532 nm
Single pulse energy	≥ 30 mJ
Pulse duration	20 - 50 ps
Repetition rate	1 - 5 pps
Laser dimensions (main body)	132 × 32 × 25 cm

Using this system, the Lageos satellite laser ranging have been performed successfully. Up to date, at Shanghai Observatory fixed station and Wuhan transportable laser ranging station the laser has been operating over one year.

I. Theory and optical scheme of the laser system

For our new modified SFUR, the recollimating mirror is replaced by a flat mirror which allows a shorter cavity for the same magnification. In this case, a slightly displaced position,.

$\Delta = L_1 - f_1$ with respect to the f_1 focal plane is needed. The aperture a is as follow:

$$a = [\, 0.61 \,(2 - L_1 / f_1) L_1 \,]^{1/2}$$

In this configuration, the output beam is divergent. The magnification of the cavity is

$$M = -(2 L_2 + \Delta) / f_1$$

M as a parameter, according to [1], has the following expressions:

$$\Delta = - f_1 / M$$

$$L_1 = (1 - 1 / M) f_1$$

---

[1] IEEE J. QE - 24 (8): (1988) 1543 - 1547

$$f_2 = d - M(1 - 1/M^2) f_1$$

For our new modified SFUR, d = 0, then, f is the radius of curvature of the laser beam reaching the aperture. The concave mirror with a pinhole is taken as self-filtering component, also used for compensate the pure geometrical divergence. So, the redius of curvature of the concave mirror R = 2 f .

(1) Mirror R_1 =500 mm H.R. at 1.064 μm

(2) Concave mirror, R ≅ 3000 mm, aperture d ≅1 mm

(1) and (2) consist a self-filtering and collimating output coupler system.

II. Experimental and Observational Results

1. The pulse width of the output was measured by a Hamamatsu streak camera (Figure).
2. The new laser has been operational at Shanghai SLR station since October, 1995.
   About 600 passes returns from many satellites, such as Lageos 1、2, Etalon 1、2, Glonass 63、67, have been obtained. The stability of the laser is quite good.

III. Future Plans

1. Cr^{4+} , Nd^{3+} YAG, self-Q switched supershort cavity,
   pulse duration t =100 ps
   repetition rate 10 Hz
2. Diode pumping mode-locked laser (DPL)
   pulse duration 20-30 ps
   repetition rate 1 Kz

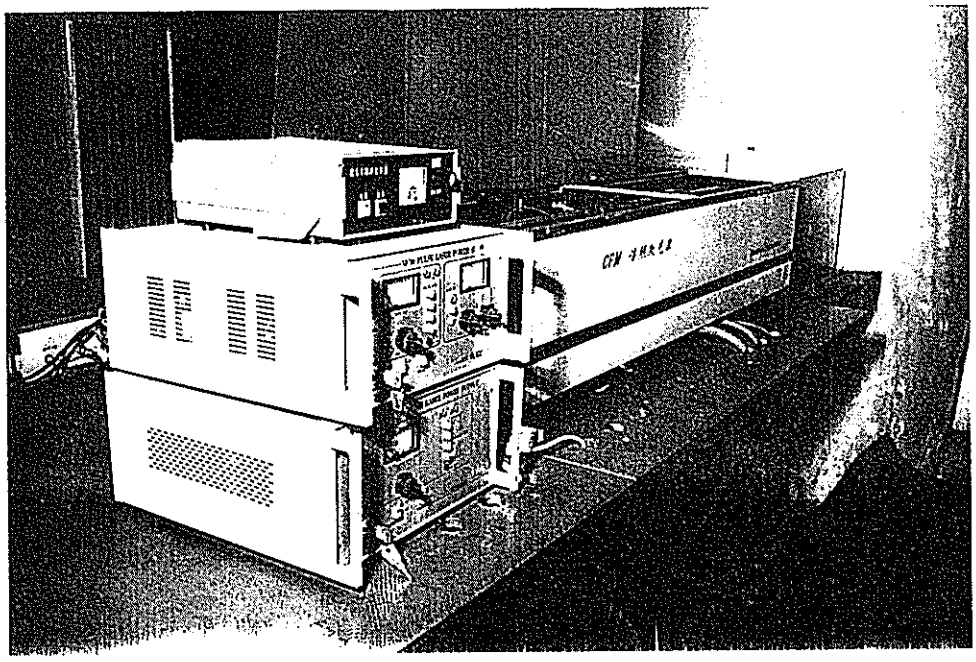

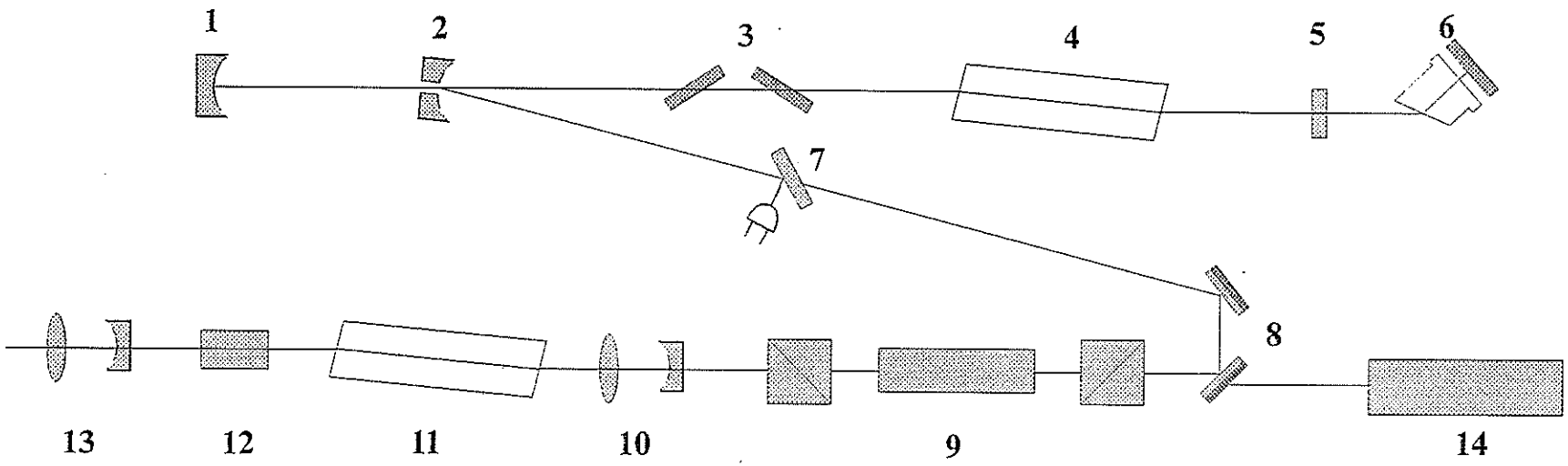

1. HR Concave Mirror (R= -500mm)
2. Pinhole and Coupling HR Concave Mirror
3. Polarizers
4. Oscillator Nd:YAG rod
   ϕ 6 × 90 mm
5. F-P
6. Dye Cell and HR Mirror
7. Sampling Plate
8. Bending Mirrors
9. LiNO3 Semi-train pulses selector
10. 1.5x Beam Expander
11. Amplifier Nd:YAG rod
    ϕ 9 × 125mm
12. KDP SHG
13. 1.5x Beam Expander
14. He-Ne Laser

Optical Layout of SFUR Nd:YAG Laser System at Shanghai

(Made by SIOM, Installed in October1995, The same laser for CTLRS)

kHz Lasers for Satellite Ranging

Yue Gao, Ben Greene, Yanjie Wang

Electro Optic Systems Pty Limited (EOS), Queanbeyan, NSW, Australia

Abstract

The design process for KSP laser with a maximum repetition rate of 1 kHz and final laser performance are presented.

1. INTRODUCTION:

Modern SLR has a wide range of performance requirements which impact the laser specification and design. eye safe, automated, and accurate tracking of multiple satellites requires a total systems design approach which can impose severe constraints on the lasers.

The requirement for low bias (hence SPAD detection) results in pressure for very short pulses (few pico-seconds) to provide precision and thus timely normal points. However, high satellites require high pulse energy, mitigating against ultra short pulses.

Satellite traffic density and data production efficiency considerations suggest high repetition rates. In addition, data yield optimisation shows that for any given average power, the repetition rate should be as high as SNR will allow. Finally, millimetre accurate satellites will have a rotation rate which requires kHz ranging rates to accurately resolve range to better than 0.5 mm.

2. SYSTEM DESIGN AND PERFORMANCE

2.1 Selection of Gain Medium

Trade-off study between different gain media, Nd^{3+}: YAG, Nd^{3+}: YLF, Nd^{3+}: YVO, and Ti^{3+}: sapphire was conducted. The second harmonic generation (SHG) and third harmonic generation (THG) of Nd^{3+}: YAG at 532 and 355 nm are nearly as good as 423 nm and 846 nm generated by Ti^{3+}: sapphire laser for two colour satellite laser ranging. Other factors considered include the maximum energy that the gain medium can handle, the maximum available size, cost, how easily the output wavelength can be converted into the eye safe wavelength region. As a result, Nd:YAG is used as the gain medium, with an emission wavelength of 1.064 μm.

2.2 System Description

The laser system consists of an aircraft detection and a satellite ranging sub-systems.

Satellite laser ranging raises significant safety issues since the laser energy used to track satellites presents a significant hazard. The hazard to personnel, in some modes, is significant at distances of kilometres. Thus there is a possibility of hitting an aircraft or helicopter and causing temporary reduction in vision and possibly permanent damage to the eyes. The possibility of eye damage can be eliminated by preceding every ranging pulse with the transmission of a laser pulse at the 'eye-safe' wavelength of 1.57 μm. This pre-ranging pulse leads the ranging pulse by 300 micro-second and presents no hazard at the exit aperture of the ranging telescope. If a reflection of any of the energy of the pre-ranging pulse is detected, the interlock system blocks firing of the following satellite ranging pulse.

The aircraft detection laser comprises a nano-second Nd:YAG laser and an Optical Parametric Oscillator (OPO) which is able to convert non-eye safe pulses at 1.064 μm into nano-second pulses at 1.57 μm which is eye safe according to Laser Safety Standard ANSI Z136.1 (1993).

The satellite ranging sub-system comprises a diode pumped mode-locked laser oscillator, a diode pumped regenerative amplifier, two power amplifiers, a second harmonic generator (SHG) and a third harmonic generator (THG), if applicable, and generates pico-second pulses.

The laser table layout is shown in Figure 1.

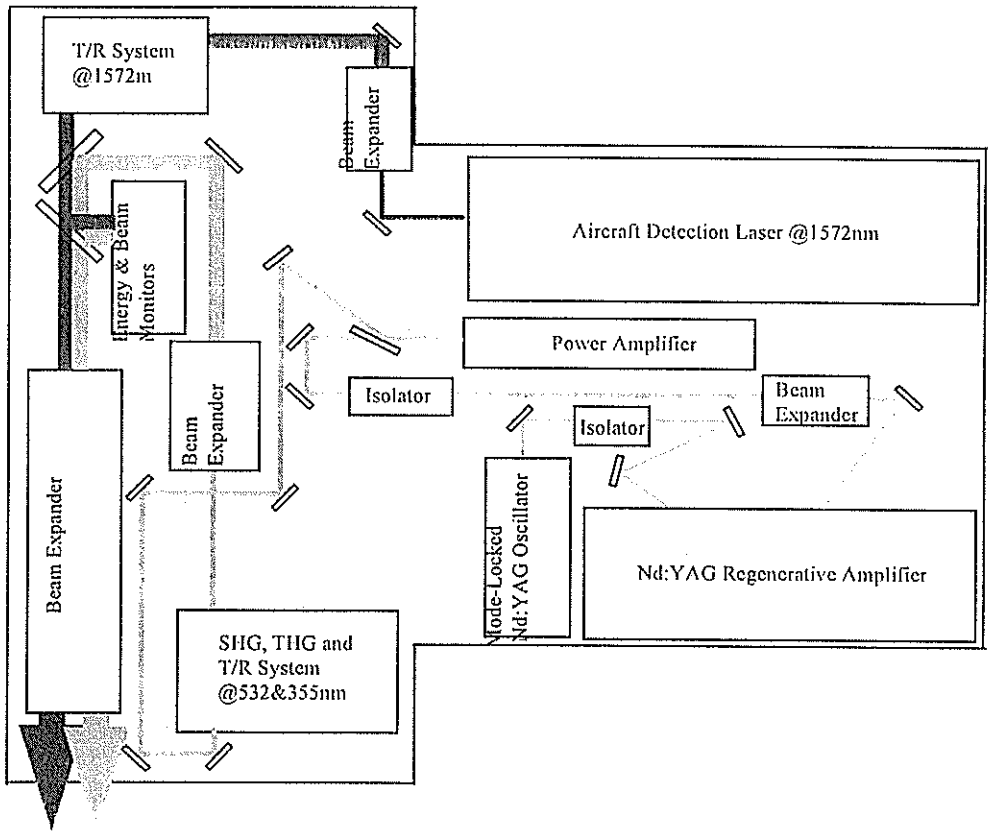

Figure 1. Laser Table Layout

The second harmonic at 532 nm of the Nd:YAG is used as the main wavelength for satellite laser ranging in eye safe and non-eye safe modes. The satellite ranging sub-system allows multi-wavelength output utilising second harmonic at 532 nm and third harmonic at 355 nm.

The laser system is automatically controlled. Changing the repetition rate and energy level, and monitoring of the laser beam quality and energy at 1.57 μm, 532 nm are automated. The temperature of the key laser elements are continuously monitored.

A security system is able to activate a shutdown or recovery of the laser system. Interlocks are provided at the access to the laser area and in the laser system. In case un-authorised personnel enter the laser area the laser system will be shutdown and stay in stand-by mode until security status is clarified.

2.3 Satellite Ranging Sub-system Operating Modes

The sub-system has two operation modes for satellite ranging:

- Reduced transmitted power mode which could be essentially eye safe according to ANSI Z136.1 (1993).
- Full power mode which might not be eye safe

The sub-system is capable of being switched from eye safe to non-eye safe full power mode to maintain data acquisition if weather conditions deteriorate.

2.3.1 Reduced Transmitted Power Mode

In this mode only the oscillator and regenerative amplifier operate and the beam will pass through the power amplifiers while the power amplifiers remain idle. The satellite ranging sub-system is able to produce pulse energy in the range of 50 to 500 μJ at 532 nm and at repetition rates up to 1000 Hz. The energy output will be set so that when converted through a second harmonic generator, the output is in the eye safe range. The design of the regenerative amplifier was one of the challenges at the beginning of the design process in terms of whether a single output pulse and the desired output energy can be achieved at all the specified repetition rates, whilst maintaining good beam quality.

Figure 2 shows the beam profile of the regenerative amplifier output before the beam passes through the power amplifier. Beam profiles with a good Gaussian fit were obtained at 10, 20, 50, 100 and 1000 Hz.

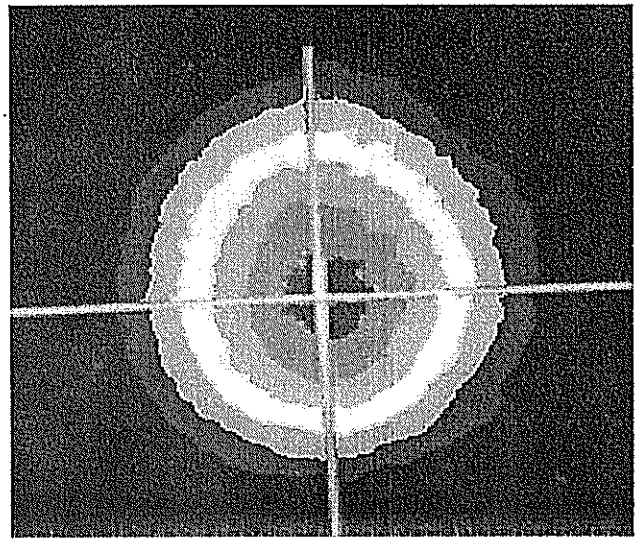

Figure 2. Beam profile of regenerative amplifier output at 10Hz

As shown in Figure 3 the output pulses measured at 10, 100, 500, and 1000 Hz are clean single pulses.

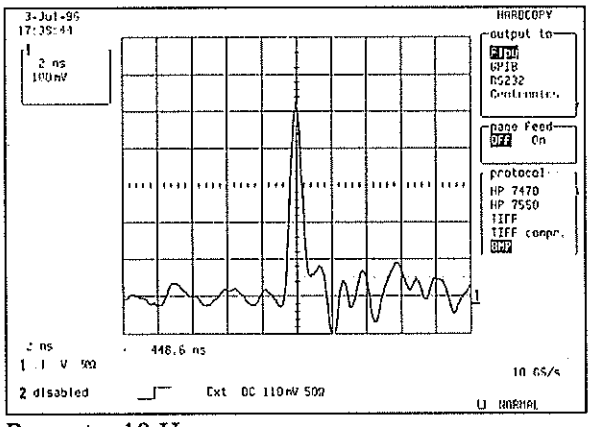

Rep rate: 10 Hz

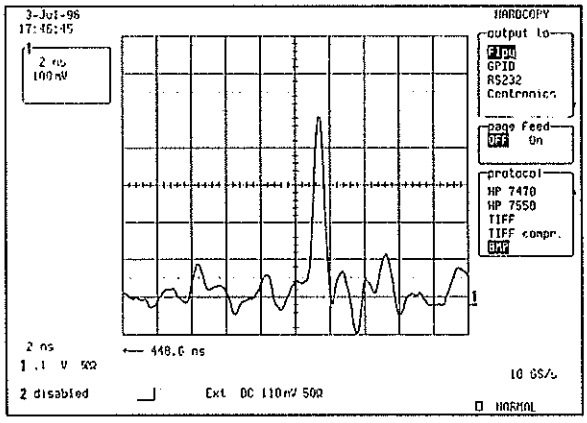

Rep rate: 500 Hz

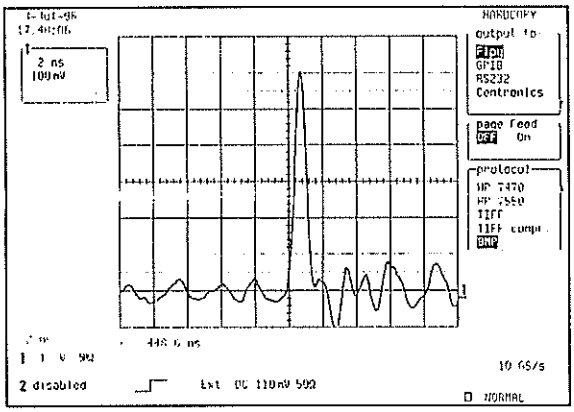

Rep rate: 100 Hz

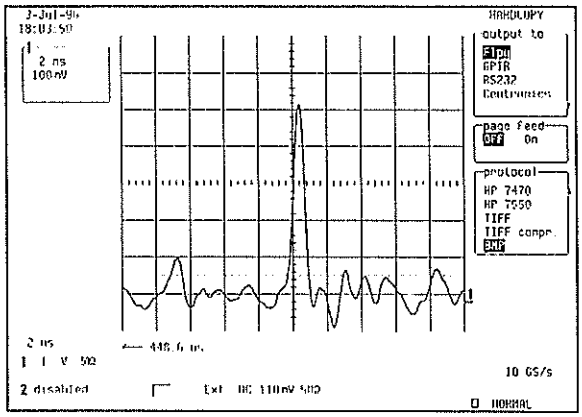

Rep rate: 1000 Hz

Figure 3 Regenerative Amplifier Output Pulses at 10, 100, 500 and 1000 Hz

The pulse width of the regenerative amplifier output was measured using an autocorrelator and is basically the same as the pulse width of the mode-locked oscillator.

It should be mentioned that air turbulence plays an important role in the performance of the regenerative amplifier at a repetition rate higher than 50 Hz. Both the beam quality and energy stability deteriorate when the ambient air turbulence increases. This effect is also very significant to the power amplifier output.

Table 1 shows the design specification and results achieved in the reduced transmitted power mode.

	Design Specification	Results Achieved
Pulse Energy (μJ)	50-500	60-150
Pulse Width (ps)	< 30	< 30
Pulse Repetition Rate (Hz)	10, 20, 50, 100 and 1000	10, 20, 50, 100, and 1000
Mode Structure	> 60% Gaussian fit	> 60% Gaussian fit

Table 1. The design specification and results achieved in the reduced transmitted power mode

The beam profile measured after the beam passes through the power amplifier while it remains idle is shown in Figure 4. Very even energy distribution is obtained.

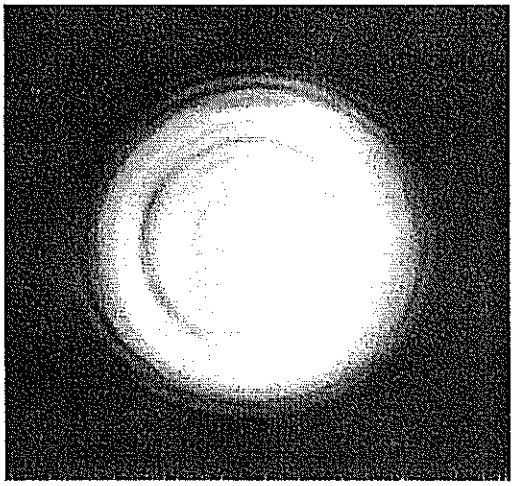

Figure 4. Beam profile after the power amplifiers

2.3.2 Full Power Mode

In this mode the oscillator, regenerative amplifier and power amplifiers operate and the satellite ranging sub-system will produce maximum pulse energy up to 50 mJ at 532 nm after the Second Harmonic Generator (SHG).

The maximum pulse energy at 532 nm is 25 mJ after the Third Harmonic Generator (THG), if applicable. The energy output at 355 nm will be greater than 7 mJ. In this mode the output energies at 532 nm and 355 nm are controlled from the computer. The repetition rate is variable from 10 to 100 Hz in 4 discrete steps at 10, 20, 50 and 100 Hz. The design specification and results achieved are in Table 2.

	Design Specification	Results Achieved
Maximum Pulse Energy (mJ)	≥ 50 @ 532 nm after SHG	≥ 57 @ 532 nm after SHG
	≥ 25 @ 532 nm after THG	≥ 37 @ 532 nm after THG
	≥ 7 @ 355 nm after THG	≥ 10.7 @ 355 nm after THG
Pulse Width (ps)	< 30	< 30
Pulse repetition rate (Hz)	10, 20, 50, 100	10, 20, 50, 100

Table 2. Design specification and results achieved in full power mode

The design of the power amplifier was the second challenge in the design process in terms of whether a good beam quality can be achieved at all the specified repetition rates, since the thermal lensing effect is very significant in this case. As shown in Figure 5, the beam profiles of power amplifiers output measured at 10, 20, 50, and 100 Hz are consistent.

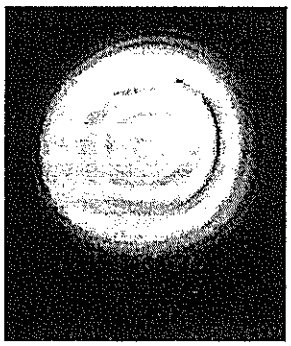

Beam profile of power amplifier output at **10Hz, 70 mJ**

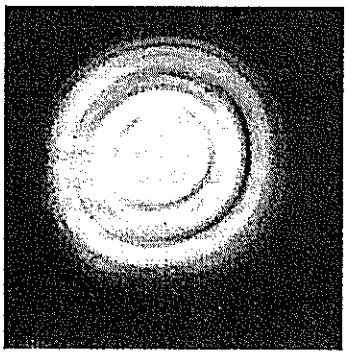

Beam profile of power amplifier output at **20Hz, 70 mJ**

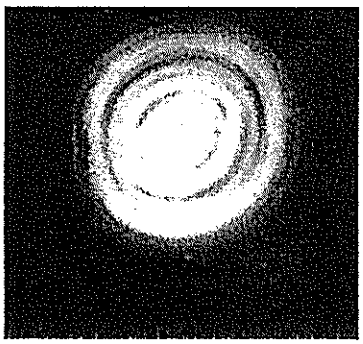

Beam profile of power amplifier output at **50Hz, 70 mJ**

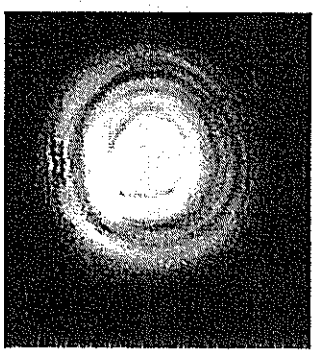

Beam profile of power amplifier output at **100Hz, 30 mJ**

Figure 5. The beam profiles achieved at different repetition rates in full power mode

2.4 AIRCRAFT DETECTION LASER

A repetition rate variable nano-second Nd:YAG laser and an efficient OPO are the two key components of the aircraft detection laser system. Consistent beam quality over a wide range of pulse repetition rates is necessary because the satellite ranging laser is designed to operate at repetition rates between 10 Hz and 1 kHz. Sufficient conversion of pulse energy at a wavelength of 1.06 μm to 1.57 μm by the OPO can ensure that all the necessary altitude at which the aircraft may fly can be covered.

As shown in Table 3, all the design specifications have been achieved.

	Design Specification	Results Achieved
Maximum Pulse Energy at 1.57 μm (mJ)	30	31
Energy Stability (shot to shot)	5%	1.1%
Pulse Width (ns)	2.7 ± 0.2	2.7 ± 0.2
Pulse Repetition rate (Hz)	10, 20, 50, 100	10, 20, 50, 100
Mode Structure	Top hat	Top hat

Table 3. Aircraft detection laser design specification and results achieved

Figure 6 shows the beam profile of OPO output at 1.57 μm. Ideal 'top hat' beam profile is achieved.

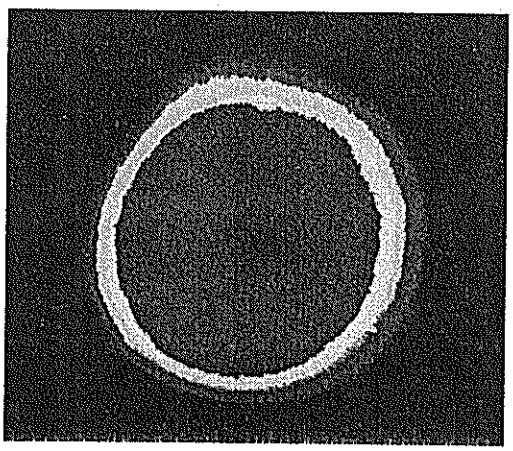

Figure 6. Beam profile of optical parametric oscillator (OPO) output at 10Hz

The pulse width of the OPO signal pulse is basically the same as that of the pump pulse, as shown in Figure 7. A sharp leading edge is obtained with the OPO signal pulse which is very good for ranging.

In conclusion, all the major design specifications have been achieved for kHz satellite ranging.

Figure 7. OPO pump and signal pulses

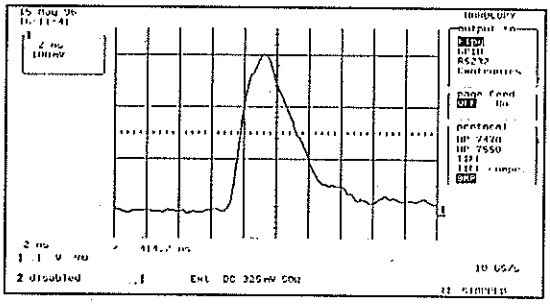

The OPO pump pulse

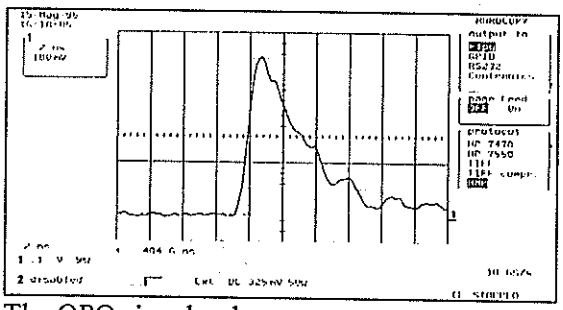

The OPO signal pulse

Eyesafe Systems

Integration of the SLR Radar into the Geophysical Laboratory

H. Donovan, T. Varghese, R. Allshouse,
D. Patterson, R. Suvali, J. Miller

NASA SLR Program
AlliedSignal Aerospace
AlliedSignal Technical Services Corporation
Lanham, Maryland, 20706, USA

J. Degnan

NASA Goddard Space Flight Center
Geosciences Technology Offices

Presented for the 10th International Workshop on Laser Ranging Instrumentation
Shanghai, China
November 11-15, 1996

SLR Radar

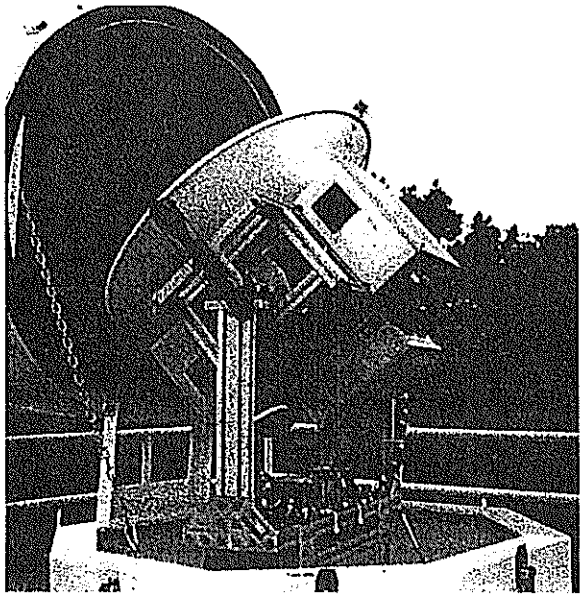

SLR Radar

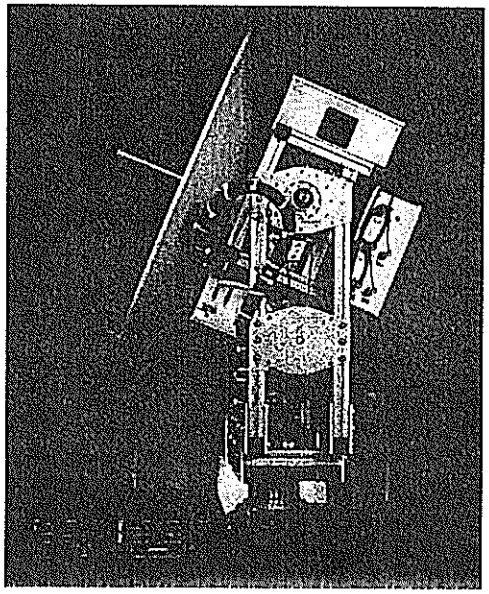

The SLR Radar System

The SLR Radar System provides a means of detecting aircraft before they intersect a transmitted laser beam. Once an aircraft is detected, a control signal is issued which can be used to disable the transmitted laser beam. The aircraft detection capabilities of the SLR Radar are from a quarter of a mile to more than twenty-five miles which covers the ocular hazard distances typically found in current laser ranging systems.

Key Points

- Field proven system
- Very low maintenance
- Adaptable to a variety of interface schemes
- Decreased station operational staffing requirements

SLR Radar Features

High Reliability

- The radar transmitter and receiver are commercial units which have been modified for automated operational functions to obtain optimum receiver tuning and gain.
- The radar is mounted on an ruggedized pedestal constructed of light weight T-slotted extruded aluminum. Pedestal drive is simplified through the use of DC torquer motors with integral tachometers coupled to harmonic drives.

Low Maintenance

- Use of highly reliable components and placing the radar inside an environmentally controlled radome greatly reduces the need for maintenance. Also, mean-time-to-repair is low as the result of inbuilt software diagnostic programs which can detect faults down to the field replaceable board level. Finally, these programs can be accessed remotely via modem for direct factory support or for system monitoring.

SLR Radar Features

Universal Interface

- The microprocessor based Data Translator Board allows the Radar Local Controller to accept a variety of position signals which can be converted for slaving the radar to the host telescope. The DTB can accept parallel or serial protocol and perform coordinate conversions and/or error corrections. The DTB is:

  -TTL compatible
  -Able to support 33 bits of parallel data per axis
  -Supports RS-232 protocol, asynchronous or synchronous
  -Coordinate conversions from BCD or other based systems
  -Minimum of one tenth of one degree position accuracy required from host

SLR Radar Specifications

Power Requirements	
•Voltage, Frequency	100/220VAC,50 - 60 Hz
•Phase	Single Phase
•Power	Consumption 100W
Signal Interfacing	
•Interunit	FSK, RS-232C
•Input from Host	RS-232C, Binary, BCD
RF Characteristics	
•Center Frequency	9410 MHz +/-30 MHz
•Peak Power Output	4kW (2.1 watts CW)
•PRF	750 Hz
•Pulse Width	700nsec
IF Amplifier	
•Center Frequency	60 MHz
•Bandwidth	3 MHz at -3 dB
•Overall Noise Figure	<6dB
Antenna	
•Diameter	33 inches
•Gain @ 9.4GHZ	36.5 dB
•Beam Width @ 3 dB	2.8 degrees
•First Side Lobe	-23 dB @ 12 degrees
•Second Side Lobe	-30 dB @ 20 degrees
Pedestal	
•Azimuth Rotation	Unlimited
•Elevation Rotation	0 to 180 degrees
•Position Resolution	0.09 degrees (both axis)

The Effects of SLR Radar Emissions Upon Radio Astronomy Observatories

Quantitative analysis has shown:

- **SLR Radar isotropic radiation emissions are well below the ITU VLBA guidelines for near and far distances**
- **SLR Radar isotropic directional emissions lie outside the allocated band for VLBA radio astronomy**

Radio Astronomy Allocations Within VLBA Bands

VLBA Band	Radio Astronomy Allocated Band	Allocation Status	Sharing Services R.A. Lines, etc.
312 - 342 MHz	322 - 328.6 MHz	P	Fixed, Mobile Deuterium line
596 - 626 MHz	608 - 614 MHz	P S	Region 2 Regions 1, 3 except African Broad-casting Area (Alloc. band was U.S. TV Ch. 37)
1350 - 1750 MHz	1400 - 1427 MHz 1610.6 - 1613.8 MHz 1660 - 1670 MHz 1718.8 - 1722.2 MHz	P (Pas) P P S	Hydrogen line Mobile Sat. Serv. Radio-determination Sat. Serv., OH line Fixed, Mobile, Met. Sat., OH line Fixed, Mobile, OH line
2150 - 2350 MHz	None		2290 - 2300 MHz Space Res., Deep Sp., Sp.-to-Earth
4600 - 5100 MHz	4800 - 4990 MHz 4990 - 5000 MHz	S P	Fixed, Mobile, ^{2}HCO line Fixed, Mobile
8000 - 8800	None		8400 - 8500 MHz, Space Res., Sp.-to-Earth
10.2 - 11.2 GHz	10.6 - 10.68 GHz 10.68 - 10.7 GHz	P P (Pas)	Fixed, Mobile
12.0 - 15.4 GHz	14.47 - 14.5 GHz 15.35 - 15.4 GHz	S P (Pas)	Fixed, Fixed Sat., Mobile H_2CO line
21.7 - 24.1 GHz	22.21 - 22.5 GHz 23.6 - 24.0 GHz	P P (Pas)	Fixed, Mobile, ^{2}B line NH_3 lines
41.0 - 45.0 GHz	42.5 - 43.5 GHz	P	Fixed, Fixed Sat., Mobile SiO lines

"P" Primary Allocation; "S" Secondary Allocation; "Pas" Passive Band

ITU Guidelines vs SLR Radar Spurious Emission

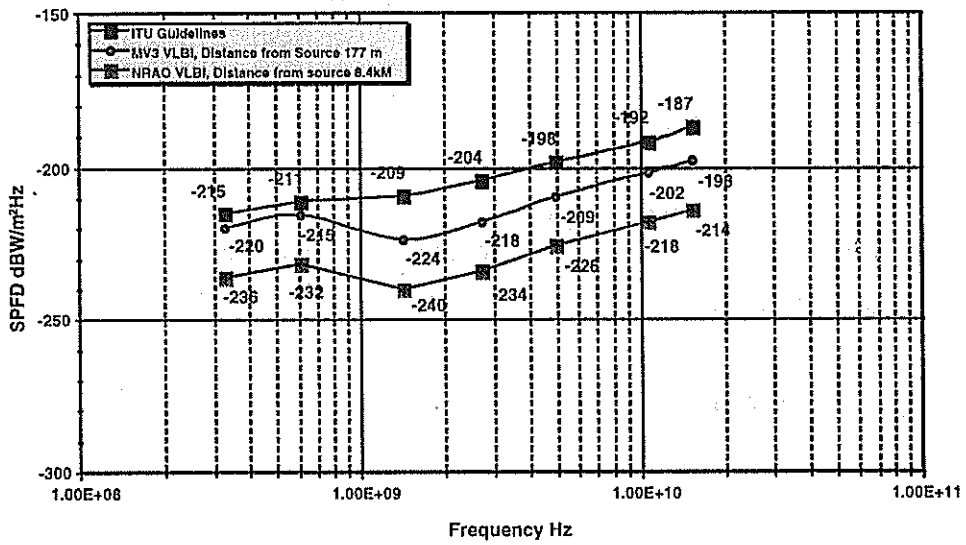

AlliedSignal AEROSPACE

SLR Radar Isotropic Spectral Emissions

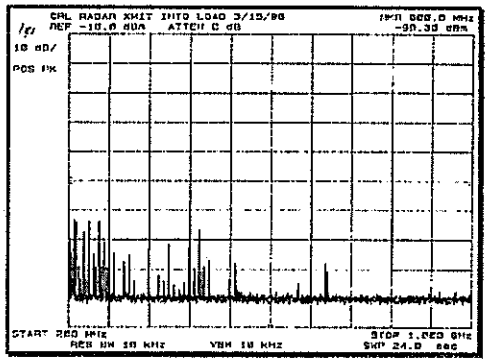

200MHz to 1GHz

1GHz to 2GHz

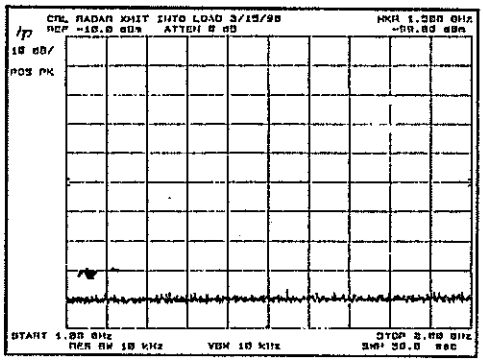

AlliedSignal AEROSPACE

SLR Radar Isotropic Spectral Emissions

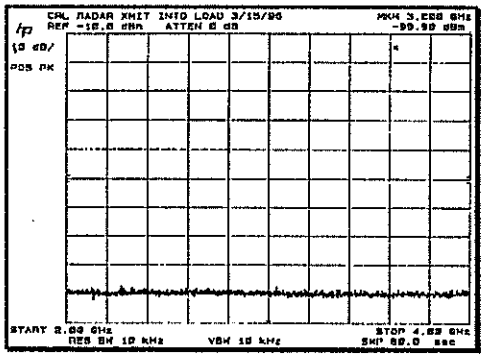

2GHz to 4GHz

4GHz to 6GHz

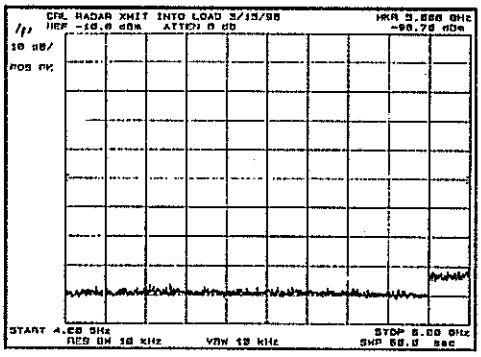

AlliedSignal AEROSPACE

SLR Radar Isotropic Spectral Emissions

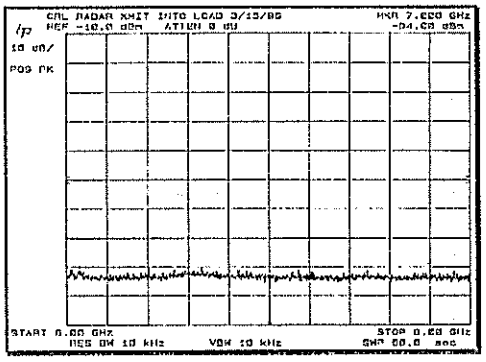

6GHz to 8GHz

8GHz to 10GHz

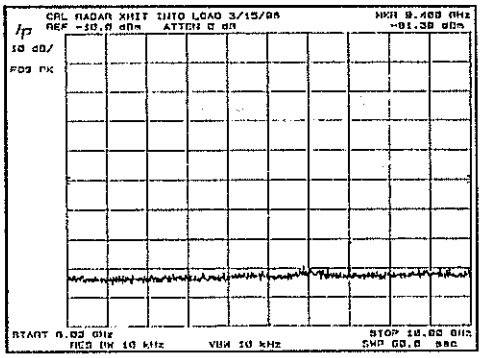

AlliedSignal AEROSPACE

SLR Radar Isotropic Spectral Emissions

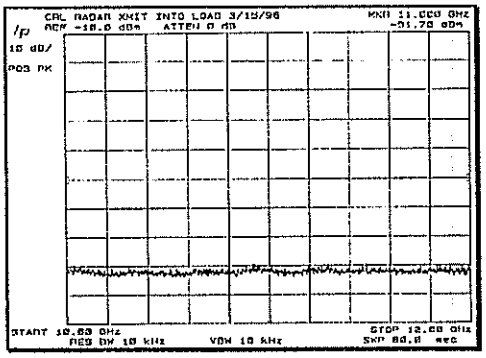

10GHz to 12GHz

12GHz to 14GHz

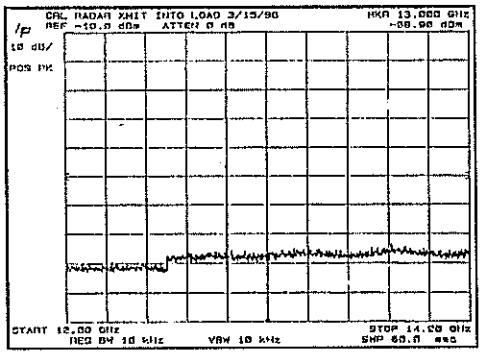

SLR2000: AN INEXPENSIVE, FULLY AUTOMATED, EYESAFE SATELLITE LASER RANGING SYSTEM

John Degnan, Jan McGarry, Thomas Zagwodzki
NASA Goddard Space Flight Center

Paul Titterton, Harold Sweeney
EOO, Inc.

Howard Donovan, Michael Perry, Brion Conklin, Winfield Decker
AlliedSignal Technical Services Corporation (ATSC)

Jack Cheek, Anthony Mallama, Peter Dunn
Hughes STX

Randall Ricklefs
University of Texas

ABSTRACT

SLR2000 is an autonomous, unmanned satellite laser ranging station with an expected single shot range precision of about one centimeter and a normal point precision better than 3 mm. The system will provide continuous 24 hour tracking coverage and reduce capitalization, operating and maintenance costs by an order of magnitude relative to current outlays. Computer simulations have predicted a daylight tracking capability to GPS and lower satellites with telescope apertures under 50 cm and have demonstrated the ability of our current autotracking algorithm to extract mean signal strengths as small as 0.0001 photoelectrons per pulse from noise.

The dominant cost driver in present SLR systems is the onsite and central infrastructure manpower required to operate the system, to service and maintain the complex subsystems (most notably the laser), and to ensure that the transmitted laser beam is not a hazard to onsite personnel or overflying aircraft. In designing the SLR2000 system, preference was given to simple hardware over complex, to commercially available hardware over custom, and to passive techniques over active resulting in the prototype design described here. This general approach should allow long intervals between maintenance visits and the "outsourcing" of key central engineering functions on an "as needed" basis. In unassembled "kit" form, the per system hardware costs for SLR2000 are expected to be less than $300K. A fully assembled and tested field system should be reproducible for about $500K per system in quantities of eight or more.

SLR2000 consists of seven major subsystems: (1) Time and Frequency Reference Unit; (2) Optical Head; (3) Tracking Mount;(4) Correlation Range Receiver; (5) Meteorological Station; (6) Environmental Shelter with Azimuth Tracking Dome; and (7) System Controller. The Optical Head in turn consists of a 40 cm aperture telescope and associated transmit/receive optics, a Q-switched microlaser operating at 2KHz, a start detector, a quadrant stop detector, a CCD camera for automated star calibrations, and spectral and spatial filters. The current design status of each of these subsystems is addressed in the present paper.

1. INTRODUCTION

The feasibility of a fully autonomous, satellite laser ranging system operating at visible wavelengths with eyesafe energies (on the order of 100 μJ for a 30 to 40 cm telescope aperture) and high repetition rates (on the order of 2 KHZ) was first postulated by Degnan[1], and some early concepts and analyses were described at the last SLR Workshop in Canberra [2,3]. The present paper gives a progress report on the engineering design of the overall SLR2000 system, while four companion papers in these proceedings describe in more detail the microlaser transmitter[4], the correlation range receiver algorithms and analysis [5], the results of recent system simulations [6], and the feasibility of SLR2000 ranging over interplanetary distances to an asynchronous laser transponder incorporating many of the SLR2000 subsystems [7]. The simulations, which are based on realistic models of the hardware and atmospheric channel, suggest that ranging to GPS in daylight is feasible with a telescope aperture as small as 40 cm[5,6].

When designing an autonomous and inexpensive system such as SLR2000, it is necessary to make certain assumptions regarding the environment into which it will be placed. Specifying an environment which is unrealistically isolated and forbidding will only drive up the fabrication and operational costs. The typical SLR2000 site is anticipated to have: (1) generally good weather and visibility; (2) good site stability with access to bedrock; and (3) easy access to basic services such as stable commercial power, communications (telephone, Internet), transportation (airports), "industrial level" security (i.e. limited personnel access), and janitorial/custodial services.

To keep construction and maintenance costs at a minimum, we have also adopted the following design philosophies:

(1) Use off the shelf commercial components wherever possible; this allows rapid component replacement and "outsourcing" of engineering support;

(2) Use TLRS-size telescopes; this constrains the cost of the optical tracking mount and telescope;

(3) For low maintenance and failsafe reliability, use passive techniques and components rather than active ones (e.g. eyesafe beams vs active radars, passive T/R switches, passively Q-switched lasers and passive multipass amplifiers).

Adherence to these fundamental assumptions and design philosophies have led to the SLR2000 design described here.

2. MAJOR SUBSYSTEMS

SLR2000 is composed of the following seven major subsystems:

Time and Frequency Reference Unit
Optical Head
Tracking Mount
Correlation Range Receiver
Meteorological Station
Environmental Shelter with Azimuth Tracking Dome
System Controller

In the following subsections, the status of each subsystem will be described.

2.1 Time and Frequency Reference Unit

The Hewlett Packard Model HP58503A GPS Time and Frequency Reference Receiver has been selected to serve as the station clock and frequency reference. The unit consists of a GPS-disciplined Quartz crystal oscillator and provides clock outputs at both 1 Hz and 10 MHz.

The one pps output has a pulse-to-pulse jitter of less than 750 psec with only one GPS satellite in view. Its time accuracy, when locked to GPS, is specified at less than 110 nsec with respect to UTC (i.e. the master clock at the US Naval Observatory in Washington, DC). In the prolonged absence of a GPS signal (unlocked), the accumulated time error is less than 8.6 μsec in 24 hours. The 10 MHz output has a Root Allen Variance, when locked to GPS, of 1.5×10^{-11} for a 100 msec sample time typical of artificial satellite laser ranging. Thus, ranging errors introduced by variations in the clock frequency will be submillimeter for all satellites up to and including the highest satellites, GPS, GLONASS, and ETALON.

2.2 Optical Head

The optical head consists of the telescope, a passive transmit/receive switch , a Q-switched microlaser operating at 2KHz, a start diode, a quadrant stop detector with bias supply and gating circuit, a CCD camera for automated star calibrations, and spectral and spatial filters. The outgoing single pulse energy is maximized, within eye hazard constraints, by filling the available telescope aperture with the transmit beam and by using a passive wavelength-dependent transmit/receive switch to separate the transmitted and received beams.

A block diagram of the preliminary optical head design is shown in Figure 1. A 2KHz pulse train from the Nd:YAG microlaser transmitter (21), described in a companion paper in these proceedings [4], is transmitted through a dichroic mirror (16) which passes infrared radiation at 1064 nm and reflects the frequency doubled green radiation at 532 nm. The low energy pulse train is focused by a lens (14) into a doubling crystal (15) and the resulting green radiation at 532 nm is magnified and recollimated by a second lens. After passing through a second dichroic beamsplitter (10), which is coated to pass the majority of the 532 nm radiation, a final diverging lens (8) matches the outgoing green beam to the focal length of the telescope primary for further magnification and collimation of the outgoing transmitter beam. The position of the diverging lens (8) is adjustable under computer control and can be used to correct for thermally induced variations in system focus. The outgoing reflections of the transmit beam off the two beamsplitters are used to monitor the infrared (23) and green (25) energies from the laser and doubling crystal respectively. Filter (24) blocks 1064 nm light from entering the green detector. The green radiation reflected from the satellite retraces the same optical path until it is reflected by the dichroic beamsplitter (16) into the quadrant detector (20) after first passing through a narrowband spectral filter (17), an imaging lens (18), and a variable spatial filter (19). Thus, the combination of dichroic mirror (16) and doubling crystal (15) provides a passive, wavelength-dependent transmit/receive switch [8] which is independent of polarization and allows the entire telescope primary (2) to be used simultaneously by both the transmitter and receiver.

During star calibrations, collimated starlight reflects off dichroic beamsplitter (10), passes through a broadband filter (11) centered on the 532 nm laser wavelength, and is focused by a lens (12) onto a 324 x 242 pixel Electrim Model EDC-1000M CCD array (13) which in turn measures the position of the star and provides pointing error information to the system computer for periodic mount modelling and pointing verification. It is also used to periodically check and

verify accurate system focus by minimizing the star spot diameter. The star calibration optical train provides a field of view of approximately two arcminutes.

The quadrant stop detector lies behind the focal plane so that the incoming reflected laser energy and background noise is spread over the four quadrants, allowing estimation of the position of the satellite in the receiver field of view by the correlation range receiver as described in Subsection 2.4.3.

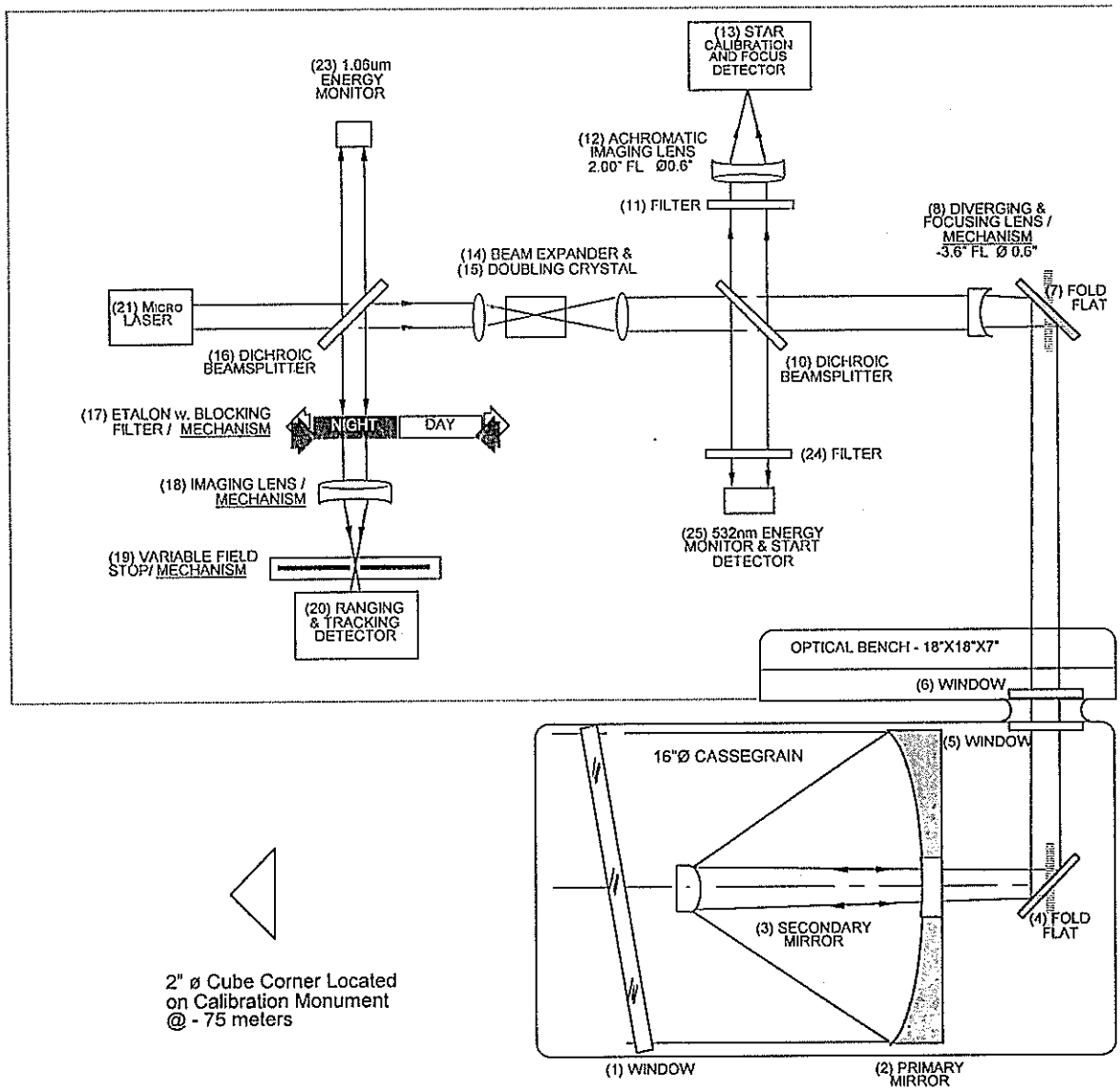

Figure 1: Preliminary block diagram of the SLR2000 optical head.

2.3 Tracking Mount

The optical head will be mounted in one of the Aerotech Model AOM360-D series of tracking mounts, to be selected upon completion of the optical head preliminary design. The latter mounts can accommodate loads up to 50 cm in diameter and are driven by direct-drive DC torque motors. The absence of gear trains and other drive mechanisms eliminates position error contributions due to mechanical hysteresis and backlash. The mount has a high axis positioning accuracy of one

arcsecond, a bidirectional repeatability to one arcsecond, and a low axis wobble, also at the one arcsecond level. Orthogonality of the axes is good to 3 arcseconds, but this error can be taken out with star calibrations and mount modelling. Thermal stability is 0.4 arseconds/°C. The use of Inductosyns, rather than optical encoders, for angle sensing allows electrical cables to be passed from the environmental shelter to the optical head through the center of the azimuth and elevation drive bases. The mount will be equipped with military style electrical connectors and bearing seals to provide additional environmental protection over and above that provided by the dome.

2.4 Correlation Range Receiver (CRR)

The correlation range receiver performs several critical functions which include: (1) precise time of flight (TOF) measurements; (2) the discrimination of signal from noise; and (3) the generation of subarcsecond pointing corrections. The power of the CRR is that it carries out these functions simultaneously using all of the ranging signal available to it. Like the microlaser transmitter, the CRR must operate at KHz rates. To fully understand the design and operation of the CRR, one must first describe the manner in which the TOF measurement is made under these high repetition rate conditions.

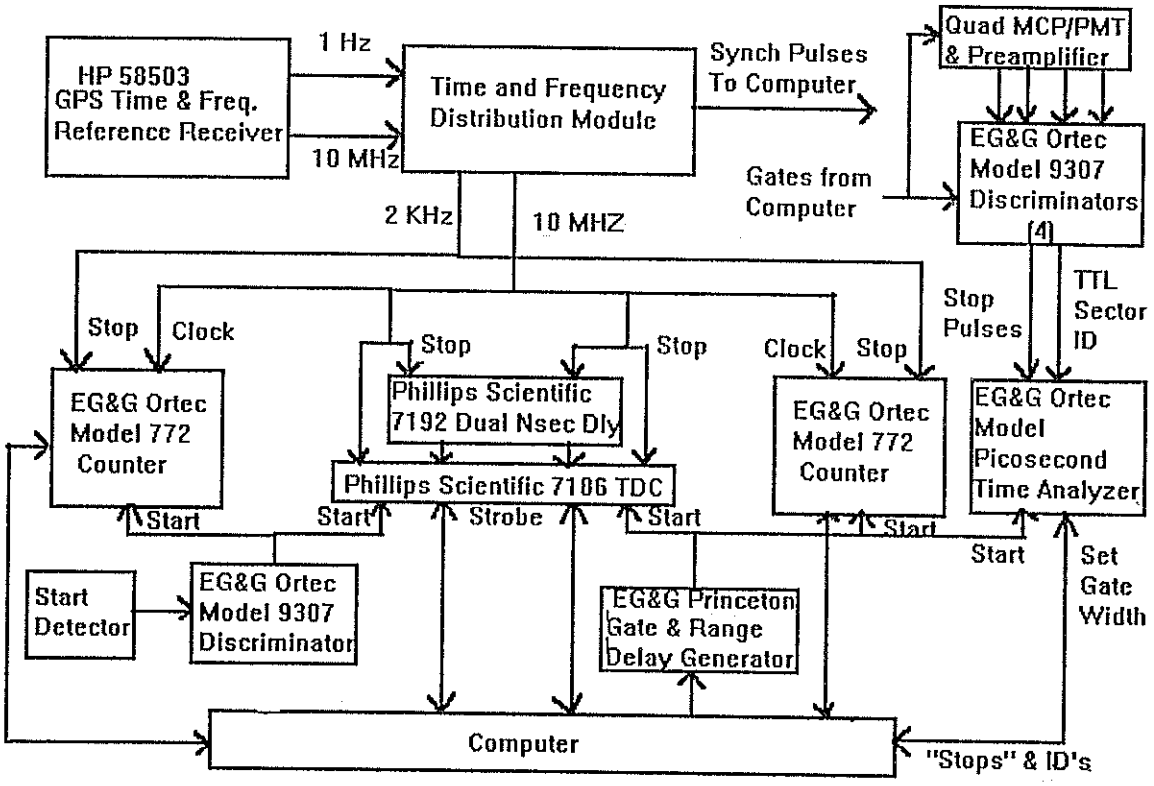

Figure 2: A correlation range receiver configuration designed using commercially available nuclear timing instrumentation.

2.4.1 CRR Time-of-Flight Measurement

Figure 2 shows a baseline design for the CRR which is built up entirely from NIM/CAMAC nuclear timing instrumentation commercially available from three companies: EG&G Ortec, EG&G Princeton and Phillips Scientific. The timing is centered around the nominal 2 KHz fire rate of the microlaser transmitter as illustrated by the timing diagram in Figure 3. The 10 MHz output of the HP Time and Frequency Reference Receiver is used to generate a 2 KHz train of

synchronized clock pulses. Within each 500 μsec fire interval, there will be one "start" pulse and potentially one "stop" pulse plus noise counts. Since each fire interval corresponds to a one-way distance interval of 75 Km, the stop pulse occurring during satellite ranging in the (n+m)th interval originates from the "start" pulse occurring in some earlier (nth) interval. The (n+m)th 2 KHz clock pulse starts the "start" counter for that interval. The arrival of the (n+m)th "start" pulse stops the "start" counter and starts a time to digital converter (TDC) which is then stopped by the next 10 MHz clock pulse. Thus, the temporal position of the "start" laser pulse within the fire interval is determined by adding the "start" counter and "start" TDC vernier outputs. Similarly, the range gate from the EG&G Princeton Research Gate and Time Delay Generator starts a second "stop" counter, a second "stop" TDC, and an EG&G Model 9308 Picosecond Time Analyzer (PTA). The "stop" TDC is stopped by the next 10 MHz clock pulse and the "stop" counter is stopped by the next 2 KHz clock pulse. Adding the outputs of the second TDC vernier and the "stop" counter gives the time interval between the range gate and the (n+m+1)th 2 KHz clock pulse. The PTA is capable of recording multiple events separated by at least 50 nsec and gives the temporal positions of any signal or noise counts occurring within the range window relative to the range gate. The width of the PTA range window is programmable down to a minimum of 80 nsec. The time resolution of the PTA is the window divided by 64,000 or about 1.2 psec for its narrowest window setting. Thus, all "events" occurring within each 500 μsec fire interval are well-positioned with respect to the 2 KHz clock pulses which bound that interval.

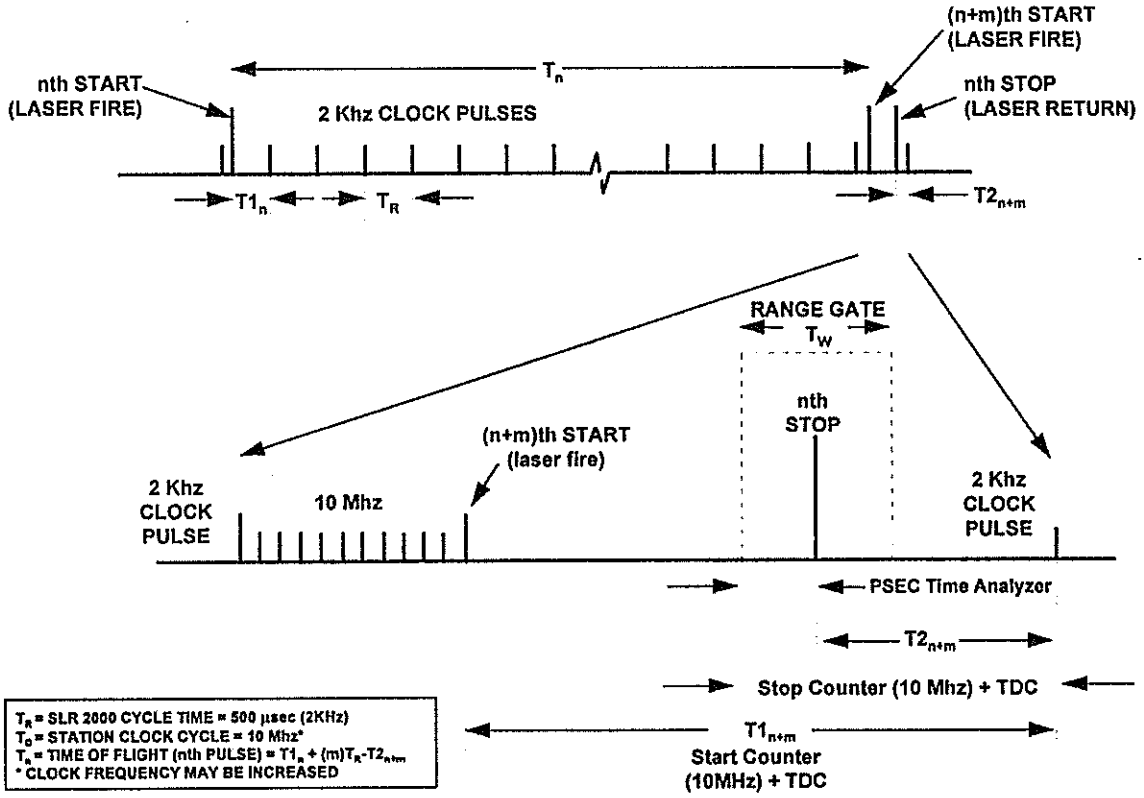

Figure 3: SLR2000 Timing Diagram

To compute the range to the satellite as measured by the nth start pulse, one must now use the following formula (see Figure 3)

$$T_n = T1_n + mT_R - T2_{n+m}$$

where $T1_n$ is the interval between the nth clock pulse and the nth start pulse as measured by the "start" counter and "start" TDC, T_R = 500 μsec is the fire interval between 2 KHz clock pulses, $T2_{n+m}$ is the interval between the (n+m)th signal arrival time and the (n+m+1)th clock pulse as measured by the "stop" counter, "stop" TDC, and PTA, and m is the number of intervening 2 KHz clock cycles between a "start" pulse and its corresponding "stop" pulse and can be computed a priori from our approximate knowledge of the station and satellite positions.

We are looking into possible enhancements which would improve the timing precision of the baseline CRR, such as multiplying the 10 MHz to higher clock frequencies (~100 MHz) or modifying the event timer developed by ATSC for the Matera Laser Ranging Observatory [9] to perform all of the CRR functions.

2.4.2 Post-Detection Poisson Filtering of CRR Range Data

The timing outputs (starts, stops, and noise events) from the CCR are transferred to the SLR2000 ranging computer which assigns them to "time bins" in accordance with satellite-dependent algorithms described in detail in [5] and simulated in [6]. Signal counts from the satellite would be bunched in a narrow time interval whereas dark current or background noise counts would be spread over the full width of the range gate. Put simply, the ranging computer looks at the number of counts in each time bin to identify the probable presence of the signal, applies an iterative filter, computes an updated range and time bias, and gradually reduces the range gate width to decrease the number of noise counts in future frames.

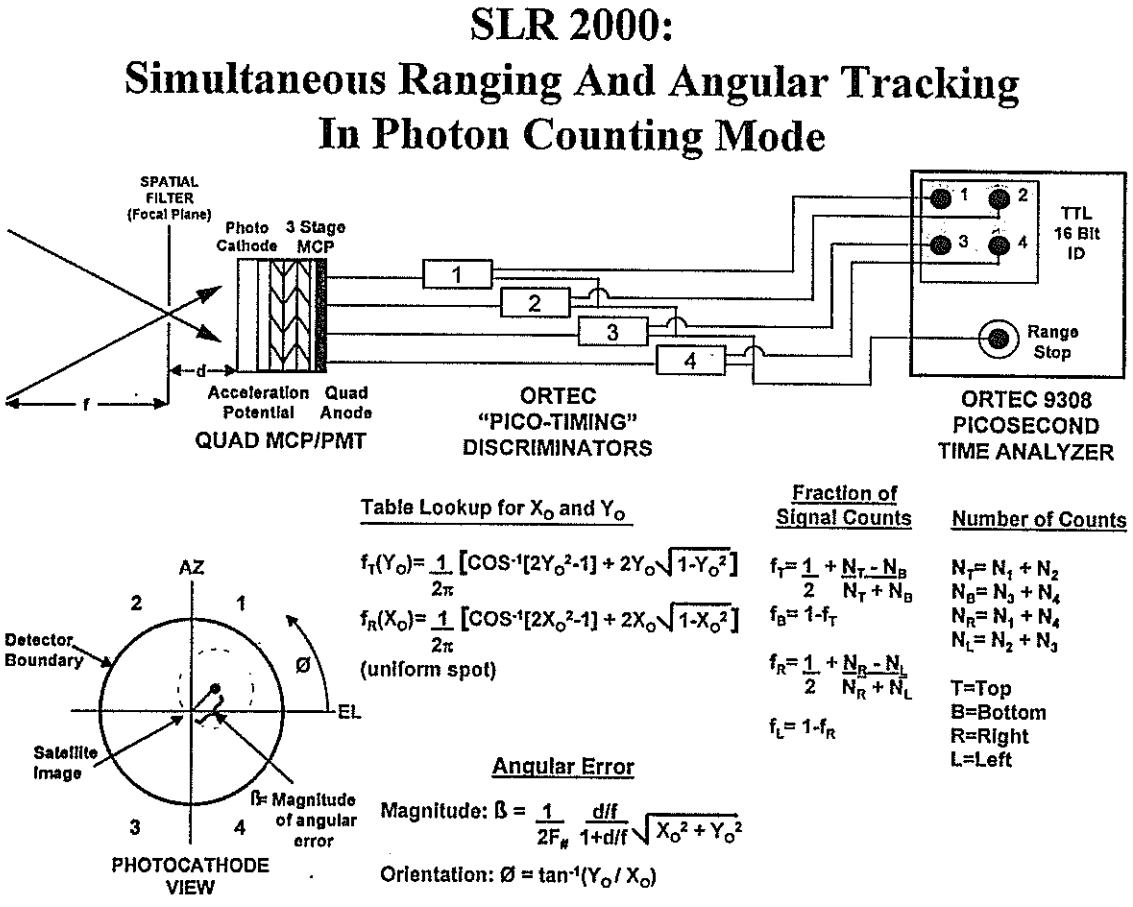

Figure 4: Correcting pointing error in the photon counting mode using the correlation range receiver.

2.4.3 CRR Derivation of Subarcsecond Pointing Error

As mentioned in Section 2.2, the stop detector is placed behind the telescope focal plane so that the satellite image is enlarged and distributed over the four quadrants as in Figure 4. Following a photon event in one of the quadrants, the corresponding anode produces an electronic pulse which is input to one of four EG&G Ortec Model 9307 "Pico-timing Discriminators". The latter device produces both a fast ECL logic "stop" pulse, which is summed with the other three discriminator channels and input to the PTA timing circuitry, and a second TTL logic pulse, which is input to a second circuit in the PTA and identifies which of the four quadrants the timing signal came from. One would expect, on average, that noise counts would be equally distributed among the four quadrants whereas, if there were a small pointing error, signal counts would pile up preferentially in one or more quadrants. Following the filtering of noise counts based on time of arrival by the postdetection Poisson filter, a subarcsecond pointing angle correction can be computed by adding or subtracting the residual counts in each quadrant using the algorithms summarized in Figure 4.

2.5 Meteorological Station

The meteorological subsystem measures pressure, temperature, and relative humidity with the requisite accuracy for millimeter ranging. In order to protect the system from the external environment and extend component lifetimes, the meteorological subsystem also monitors: (1) wind speed and direction ; (2) the presence, type, and accumulation of various forms of precipitation (rain, snow, etc.); (3) local visibility out to 50Km; and (4) cloud cover.

The meteorological station consists of four principal parts, three of which are commercially available:

(1) Paroscientific MET3-1477-001 Pressure, Temperature, and Relative Humidity Monitor

Pressure: Range 800 to 1100 mbar; Accuracy ~0.1 mbar; Stability < 0.1 mbar/year
Temperature: Range -40 to 70°C; Accuracy < 0.5°C; Stability < 0.1°C/year
Relative Humidity: Range 0 to 100%; Accuracy $\pm$2%, Stability<1%/year

(2) Vaisala FD12P Precipitation and Visibility Sensor

The FDP12 consists of an optical transmitter, receiver, controller, and a capacitive rain sensor. It utilizes an optical forward-scatter sensor that not only sees fog but also distinguishes between precipitation particles. An ambient temperature sensor is included to increase the reliability of precipitation type assessment. The unit measures visibility optically from 10 m to 50 Km and the
type, intensity, and accumulation of precipitation.

(3) Belfort 200 Wind Monitor

Wind speed is sensed by an 18 cm diameter helicoid propellor. A six pole permanent magnet attached to the shaft induces a sinusoidal AC signal in a stationary coil with a frequency proportional to the wind speed. Wind direction is sensed by rotation of the sensor on its vertical shaft Vane position is transmitted by a 10K ohm conductive potentiometer. With a reference voltage applied to the potentiometer, an analog voltage proportional to azimuth angle is produced as output.

Wind Speed: Range 0 to 135 mph; ±0.6 mph
Wind Direction: Range 0 to 360°; Accuracy ±3°

(4) Cloud Sensor

Presently we are looking at two very distinct options for detecting clouds. One approach is to add a crude lidar channel to the receiver to monitor the laser backscatter from clouds, but this requires the system dome to be open and the laser ranging system to be operating. A potentially more attractive option is to have a CCD camera outside the dome view the hemispherical sky from a convex mirror. In daylight, the sky would be viewed alternately through blue and green filters (blue sky = clear) whereas, at night, approximate cloud cover would be inferred from the presence or absence of low magnitude stars. In both cases, the image would be used in determining whether or not to open the dome, and, if partially clear, which parts of the sky should be avoided in scheduling satellite tracks.

2.6 Environmental Shelter with Azimuth Tracking Dome

The Aerotech tracking mount will be positioned (three-points of contact) and leveled, using two attached differential leveling bubbles, on a central concrete monument. A mount model, updated by frequent star calibrations, further defines and maintains the system orientation and alignment. The telescope and calibration targets will be more than 2 meters off the ground, making access by unauthorized personnel difficult.

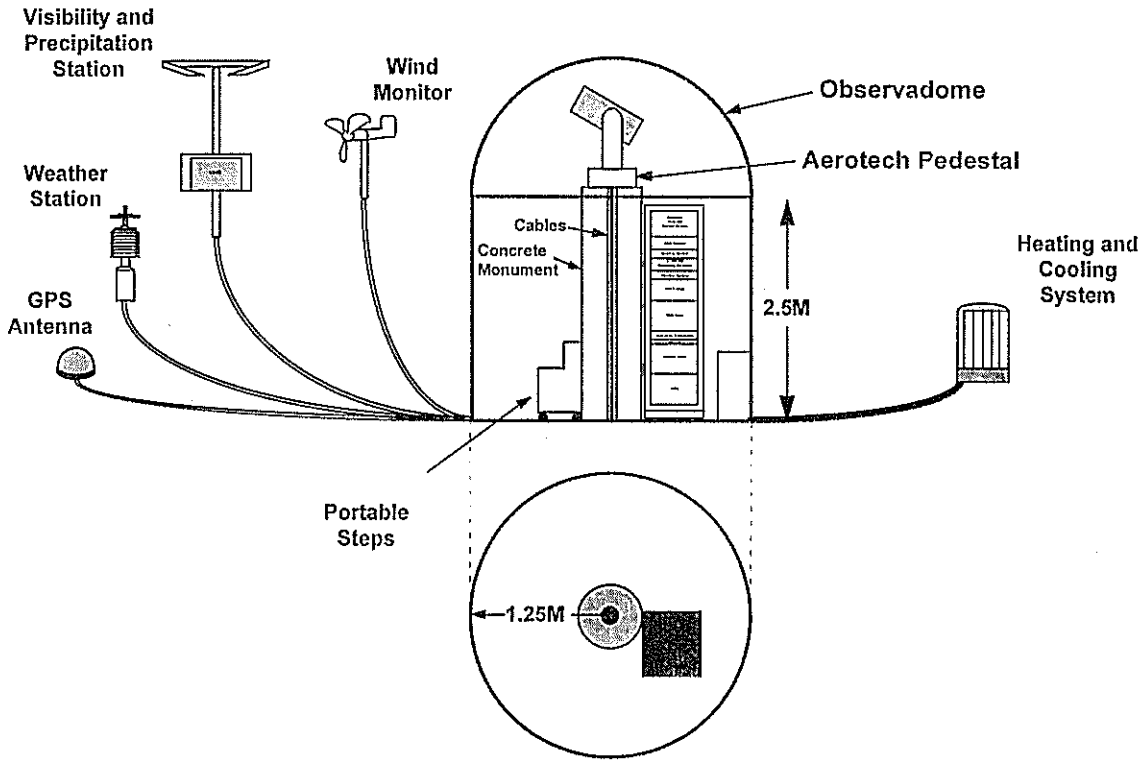

Figure 5: SLR2000 field installation concept.

The central monument sits inside an environmental shelter and a protective astronomical dome as in Figure 5. The interior of the environmental shelter is maintained at nominal room temperature (≅23°C) by an external heat pump. This stabilizes the timing electronics, provides a source of heated dry air for preventing condensation on the optics, helps to stabilize the temperature of

certain elements in the optical head, and provides a comfortable workplace for visiting maintenance personnel. To allow the optical head and tracking mount to follow the external ambient temperature and thereby minimize thermal gradients in the optical head during system operation, the heated (or cooled) "electronics room" is thermally isolated from the dome area by a removable "ceiling". A technician can gain access to the optical head and tracking mount by removing the "ceiling" and using a set of portable steps permanently stored in the shelter. Diagnostic tests can be performed onsite by plugging a laptop computer into the central computer system. Internet and telephone communications are also provided in the shelter. A modem provides a backup means of communicating with the system when the Internet is inaccessible.

The 2.5 meter dome is built by Observadome™ and has a motorized slit (shutter) and azimuth drive. Both are under computer control and the dome azimuth drive is slaved to the Aerotech tracking mount azimuth.

Electrical signal and power cables are passed from the electronics rack through the center of the Aerotech azimuth stage Inductosyn , through one arm of the mount yoke, and through the elevation Inductosyn in order to power the optical head and tracking mount and to extract the ranging, star calibration, and housekeeping signals. Small hoses bearing filtered, heated (or cooled) dry air from the electronics room can also pass through the same path as necessary to prevent condensation on optics and to provide a heat exchange medium for temperature-sensitive elements in the optical head (e.g. diode pump lasers, spectral filters, etc) .

It is expected that the shelter will be equipped with additional inexpensive security devices for automatically detecting and reporting threats to system security, via Internet and/or recorded phone messages. These might include motion and intrusion sensors and surveillance cameras for detecting and reporting unauthorized personnel in the vicinity, thermal sensors for detecting heat pump failure, etc.

2.7 System Controller

The SLR2000 computer consists of three Pentium-based processors, two in a VME backplane and the third in a PC/ISA crate. The VME bus was chosen for its higher bus speed (40MB/sec), while the ISA bus was needed to handle specialized interface cards for the camera, Picosecond Time Analyzer, and mount. The ISA computer functions simply as an Input/Output processor, passing data to and from the VME computers via shared memory. The VME processors perform all of the decision making, data analysis, and external communication. One of these processors, called the "Pseudo-Operator", performs the functions of a human operator, making decisions on whether the weather permits opening the dome and tracking, which satellite should be tracked, and whether the returns in the ranging window are signal or noise. The Pseudo-Operator also monitors the system temperatures and voltages, and acts to protect the system if it detects system health or safety problems. The second VME processor, called the Analysis CPU, computes the Normal Point data from the raw tracking/ranging data and sends this data out to a central archive. This processor also gets predictions for the system, and converts it to the appropriate format. Information is communicated between the two VME processors via file and memory sharing. Both processors are expected to be running the Lynx Real-Time Operating System.

Human interaction with the SLR2000 system requires communicating with the Analysis CPU through the internet. A laptop PC running a special software package will allow personnel to monitor the operation of the system via graphical displays, get information from the system to analyze off-line, run diagnostic tests, and change system parameters.

3. SUMMARY

SLR2000 is an autonomous, unmanned satellite laser ranging station with an expected single shot range precision of about one centimeter and a normal point precision better than 3 mm. The system will provide continuous 24 hour tracking coverage for all satellites up to and including GPS and will reduce capitalization, operating and maintenance costs by an order of magnitude relative to recent outlays. The dominant cost driver in present SLR systems is the onsite and central infrastructure manpower required to operate the system, to service and maintain the complex subsystems (notably the laser), and to ensure that the transmitted laser beam is not a hazard to onsite personnel or overflying aircraft. In designing the SLR2000 system, preference was given to simple hardware over complex, to commercially available hardware over custom, and to passive techniques over active resulting in the prototype design described here. This general approach should allow long intervals between maintenance visits and the "outsourcing" of key central engineering functions on an "as needed" basis. In unassembled "kit" form, the per system hardware costs for SLR2000 are expected to be roughly $300K. A fully assembled and tested field system, including shelter and monument, should be reproducible for about $500K per system in quantities of eight or more.

REFERENCES

1. Degnan, J.J., "SLR2000" in Satellite Laser Ranging in the 1990's : Report of the 1994 Belmont Workshop, NASA Conference Publication 3283, pp. 101-106, 1994.

2. Degnan, J. J. , "SLR2000: An Autonomous and Eyesafe Satellite Laser Ranging Station", Proc. Ninth International Workshop on Laser Ranging Instrumentation, pp. 312-323, Canberra, Australia, November, 1994.

3. McGarry, J. , J. J. Degnan, P. Titterton, H. Sweeney, B. P. Conklin, and P. J. Dunn, "Automated Tracking for Advanced Satellite Laser Ranging Systems", Proc. Spring SPIE Meeting, SPIE Vol. 2739, pp. 89-103, Orlando, FL, April 10-11, 1996.

4. Degnan, J. J., "Optimal Design of Q-switched Microlaser Transmitters for SLR", these proceedings.

5. Titterton, P., and H. E. Sweeney, "Correlation Processing Approach for Eyesafe SLR2000", these proceedings

6. McGarry, J., "SLR2000 Performance Simulations", these proceedings

7. Degnan, J. J. , "Compact Laser Transponders for Interplanetary Ranging and Time Transfer", these proceedings

8. Hamal, K. and B, Greene,"Second Harmonic Generator T/R Switch" , these proceedings.

9. Selden, M., C. Steggerda, R. Stringfellow, D. McClure, C. B. Clark, and G. Bianco, "Instrument Development and Calibration for the Matera Laser Ranging System ", these proceedings.

Correlation Processing Approach for Eyesafe SLR 2000*

Paul J. Titterton and Harold E. Sweeney
EOO, Inc.
269 North Mathilda Avenue, Sunnyvale, CA 94086-4830
(408) 738-5390; FAX: (408) 738-5399. e-mail: EOOInc@aol.Com
*Supported in part by NASA Goddard Space Flight Center

The SLR 2000 design, discussed in the Canberra meeting two years ago, employs a high PRF / low energy-per-pulse 532 nm transmitter beam which is expanded to fill a large aperture. The system is also designed to be capable of fully unattended operation. The following table summarizes the top level electro-optical parameters for the SLR-2000, as presently configured.

Transmitter Side	Receiver Side
Wavelength: 532 nm	Filter Bandpass : 1.2 Å (50% throughput) [B_{opt}]
Energy Per Pulse: 207 μjoule [$E_p\gamma_t$]	Quantum Efficiency: 40 % [η]
Pulse Repetition Frequency: 2000 Hz	Total Dark Counts: < 10^4 /second @ 20 °C
Pulsewidth: 140 psec	Resolution: < 100 psec
Transmitter Aperture: 50 cm diam. [D_t]	Receiver Aperture: 50 cm diam. [D_r]
Optical Transmission: > 80 % [γ_t]	Optical Transmission: > 30 % [γ_r]
Half Angle Beamwidth: 20 μrad [θ_t]	Half Angle Beamwidth: 20 μrad [θ_r]
Power Distribution - At Aperture: Top Hat - Far Field: Airy Disc	Field-of-View : Sharp Edged Uniform Sensitivity
Pointing Jitter: < 5 μradians (nominal)	Boresight with Transmitter: < 5 μradians
Pointing Offset: < 5 μradians (nominal)	Special: Quadrant Detector

System eye safety is based on ANSI Z136.1-1993, Section 8.2, Table 5 and the accompanying Errata Sheet. The governing equation is

$$C_{\#}MPE = \frac{E_p\gamma_t}{\pi D_t^2/4} \qquad (1)$$

for C# = Multiple pulse correction to the allowable single pulse MPE

$= \left[PRF(Exposure\,Duration)\right]^{-1/4}$, for PRF = laser pulse repetition frequency (Hz),

MPE = Maximum Permissible single pulse/single exposure energy density,

C# = $\left[PRF(0.25)\right]^{-1/4}$ (in the green, for short pulses) = 0.2115 for PRF = 2000 Hz,

MPE = 5 (10^{-7}) joules/cm^2 (in the green for short pulses).

Evaluating Equation 1 we find in general that

$$E_p\gamma_t = 8.305\left(10^{-8}\right)D_t^2 \quad \text{joules.} \qquad (2)$$

The 50 cm aperture case is used in the baseline SLR-2000 configuration, and corresponds to the 207 μjoule value for energy per pulse at the aperture.

The range equation (cf. Bibliography) is

$$n_{pe}^{s} = \eta\left(\frac{E_p \gamma_t}{h\nu}\right)\tau_a \tau_{c\ell}\left(\frac{\sigma}{\pi\theta_t^2 \gamma_{turb}^2 R^2}\right)\tau_{c\ell}\tau_a \gamma_r \left(\frac{A_r}{\pi R^2}\right)\overline{G} \qquad (3)$$

for n_{pe}^{s} = signal photo-electrons (pe's) per pulse; hν = energy per photon; τ_a = one-way clear atmosphere path transmission; τ_{cl} = one-way cirrus cloud path transmission; σ = satellite optical cross-section; γ_{turb} = impact of atmospheric turbulence on beam divergence; R = range from ground station to target; $A_r = \pi D_r^2/4$; $\overline{G}$ = normalized impact of transmitter truncation and beam shape at the satellite = 0.5.

The elevation angle dependence of the parameters and the optical cross sections are shown in the following table for the Starlette, LAGEOS and ETALON satellites. (The cross sections are ~ 80% of typical values, which provides performance margin.) Equation 3 is evaluated for these parameters in the following figure.

Elevation Angle (Degrees)	Range to Starlette(km)	Range to LAGEOS (km)	Range to ETALON (km)	τ_a	τ_{cl}	γ_{turb}
20	2034	8532	22861	0.75	0.12	1.6
30	1626	7776	21783	0.84	0.36	1.4
40	1362	7164	21006	0.87	0.53	1.27
50	1188	6687	20360	0.89	0.65	1.14
60	1074	6333	19854	0.90	0.72	1.07
70	1002	6089	19491	0.911	0.75	1.03
80	963	5947	19273	0.915	0.77	1.01
90	960	5900	19200	0.92	0.78	1.00
σ (10^6 m^2)	0.52	5.7	48			

Signal Photo-electrons per Pulse vs Elevation Angle

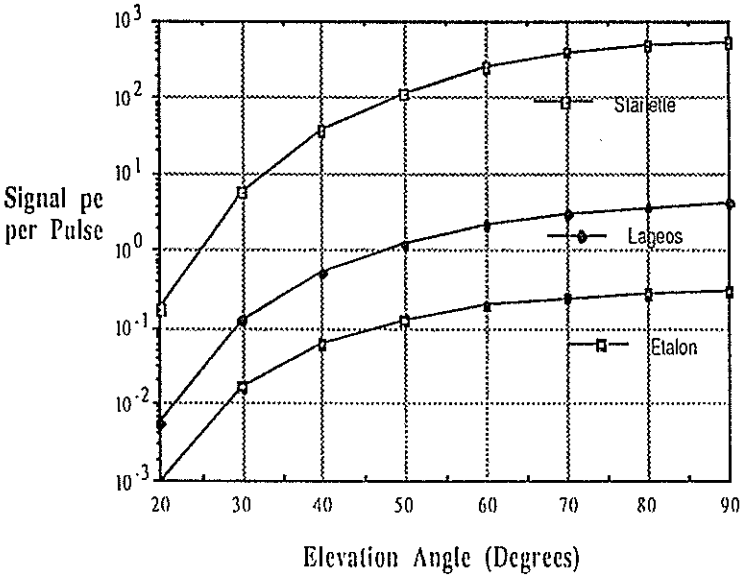

During initial acquisition (at the lowest elevation angles), the signal levels per pulse are very small: 0.159 /Starlette /20°, 0.0054 /LAGEOS /20°, and 0.00165 / ETALON / ~ 22°.

There are three functions which the system must perform at these low signal levels: acquisition, ranging, and tracking/pointing during ranging. The assumed requirements during acquisition are shown in the next table --- the basic acquisition requirement is to narrow the initial range, angle and time uncertainties.

Initial Uncertainties	Starlette	LAGEOS	ETALON	Desired Performance
Angle (μrad)	± 100 x ± 80	± 80 x ± 80	± 80 x ± 80	± 5
Range (nsec)	± 100	± 100	± 100	± 5
Range Rate(nsec/sec)	~ 300	~ 10	~ 1	Target Specific
Time to acquire (sec)	< 10	< 120	< 300	

Ranging must occur with the requirements shown in the next table.

	Starlette	LAGEOS	ETALON
Normal point Precision	~ mm	~ mm	~ mm
Time per Normal Point (sec)	30	120	300

During ranging, slow system pointing errors often occur, and so the final functional requirement is to develop a pointing error from the characteristics of the returned light, and update the pointing angles to enable correcting for these errors.

To meet these requirements at very low signal levels, we use the relative temporal location of the signal pulses over many intervals. The concept is illustrated in the following figure. The basic insight is that signal pulses will reside in time correlated "bins" within the gates, while noise counts will be randomly distributed.

n_{bin} = # of pulse resolution intervals per gate,

N^s_{pe} = mean # of signal pe after K gates

K = # of gates before detection decision; Frame = K range gates

$T = n_{bin}(\Delta t)$ and $N^s_{pe} = K\left(n^s_{pe}\right)$

We assume that both n^s_{pe} and N^s_{pe} are Poisson distributed. The probability that signal photo-electrons will be detected in corresponding time bins in separate range gates is

$$P_K(\geq 3) = 1 - \left(1 + N^s_{pe} + \frac{\left(N^s_{pe}\right)^2}{2!}\right) e^{-N^s_{pe}}, \text{ k (\# of pe correlations)} \geq 3 . \qquad (4)$$

Equation 4, and corresponding ones for k=2 and 4, are evaluated in the following figure.

Correlated Detection Probabilities vs Mean Number of Detected Photo-electrons per Frame

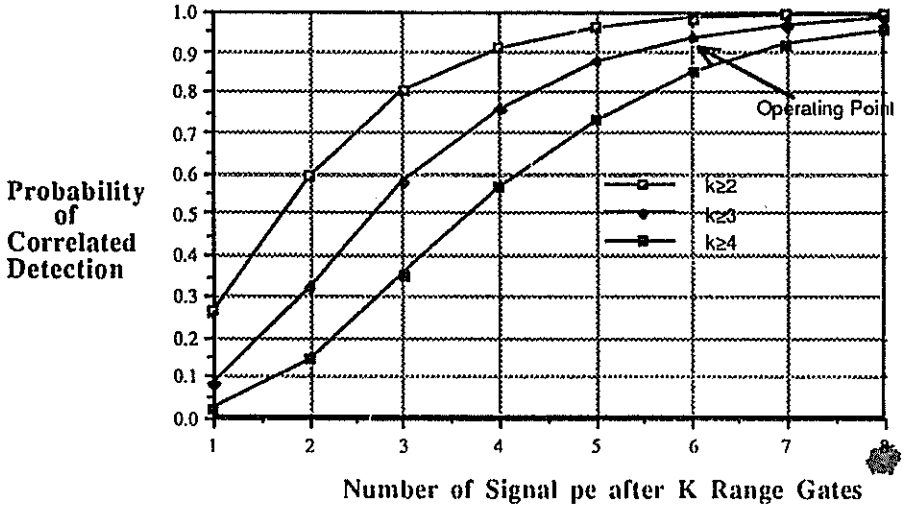

After an average of 6 signal photo-electrons are detected, k ≥ 3 correlation detection provides ~ 94% probability of signal acquisition. The corresponding times required to accumulate the 6 signal photo-electrons are shown in the next figure.

Time to achieve a Mean Photo-electron count ≥ 6 in ≥ 3 pulses vs Elevation Angle

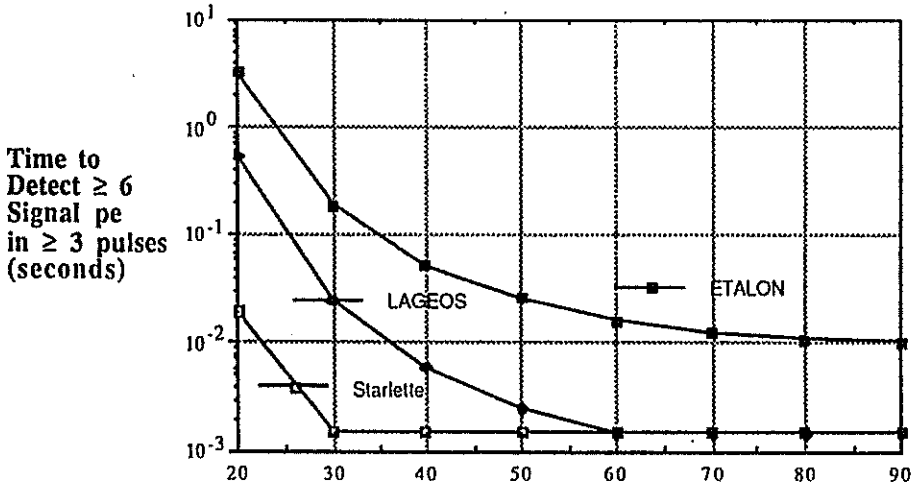

This figure is interpreted as the time it should take to acquire these satellites, which is a function of elevation angle. The times are: 0.0189 seconds / Starlette / 20°; 0.532 seconds / LAGEOS / 20°; 1.818 seconds / ETALON / 22°. During this same time noise counts occur. Using the formulation in the bibliography, and the parameters in the initial table in this paper, we find for the assumed quadrant photo-detector:

Clear Daytime Optical Background, pe's per range gate:		0.0278 Total 0.00695 per quadrant
Dark Counts: 10^4 / second , pe's per range gate:		0.0020 Total 0.0005 per quadrant
Signal Backscatter:	Prevented by Appropriate Receiver Blanking Programmably vary Laser Firing Time to Prevent "Collisions"	

Net Noise Photo-electron rate:	Day	14.9 / second / quadrant
	Night	1 / second / quadrant

To analyze the probability of false acquisition, we define m = # of noise photo-electrons present in a Frame and n_{bin} = # of time bins per range gate. The probability that these noise photo-electrons will lead to a (false) correlation is given by

$$P_{FAQ} = 1 - \left\{ e^{-\frac{m}{n_{bin}}} \sum_{j=0}^{k-1} \frac{\left(\frac{m}{n_{bin}}\right)^j}{j!} \right\}^{n_{bin}} \qquad (5)$$

m = [noise pe rate] x [time to detect 6 signal pe]

n_{bin} = [(range rate uncertainty) x (time to detect 6 signal pe)]$^{-1}$ x [range gate width].

Equation 5 is evaluated for a single ± 20 μradian beam at minimum elevation angle, k ≥ 3, and a 200 nsec gate in the following table.

		Time for 6 signal pe (sec)	Range Rate Uncertainty (nsec/sec)	m	Bin Width (nsec)	n_{bin}	$P_{FalseAcq}$
Starlette 20°	Day	0.0189	300	0.282	5.67	35	0.025 %
	Night	0.0189	300	0.0192	5.67	35	< 0.00001 %
LAGEOS 20°	Day	0.532	10	7.93	5.32	38	4.75 %
	Night	0.532	10	0.53	5.32	38	0.0017 %
ETALON ~22°	Day	1.818	1	27.1	1.818	110	20.4 %
	Night	1.818	1	1.82	1.818	110	0.0082 %

For Daytime ETALON, the SLR 2000 system parameters and k ≥ 3 correlation detection will find the signal ~ 94% of the time that it is present, and falsely identify noise counts as signal ~ 20% of the time when the signal is absent, for a single ± 20 μradian spot. The total time to acquire includes the effect of scanning the ± 20 μradian beam over the full angular uncertainty, including the effect of spot overlap and revisit, both included in an overhead factor. The resulting times are shown in the next table.

		Initial Angular Uncertainty (μradians)	Time per Spot (seconds)	Approximate Overhead	# of Spots	Maximum Acquisition Time (seconds)	Required Acquisition Time (seconds)
Starlette	Day	± 100 x ± 80	0.0189	33%	27	0.51	< 10
	Night	± 100 x ± 80	0.0189	33%	27	0.51	< 10
LAGEOS	Day	± 80 x ± 80	0.532	50%	24	12.55	< 120
	Night	± 80 x ± 80	0.532	33 %	21	11.17	< 120
ETALON	Day	± 80 x ± 80	1.818	100 %	32	58.2	< 300
	Night	± 80 x ± 80	1.818	33%	21	38.2	< 300

Before ranging, we center the spot on the quadrant to enable tracking, narrow the range gate to 10 nsec, and narrow the time bins to 100 psec . The resulting ranging performance, maintaining k ≥ 3 correlation to correctly identify 100 psec time bins, and defining precision per measurement point: $\left(\frac{c\Delta t}{2}\right) \approx 15$ mm, is given in the next table.

Satellite	Elevation Angle (Degrees)	# of Measurement Points per Normal Point	Approximate Precision (15 mm ÷ $\sqrt{\#}$ of meas. pts)
Starlette	20	1580	0.38 mm
	90	20,000	0.10 mm
LAGEOS	20	225	1.0 mm
	90	20,000	0.10 mm
ETALON	~ 22	165	1.17 mm
	90	30,000	0.087 mm

Tracking is achieved by using the quadrant signal to provide "slow" pointing updates. Signal counts per quadrant are accumulated until an adequate SNR exists.

$$SNR_{opt} = \frac{n^s_{pe}}{\left[n^s_{pc} + n^n_{pc}\right]^{1/2}} \rightarrow SNR_{opt} = \frac{\dot{n}^s_{pe} T_s}{\left[\dot{n}^s_{pe} T_s + \dot{n}^n_{pe} T_s\right]^{1/2}} = \frac{\dot{n}^s_{pe}}{\left[\dot{n}^s_{pe} + \dot{n}^n_{pe}\right]^{1/2}} T_s^{1/2} \qquad (6)$$

for T_S = measurement time. For a 10 nsec range gate, signal spot centered on the quadrant, and a $SNR_{quadrant}$ = 10 dB, tracking performance is shown in the next table.

Satellite	Elevation Angle	T_S (seconds)	Angular Motion per Update (milli-degrees)
Starlette (Daytime)	20°	0.127	15
	90°	0.0005	0.22
LAGEOS (Daytime)	20°	4.73	156
	90°	0.005	0.28
ETALON (Daytime)	~ 22°	23.1	230
	90°	0.22	2.53

For realistic system parameters, correlation detection provides :

Satellite Acquisition Probability	≥ 90 %
Initial Acquisition Times: (Daytime)	Starlette ~ 0.5 seconds at 20° LAGEOS ~ 13 seconds at 20° ETALON ~ 60 seconds at ~ 22°
Ranging Precision per Normal Point: (Daytime)	Starlette ~ 0.4 mm at 20° LAGEOS ~ 1 mm at 20° ETALON ~ 1.2 mm at ~ 22°
Tracking/Pointing Update Rate: (Daytime)	Starlette ~ every 15 milli-deg at 20° LAGEOS ~ every 156 milli-deg at 20° ETALON ~ every 230 milli-deg at ~ 22°

Bibliography

J. J. Degnan, Millimeter Accuracy Satellite Laser Ranging: A Review, Geodynamics Series Volume 25, Contributions of Space Geodesy to Geodynamics: Technology, 1993.

J.J. Degnan, "SLR 2000" in "Satellite Laser Ranging in the 1990's", Proceedings of the Belmont Workshop, Elkridge, MD, NASA Conference Publication 3283, Ed. J.J. Degnan, pp. 101-106, February 1-2, 1994.

J.J. Degnan, SLR 2000: An Autonomous and Eyesafe Satellite Laser Ranging System, Ninth International Workshop on Laser Ranging Instrumentation, Canberra 1994, J. McK. Luck Ed., Volume 1, pps. 312-323.

J.F. McGarry, B. Conklin, W. Bane, R. Eichlinger, P. Seery and R.L. Ricketts, Tracking Satellites with the Totally Automated SLR2000 System, Ninth International Workshop on Laser Ranging Instrumentation, Canberra 1994, J. McK. Luck Ed., Volume 2, pps. 717-725.

P. Titterton and H. Sweeney, SLR 2000 Design and Processing Approach Sensitivity, EOO Report 94-003, Dec. 15, 1994. GSFC PO# S-44974-Z.

P. Titterton, H. Sweeney and T. Driscoll, SLR 2000 Analytical Study of 1060 nm Aided Acquisition and Tracking, EOO Report 95-007, Nov. 1, 1995, GSFC PO# S-61158-Z.

J.F. McGarry, J.J. Degnan, P.J. Titterton, H.E. Sweeney, B.P. Conklin and P.J. Dunn, Automated tracking for advanced satellite laser ranging systems, Paper 2739-08 in Acquisition, Tracking and Pointing X, Proceeding of the SPIE Volume 2739, M.K, Mastern and L.A. Stockum Editors, 10-11 Apr. 1996, pps. 89-103.

J. J. Degnan, J.F. McGarry, T. Zagwodski, P. Titterton, H. Sweeney, H. Donovan, M. Perry, B. Conklin, W. Decker, J. Cheek, T. Mallama and R. Rickleffs, An inexpensive, fully automated, eyesafe satellite laser ranging system, Tenth International Workshop on Laser Ranging, Shanghai, 1996, these Proceedings.

J. McGarry, SLR2000 performance simulations, Tenth International Workshop on Laser Ranging, Shanghai, 1996, these Proceedings.

SLR2000 PERFORMANCE SIMULATIONS

Presented in the Eyesafe Systems Session of the
Tenth International Workshop on Laser Ranging Instrumentation
November 11-15, 1996

Jan McGarry
NASA/Goddard Space Flight Center
Greenbelt, Maryland 20771 USA

The SLR2000 Simulator is a software package designed to allow testing of new tracking and ranging algorithms prior to the actual hardware development of NASA's next generation of Satellite Laser Ranging Systems, called SLR2000. The simulator is written in FORTRAN, currently runs in the HPUX environment, and models relevant errors in the receiver system, tracking mount, weather sensors, station location, system timing, predictions, and others. Recent work includes adding a new signal to noise algorithm, improving the tracking mount model, and developing an acquisition search algorithm. As a consequence of this work, we feel that the simulation results now provide a more realistic example of SLR2000 performance. Simulations of SLR2000 tracking and ranging performance will be presented.

Introduction

SLR2000 is a low cost, totally autonomous, eyesafe satellite laser ranging system currently being developed at NASA's Goddard Space Flight Center. The eye safety constraint implies a low transmit energy (200 microjoules), narrow laser divergence (+-4 arcseconds), and a rapid fire rate (2kHz). Algorithms to distinguish signal from noise must be developed since the system will be operating in a very low signal to noise environment. The operator functions must also be replaced by algorithms to perform such tasks as scheduling passes, acquiring and tracking satellites, and determining if the weather permits ranging. Lastly, the predictions must be made more accurate in order to improve pointing (for the narrower laser divergence) and to reduce the slope of the range errors in the ranging window (for the signal to noise algorithm to succeed).

The performance of SLR2000 depends heavily on the design and development of these improved models and algorithms. The simulator allows us to test the design of the algorithms, see how these algorithms affect performance prior to development of the hardware, and work in a controlled environment where absolute truth is known and can be used to judge performance.

For a more detailed description of the SLR2000 system see the paper[1] by John Degnan in this Proceedings. For a theoretical analysis of the potential acquisition, tracking and ranging performance of SLR2000 see Paul Titterton's paper[2] also in this Proceedings.

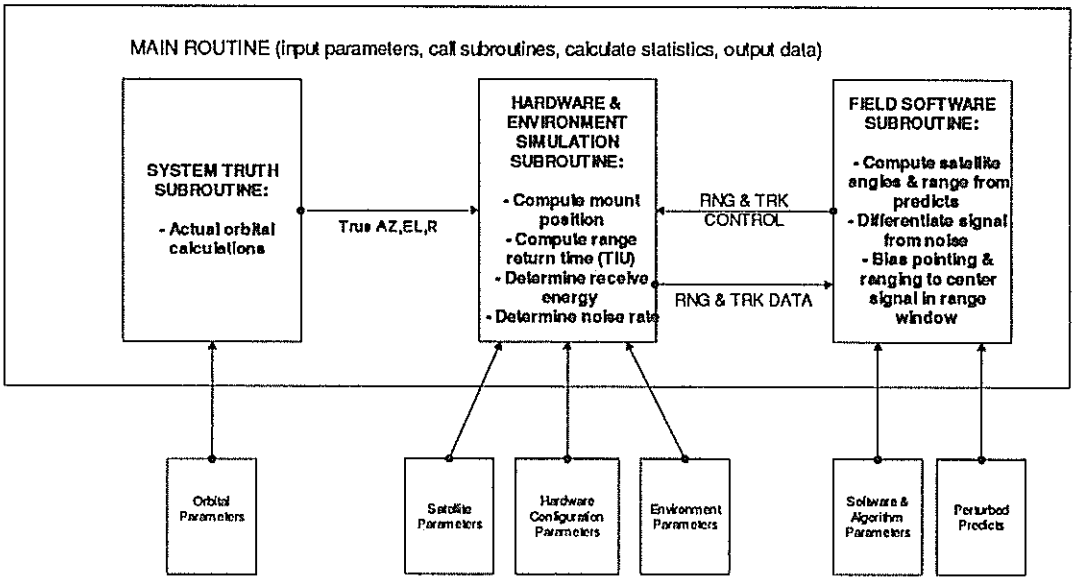

Figure 1: SLR2000 Simulator Design

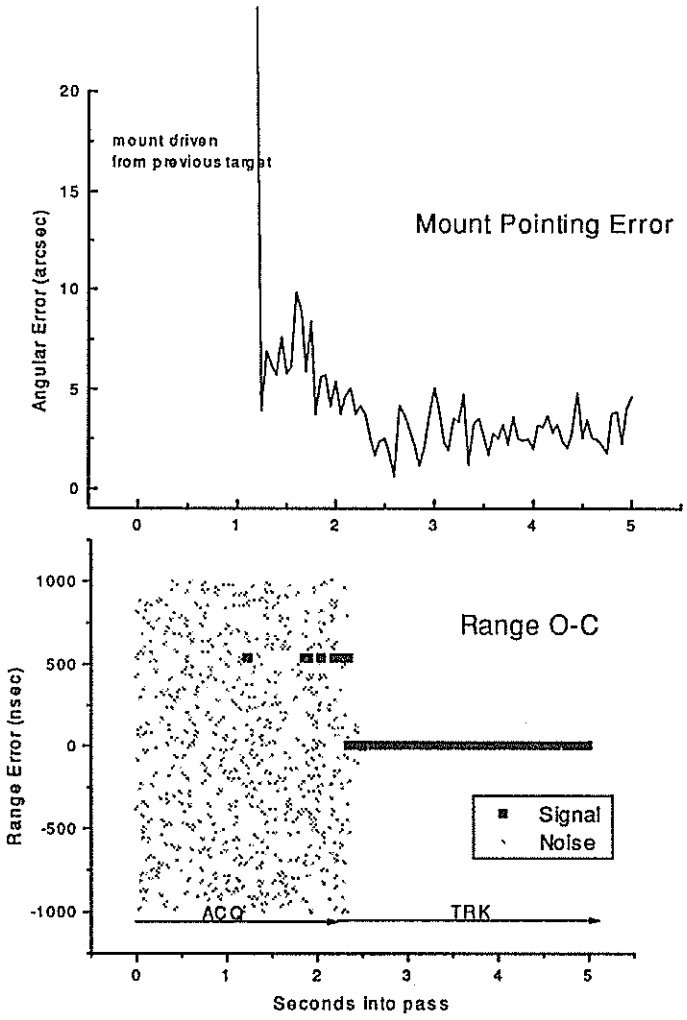

Figure 2: STARLETTE Daylight Pass

Simulator Description

The simulator models the ground instrumentation, the satellite orbit, the environment and the field software to produce a virtual SLR2000 system. The field software interacts with the hardware as in a real station to read in data and control the instrumentation. The System Truth, which includes where the satellite actually is, what the sky clarity is like, what time of day it is, and how the atmosphere is affecting the signal strength, is maintained to allow determination of actual system performance. The hardware readings are essentially System Truth perturbed by various random measurement errors and biases. The field software has no access to System Truth to ensure integrity of the testing process. Figure 1 illustrates this design. Recent enhancements include the addition of an angular search during acquisition, a model for a quadrant detector, moving clouds, and an improved tracking mount model. Listed below are some of the functions modeled in the simulator.

SLR2000 SIMULATOR HARDWARE FUNCTIONS / ERRORS MODELED

- POINTING SYSTEM
  - Bias of mount system (error in mount model and mount wobble)
  - Random jitter
  - Mount drive at 2kHz with limits on acceleration & velocity
  - Actual mount pointing kept separate from encoder readings

- RECEIVER TIMING
  - Detector modeled:
    Photomultiplier or photon-counting Avalanche Photodiode.
  - Time Interval Unit error modeled as random Gaussian noise
  - Computation of background noise above threshold
  - System delay bias applied

- RECEIVER ENERGY
  - Fixed transmitter energy
  - Gaussian pulse (spatial and temporal)
  - Computation of transmitter gain as function of laser divergence
  - Attenuation of energy with system and atmospheric transmission
  - Satellite treated as single cube with given cross-section
  - Moving cloud cover

- STATION READINGS
  - Station location biases
  - Weather sensor offsets
  - System timing bias

- QUADRANT DETECTOR
  - Simple model determines proportion of signal in each quadrant as function of pointing error
  - Noise rate is divided equally between the 4 quadrants

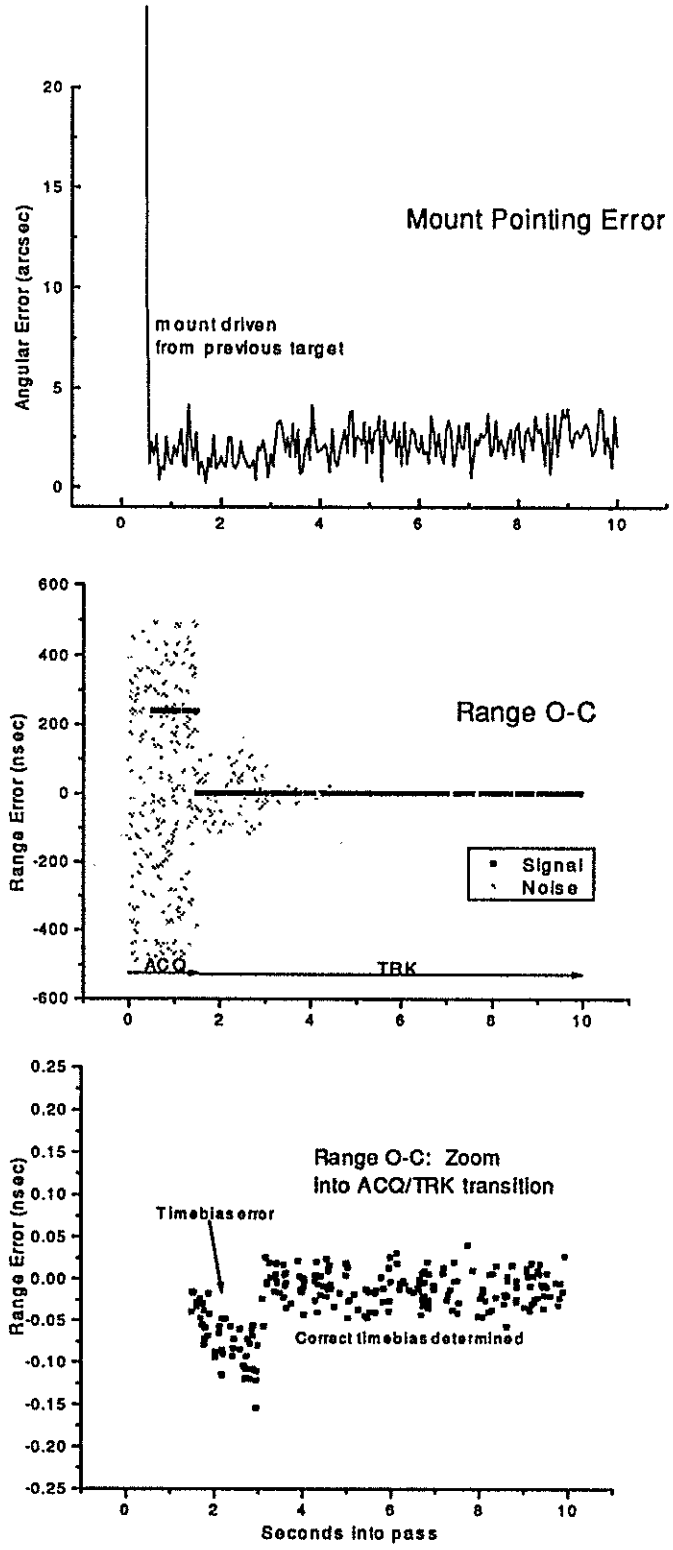

Figure 3: LAGEOS Daylight Pass

SLR2000 SIMULATOR ORBIT & FIELD SOFTWARE FUNCTIONS MODELED

- SYSTEM TRUTH
  - Orbital update using GEM10 and Texas Integrator
  - Sun position calculated and used in optical background determination
  - Environment truth maintained

- SOFTWARE POINTING COMPUTATIONS
  - Polynomial used to update satellite position (NASA SLR Network method)
  - Output to mount drive at 100Hz
  - Quadrant Detector output used as angular correction

- ALGORITHM COMPUTATIONS
  - EOO algorithm[2] used to detect Signal from Noise
  - Time and Range Bias computed from Signal
  - Angular Search used to find target (spiral scan)

The simulator is written in FORTRAN and contains approximately 4,000 lines of code. It currently runs under HPUX, but since there are few system unique calls, the simulator should be easily portable, and our plans are to convert it for Windows95. The simulator has more than 70 different variables that can be modified; each must currently be changed by editing the appropriate input file. A few of the possible parameters that can be changed, along with the values used in the Simulator Results section, are listed in Table 1. Future Windows95 versions will contain a graphical menu front end for helping the user configure the simulator and run it. There are also many possible outputs to select from, including mount errors, range O-C plots, and autotracking decisions. All of these are currently output as ASCII files which must be graphed post-run via an independent plotting package. This will also be changed in future versions, where results will be plotted from the simulator's graphical user interface.

Table 1: Important Simulator Parameters

Parameter	Value used in Simulations
Quantum Efficiency	0.40
Energy /pulse at aperture(μJ)	200
One way path transmission	0.75 @ 90° elev. and 0.12 @ 20° elev.
Optical Cross-section (m^2)	0.65(10^6) for STARLETTE 7 (10^6) for LAGEOS 20 (10^6) for GPS35
Receiver Optics Transmission	0.12
Receiver Area (m^2)	0.196 for 50 cm diam.
Transmitter half-angle beamwidth (arcsec)	4
Optical Bandpass filter (Å)	1.2
Solid angle FOV (sterad)	1.81 (10^{-9})
Background spectral radiance (watts/m^2-ster-Å)	1.46 (10^{-3}) day and 1.46 (10^{-8}) night
Dark current density (amps/cm^2)	10^{-15} (◇ background rate = 7000/sec for 1.2cm diameter cathode)
Mount jitter (arcsec)	0.5
Mount wobble / model error (arcsec)	4

Simulator Results

Figures 2 - 4 show simulations of the SLR2000 system acquiring STARLETTE, LAGEOS and GPS. The plots show Observed minus Calculated ranging data (O-C) in the range window along with the corresponding mount errors. The errors are graphed versus seconds into the pass. The darker range returns are the signal and the light gray returns represent noise. In all cases the simulator correctly finds the signal, corrects the pointing, range and time biases to center the satellite returns in the quadrant detector, and centers the signal in the range window. As the signal is acquired, the field software also closes down the range window. The mount errors shown include the time to close on the start of the pass from another mount position, the errors in the commands due to errors in the prediction polynomials, and the mount jitter and wobble. The polynomials used are those from the current NASA SLR Network and while accurate enough for the MOBLAS systems which have +-10 arcsecond beam divergences and 100 millijoule laser energies, they are not accurate enough for SLR2000 requirements and will not be used in the actual system.

Figure 2 shows a STARLETTE acquisition at 20 degrees elevation with a slant range of around 2,000km. Figure 3 is a LAGEOS pass being acquired at 20 degrees with a slant range of around 8,500km. This figure also zooms into the range window to show the timebias correction being applied (the slope of the range error being zeroed). Figure 4 shows GPS being acquired at 30 degrees elevation with a slant range of around 23,500km. All results are for a 50 centimeter telescope with parameters shown in Table 1 above. It should be emphasized that in these simulations the algorithm does not mistake noise for signal, even in the GPS case with a 1 microsecond range window. Previous simulations, using a 30cm telescope, showed false acquisitions for daylight GPS.[3] This agrees with theory which gives the probability of false acquisition for this telescope aperture to be nearly 100%. For the 50 centimeter telescope the probability of false acquisition is less than 20%.

Conclusions

Simulations of SLR2000 performance agree with the analytical conclusion that a low energy, 50cm telescope system with a quadrant detector, will be able to acquire and track, during daylight, all of the satellites currently tracked by the NASA Network from STARLETTE out to GPS.

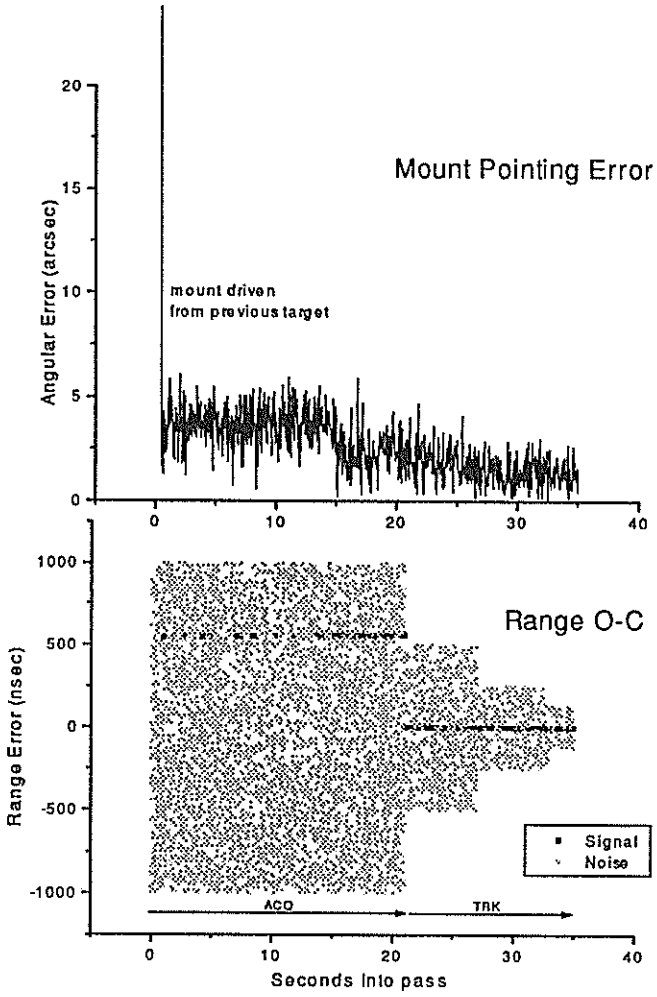

Figure 4: GPS Daylight Ranging

References

1. Degnan, John, Jan McGarry, Thomas Zagwodzki, Paul Titterton, Harold Sweeney, et al, "SLR2000: An Inexpensive, Fully Automated, Satellite Laser Ranging System," in this Proceedings.
2. Titterton, Paul, and Harold Sweeney," Correlation Processing Approach for Eyesafe SLR 2000," in this Proceedings.
3. McGarry, Jan.F, John J. Degnan, Paul Titterton, Harold Sweeney, Brion P.Conklin, Peter J. Dunn, "Automated tracking for advanced satellite laser ranging systems", in the proceedings from Acquisition, Tracking, and Pointing X, Vol. 2739, SPIE Aerosense, Orlando, April 1996.

Centimeter Eyesafe Satellite Laser Ranging

Using Raman Shifted Nd:YAG Laser and Germaniumm Photon Counter

B.Greene

Electro Optic Systems Pty Limited, Queanbeyan, NSW, Australia

H.Kunimori

Communication Research Laboratory, Nukui-kita, Tokyo, Japan

K.Hamal, I.Prochazka

Czech Technical University, Brehova 7,115 19 Prague, Czech Republic

Abstract

Centimeter eyesafe satellite laser ranging has been performed to a wide range of satellites using a Raman shifted picosecond Nd:YAG laser operating at 1543 nanometers and a novel Germanium single photon detector. The ranging has been accomplished for retroreflector equipped satellites up to an altitude of 30,000 kilometers, establishing link parameters through the atmosphere for this wavelength for the first time. The experiment paves the way for deployment of high power eyesafe lasers in space applications.

1. INTRODUCTION

Satellite laser ranging (SLR) is performed routinely by a global network of around 40 active stations. The precision of these stations is now at the centimetre level, and further improvements are anticipated in the future. SLR data has made major contributions to science in the past 3 decades in applications including geodynamics, crustal deformation, earth rotation, environmental studies, oceanography, relativity, and cosmology.

The technique of SLR involves satellites equipped with retroreflectors, tracked by ground laser stations equipped with a picosecond laser, tracking telescope, detector, and a timing system. Laser transmitters used up to now operate in the wavelength range 355 to 1064 nanometers, with pulse energies far above the eye safe (Maximum Permissasble Exposure) levels. The high power laser pulses transmitted by the station can represent a serious eye damage hazard to aircraft passengers and crew, and to the SLR station operators. The need for ground calibration extends this risk to people in the local area of the station.

To reduce the risk to acceptable levels, a strong set of safety guidelines are in force at most stations. Over billions of laser pulses sent into space, there has never been any injury from a pulse transmitted from an SLR station. However, as air traffic increases and is globally less regulated, as the tracking program multiplies in intensity, and as pressure is applied for reductions in operating costs, there is a clear need to render the SLR operations intrinsically harmless to humans.

An eyesafe SLR station is defined as one for which the emitted laser beam intensity is below statutory MPE levels. This can be achieved by reducing the transmiited energy of existing lasers (operating at 532 nm) by (typically) several orders of magnitude, which correspondingly reduces data yield and makes the tracking of high satellites (above 10,000 km) problematic. An alternative approach is to operate the laser

at another wavelength within the eye safety window near 1540 nanometers [1], where reductions in laser pulse energy to meet MPE criteria are not necessary.

This second approach has the potential to allow all traditional SLR applications to be maintained, and even expanded. The approach has been inhibited by several technical obstacles and uncertainties:

- the lack of a reliable picosecond laser source with (at least) millijoule pulses;
- the lack of a picosecond detector with suitable characteristics;
- uncertainty over the response of existing laser satellites to 1.5 um radiation; and
- uncertainty over the effect of various atmospheric conditions on link budgets at this wavelength.

Provided these difficulties and uncertaintanties could be overcome, the cost, productivity, and range of application of SLR systems and technology would be enhanced by migrating the operating wavelength to around 1.5 micron.

2. EYESAFE SLR DESIGN

The experiment was performed by adding a second (1.54 um) wavelength capability to a standard 532 nm SLR system (EOS SLR Version 3d) installed at CRL. Figure 1 shows the exerimental arrangement [2].

The 1.5 meter aperture tracking telescope is used to transmit the laser pulse to the satellite and to collect the returned signal. The same telescope aperture is used for both transmit and receive, by means of an optical switch comprising a rotating mirror synchronized to the laser firing.

The SLR system is capable of routinely tracking all satellites of scientific interest, and has an instrumental accuracy (ie excluding atmospheric dispersion correction) of around 1 mm at any range. using the Si SPAD (Single Photoelectron Avalanche Diode).

Routine SLR operations are normally carried out by transmitting 70 mJ in 150 ps (FWHM) of 532 nm radiation, and using the Si SPAD detector. This configuration typically gives a single shot precision of 15 mm. For this experiment, modifications were made to allow a second laser pulse at 1543 nm to be transmitted synchronously with the original beam, and to provide a second receiver channel at 1543 nm. No modifications were need to the SLR operating system, as it allows multiple satellite returns to be taken from two detectors.

The receiver was modified by adding a dichroic beamsplitter to create a second optical path to the Ge SPAD. The dichroic is placed so as to utilise the existing spatial filter. A bandpass filter and 532 nm block are also added to the 1543 nm channel. The use of a common spatial filter to which both detectors are aligned ensures that the satellite will be in the field of both detectors simultaneously.

The experiment requires at least 1 mJ of 1543 nm energy for useful data over a variety of atmospheric conditions and for various satellites. Considering the present picosecond laser technologies, the two principal alternatives to develop the laser transmitter are optical parametric techniques based on non-linear solid state devices (OPO/OPG/OPA), or Raman Shifted Laser (RSL). Preliminary experiments at SLR stations in Graz, Austria and Tokyo, Japan [4] were based on a RSL configuration which was further developed and applied here. For this experiment Raman stimulated emission provided 6 mJ of 1543 nm energy in 160 ps, using 50 mJ input energy at 1064 nm focussed into a Raman tube filled to 30 Bar with methane. The final beam divergence at the telescope was 10 microradians.

For this experiment, a Germanium SPAD (Ge SPAD) operated in Geiger mode with active quenching and gating [5] was developed. To reach the single photon sensitivity and subcentimeter precision the

photodiode is pulse biased above the break voltage. A similar detector (Si SPAD [3]) is in routine use at many SLR stations for 400 - 1064 nanometer wavelength SLR.

The Ge SPAD and electronics are housed in a custom-designed cryostat, allowing the detector to operate at 77K. The cryostat is a high-vacuum insulation design, allowing several days between liquid Nitrogen refills.

Detector performance was calibrated using calibration facilities at the Czech Technical University in Prague. The experimental Ge SPAD was determined to have the following characteristics:

- active area diameter 0.1 millimeter
- single photon timing jitter 32 picoseconds rms
- quantum efficiency 15% at 532 and 1543 nanometers
- dark count rate 1 Mhz.

Using ground target calibration facilities at SLR Station Graz (Austria), and ranging at 1543 nanometers using 30 picosecond pulse duration laser, these measurements were confirmed.

3. EYESAFE SLR RESULTS

The eyesafe SLR system described above was developed and installed at CRL between June 1994 and January 1996. SLR at 1543 nanometer range was achieved on January 11, 1996. The retroreflector equipped satellites Topex, Starlette, Ajisai, Lageos 1, Lageos 2, Etalon, and Glonas at distances 1000 - 20,000 kilometers have been ranged routinely since January 1996. Figures 2a and 2b show typical results from Lageos 2 and Ajisai respectively. The atmospheric dispersion effect can be noticed on Figure 2, as optical signals at different wavelengths experience different optical thickness of the atmosphere.

The Lageos satellite elevation above the horizon varied from 60 to 70 degrees during the pass on Fig. 2a and the Ajisai satellite elevation in Fig. 2b changed from 63 degrees down to 20 degrees.

The ranging precision was tested on a satellite with minimal target depth (Starlette) yielding 25 millimeters single shot precision, as expected for this initial configuration.

4. DISCUSSION AND CONCLUSIONS

- The respective signal return rates at 532 nm and 1543 nm are comparable, after consideration is given to output pulse energy, detector efficiency, detector area, and beam divergence.
- The calibrated response of the detector is 45 ps RMS per detected photon. However the observed satellite ranging precision was 165 ps [25 millimeters] RMS for a single shot, due to the laser pulse of 160 ps FWHM [which adds up to 90 ps RMS of uncertainty to the timing process] and Raman jitter. The pulse transmition epoch is referred to the Raman pump 1064 nm pulse, and therefore the overall ranging precision at 1543 nm is affected by the fluctuations in Raman generation process, which appears at different epochs relative to the 1064 nm pump pulse. Raman generation epoch fluctuations will reach a significant proportion of the pump pulse duration of 200 picoseconds.
- The results prove the feasibility of eyesafe SLR in the 1543 nanometer eyesafe window.
- The observed relative link budgets for 532 nm and 1543 nm for 2-way atmospheric transmission generally agree with predictions based on atmospheric transmission models, although more data is required over a wider variety of conditions to allow the separate model elements to be validated.

- The use of Raman techniques for reliable picosecond pulse generation over many millions of shots has been demonstrated. However operational limitations of the Raman technique, such as epoch jitter and conversion efficiency for picosecond pulses and parasitic anti-stokes conversion, remain to be overcome.
- The novel Ge SPAD detector can resolve sinlge photon events with 100 ps resolution. This detector is likely to find widespead use in photon counting over a broad spectral range.
- The response of existing retroreflectors in space to 1543 nm radiation has been established. None of the retroreflectors used were designed for or tested at this wavelength prior to launch, and the satellite response before this experiment has been unknown. It has been shown that the cross section for all satellites at 1543 nm is at least similar to the 532 nm cross section.
- As it has been demonstrated that SLR can be conducted within eye safety standards, unmanned and automated systems are now possible. This will expand the range of applications and the flexibilty of deployment of SLR and its derivative techniques.
- Routine two wavelength ranging measurements with picosecond accuracy [6] will contribute to the existing atmospheric refraction model verification and possible refining in the near infrared range.

5. Acknowledgements

The authors would like to express their appreciation to Mr.Suzaki and Mr. Oyama of Hitachi Co.Ltd, and John Guilfoyle and Tim May of Electro Optic Systems Pty Limited, for their assistance in performing the experiments.

The reseasrch was carried out with funds granted by Communications Research Laboratory and Electro Optic Systems Pty Limited.

References

[1] American National Standard: Z 136.1-1993

Japanese Industrial Standard: JIS C6802-1991

European Community Standard: EN60825:1991

[2] Kunimori H., Imamura K., Taka-hashi F., Itabe T., Aruga T., Yamamoto A., "New Development of Satellite Laser Ranging System for Highly Precise Space and Time measurements", Journal of Communication Research Laboratory, Vol.38, No.2, pp303-317, July 1991.

[3] Prochazka I., Hamal K., Kirchner G., Sopko B., "Photodiode for Subcentimeter Satellite Laser Ranging Operating at the Room Temperature", Technical Digest Series, Proceedings of the Conference on Lasers and Electro Optics, CLEO '90, Optical Society of America, pp 138, 1990.

[4] Kunimori H., Greene B., Guilfoyle J., Hamal K., Prochazka I., Kirchner G., Koidl F., "Subcentimeter eyesafe ranging", Technical Digest Series, Proceedings of the CLEO Pacific Rim '95 Conference, Tokyo, pp 17-18,1995.

[5] Prochazka I., Hamal K., Greene B., Kunimori H.,' Large aperture Germanium detector package for picosecond photon counting in 0.5 to 1.6 um range', to be published in Optics Letters.

[6] Prochazka, I. Hamal K., Kirchner G., Koidl F., "Atmospheric optical density measurement using multiple wavelengths picosecond satellite laser ranging", Proc. of the Conference on Lasers and Electro Optics CLEO'94, Teschnical Digest Series, Optical Society of America, paper CWQ3.

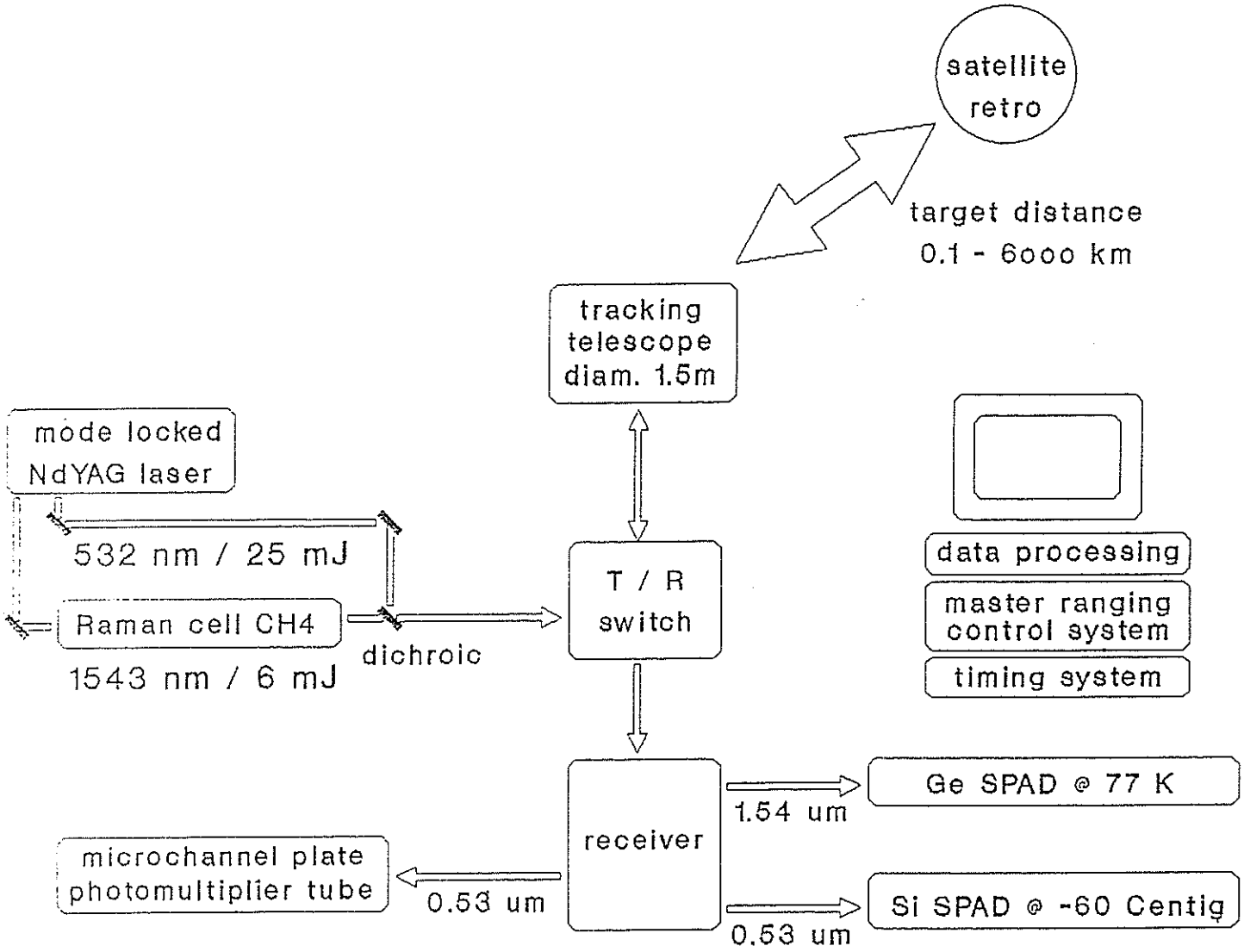

Figure 1: Satellite laser ranging station block diagram.